Report No. K-TRAN: KU-13-2 ▪ FINAL REPORT ▪ January 2016

Stabilization of Unpaved Shoulders on Moderate and Weak Subgrade Using Geosynthetics

Jun Guo
Jie Han, Ph.D., P.E.
Steven D. Schrock, Ph.D., P.E.
Xiaohui Sun, Ph.D.
Robert L. Parsons, Ph.D., P.E.

The University of Kansas

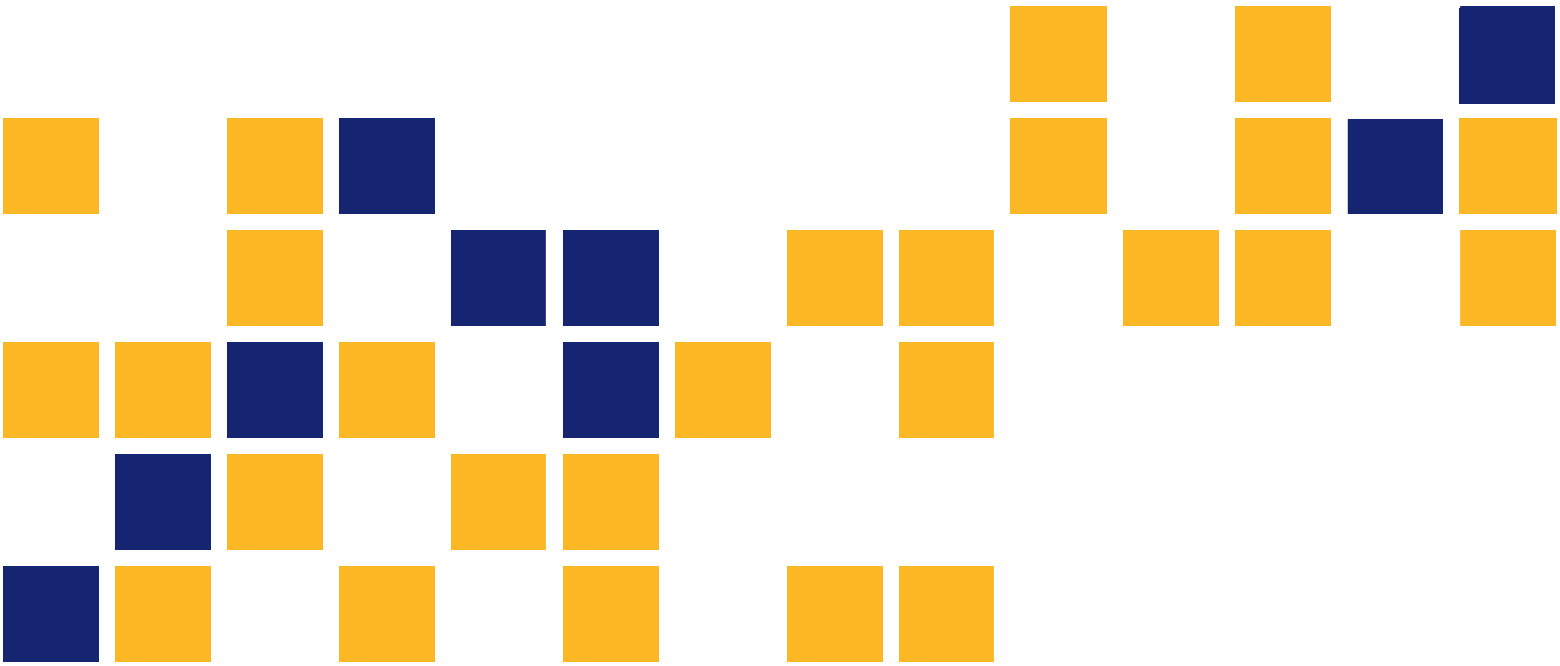

Kansas Department of Transportation

1 Report No. K-TRAN: KU-13-2	**2 Government Accession No.**	**3 Recipient Catalog No.**
4 Title and Subtitle Stabilization of Unpaved Shoulders on Moderate and Weak Subgrade Using Geosynthetics		**5 Report Date** January 2016 **6 Performing Organization Code**
7 Author(s) Jun Guo, Jie Han, Ph.D., P.E., Steven D. Schrock, Ph.D., P.E., Xiaohui Sun, Ph.D., and Robert L. Parsons, Ph.D., P.E.		**7 Performing Organization Report No.**
9 Performing Organization Name and Address The University of Kansas Department of Civil, Environmental and Architectural Engineering 1530 West 15th St Lawrence, Kansas 66045-7609		**10 Work Unit No. (TRAIS)** **11 Contract or Grant No.** C1956 C1987
12 Sponsoring Agency Name and Address Kansas Department of Transportation Bureau of Research 2300 SW Van Buren Topeka, Kansas 66611-1195		**13 Type of Report and Period Covered** Final Report April 2013–July 2015 **14 Sponsoring Agency Code** RE-0601-01 RE-0648-01
15 Supplementary Notes For more information write to address in block 9.		

Geosynthetics have been used to improve the performance of roadways, especially when weak subgrade soil exists. In this study, two types of geosynthetic products, geocell and geogrid, were investigated for their application for stabilization of unpaved shoulders on moderate and weak subgrade and for their effect on vegetation growth.

A one-year-long outdoor field vegetation test for two primary target species (tall fescue grass and perennial ryegrass) was conducted on base courses with different combinations of aggregate and topsoil to investigate the possible effect of geocell and geogrid on shoulder vegetation. During the one-year test period, soil temperature and volumetric moisture content were monitored. Weather data, such as precipitation and air temperature, were obtained from the nearby weather station at the Lawrence airport. Vegetation growth was evaluated by grass leaf blade length, root length, and grass density. Vegetation biomass was obtained at the end of the test. The test results showed no obvious effect of geocell or geogrid on the vegetation in unpaved shoulders. The vegetation test also showed that the 50% aggregate and 50% topsoil mixture had vegetation growth similarly as the topsoil.

Based on the vegetation test, the 50% aggregate and 50% topsoil mixture was selected as a base course rather than the 65% aggregate and 35% topsoil mixture for cyclic plate loading tests. When geocell was used to reinforce unpaved shoulders, six large-scale plate loading tests were conducted on base courses reinforced by a single type of geocell on 5% California Bearing Ratio (CBR) subgrade (moderate subgrade) to investigate the benefits of geocell reinforcement on different base course and topsoil combinations. Eight similar plate loading tests were conducted on eight geogrid-reinforced base courses over 3% and 5% CBR subgrade, including 150-mm-thick aggregate with and without geogrid reinforcement and 150-mm-thick soil-aggregate mixture with and without geogrid reinforcement. Earth pressure cells were installed at the interface between subgrade and base course to monitor the vertical load distribution.

The cyclic plate loading tests showed that the geocell and geogrid effectively reduced the accumulated permanent deformations as compared with the unreinforced sections. The geocell-reinforced soil-aggregate mixture slightly outperformed the unreinforced aggregate of the same thickness over a 5% CBR subgrade. The geogrid-reinforced soil-aggregate mixture performed significantly better than the unreinforced aggregate of the same thickness over 3% and 5% CBR subgrades. The plate loading tests also suggested that the topsoil cover resulted in large permanent deformations and rapid failure.

Aggregate bases are recommended for unpaved roads. A 50% soil and 50% aggregate mixture is recommended for vegetated unpaved shoulders. Topsoil should not be used as a cover if unpaved shoulders are subjected to traffic. Geogrid is recommended to improve aggregate bases if needed. Geocell is recommended to improve soil-aggregate mixture if needed.

17 Key Words Geosynthetics, Geocell, Geogrid, Unpaved Shoulders, Vegetation		**18 Distribution Statement** No restrictions. This document is available to the public through the National Technical Information Service www.ntis.gov.	
19 Security Classification (of this report) Unclassified	**20 Security Classification (of this page)** Unclassified	**21 No. of pages** 134	**22 Price**

Form DOT F 1700.7 (8-72)

This page intentionally left blank.

Stabilization of Unpaved Shoulders on Moderate and Weak Subgrade Using Geosynthetics

Final Report

Prepared by

Jun Guo
Jie Han, Ph.D., P.E.
Steven D. Schrock, Ph.D., P.E.
Xiaohui Sun, Ph.D.
Robert L. Parsons, Ph.D., P.E.

The University of Kansas

A Report on Research Sponsored by

THE KANSAS DEPARTMENT OF TRANSPORTATION
TOPEKA, KANSAS

and

THE UNIVERSITY OF KANSAS
LAWRENCE, KANSAS

January 2016

PREFACE

The Kansas Department of Transportation's (KDOT) Kansas Transportation Research and New-Developments (K-TRAN) Research Program funded this research project. It is an ongoing, cooperative and comprehensive research program addressing transportation needs of the state of Kansas utilizing academic and research resources from KDOT, Kansas State University and the University of Kansas. Transportation professionals in KDOT and the universities jointly develop the projects included in the research program.

NOTICE

The authors and the state of Kansas do not endorse products or manufacturers. Trade and manufacturers names appear herein solely because they are considered essential to the object of this report.

This information is available in alternative accessible formats. To obtain an alternative format, contact the Office of Public Affairs, Kansas Department of Transportation, 700 SW Harrison, 2nd Floor – West Wing, Topeka, Kansas 66603-3745 or phone (785) 296-3585 (Voice) (TDD).

DISCLAIMER

The contents of this report reflect the views of the authors who are responsible for the facts and accuracy of the data presented herein. The contents do not necessarily reflect the views or the policies of the state of Kansas. This report does not constitute a standard, specification or regulation.

Abstract

Geosynthetics have been used to improve the performance of roadways, especially when weak subgrade soil exists. In this study, two types of geosynthetic products, geocell and geogrid, were investigated for their application for stabilization of unpaved shoulders on moderate and weak subgrade and for their effect on vegetation growth.

A one-year-long outdoor field vegetation test for two primary target species (tall fescue grass and perennial ryegrass) was conducted on base courses with different combinations of aggregate and topsoil to investigate the possible effect of geocell and geogrid on shoulder vegetation. Eight base course combinations for investigating the effect of geocell on vegetation included 200-mm-thick unreinforced topsoil, 200-mm-thick soil-aggregate mixture (50% aggregate and 50% topsoil), 50-mm-thick aggregate over 150-mm soil-aggregate mixture (50% aggregate and 50% topsoil), 50-mm-thick topsoil over 150-mm reinforced soil-aggregate mixture (50% aggregate and 50% topsoil), 50-mm-thick topsoil over 100-mm-thick aggregate, 50-mm-thick topsoil over 100-mm-thick soil-aggregate mixture (65% aggregate and 35% topsoil), 150-mm-thick soil-aggregate mixture (65% aggregate and 35% topsoil), and 50-mm-thick topsoil over 100-mm-thick soil-aggregate mixture (50% aggregate and 50% topsoil). Four base course combinations for investigating the effect of geogrid on shoulder vegetation included 50-mm-thick topsoil over 100-mm-thick aggregate, 50-mm-thick topsoil over 100-mm-thick soil-aggregate mixture (65% aggregate and 35% topsoil), 150-mm-thick soil-aggregate mixture (65% aggregate and 35% topsoil), and 50-mm-thick topsoil over 150-mm-thick soil-aggregate mixture (50% aggregate and 50% topsoil). One control (unreinforced) section and one geocell- or geogrid-reinforced section were prepared for each base course combination with a test section size of 1.5 × 1.5 m. During the one-year test period, soil temperature and volumetric moisture content were monitored. Weather data, such as precipitation and air temperature, were obtained from the nearby weather station at the Lawrence airport. Vegetation growth was evaluated by grass leaf blade length, root length, and grass density. Vegetation biomass was obtained at the end of the test. The test results showed no obvious effect of geocell or geogrid on the vegetation

in unpaved shoulders. The vegetation test also showed that the 50% aggregate and 50% topsoil mixture had vegetation growth similarly as the topsoil.

Based on the vegetation test, the 50% aggregate and 50% topsoil mixture was selected as a base course rather than the 65% aggregate and 35% topsoil mixture for cyclic plate loading tests. When geocell was used to reinforce unpaved shoulders, six large-scale plate loading tests were conducted on base courses reinforced by a single type of geocell on 5% California Bearing Ratio (CBR) subgrade (moderate subgrade) to investigate the benefits of geocell reinforcement on different base course and topsoil combinations, which included 200-mm-thick unreinforced aggregate, 200-mm-thick soil-aggregate mixture (50% aggregate and 50% topsoil) with and without geocell reinforcement, 200-mm-thick geocell-reinforced topsoil, 50-mm-thick aggregate over 150-mm soil-aggregate mixture (50% aggregate and 50% topsoil), and 50-mm-thick topsoil over 150-mm-thick geocell-reinforced soil-aggregate mixture (50% aggregate and 50% topsoil). Eight similar plate loading tests were conducted on eight geogrid-reinforced base courses over 3% and 5% CBR subgrade, including 150-mm-thick aggregate with and without geogrid reinforcement and 150-mm-thick soil-aggregate mixture with and without geogrid reinforcement. Earth pressure cells were installed at the interface between subgrade and base course to monitor the vertical load distribution.

The cyclic plate loading tests showed that the geocell and geogrid effectively reduced the accumulated permanent deformations as compared with the unreinforced sections. The geocell-reinforced soil-aggregate mixture slightly outperformed the unreinforced aggregate of the same thickness over a 5% CBR subgrade. The geogrid-reinforced soil-aggregate mixture performed significantly better than the unreinforced aggregate of the same thickness over 3% and 5% CBR subgrades. The plate loading tests also suggested that the topsoil cover resulted in large permanent deformations and rapid failure.

Aggregate bases are recommended for unpaved roads. A 50% soil and 50% aggregate mixture is recommended for vegetated unpaved shoulders. Topsoil should not be used as a cover if unpaved shoulders are subjected to traffic. Geogrid is recommended to improve aggregate bases if needed. Geocell is recommended to improve soil-aggregate mixture if needed.

Acknowledgements

This research project was financially sponsored by the Kansas Department of Transportation (KDOT). The monitor of this project was Mr. Jonathan P. Marburger (first) and Mr. Nat Velasquez (later) at KDOT. Mr. Scott Shields from KDOT provided the vegetation related documents used in this research. Presto Geosystems provide geocell products and Tensar International provided geogrid products for the testing. Laboratory manager and technicians, Matthew Maksimowicz, David Woody, and Eric Nicholson, graduate students, Omar K. Ismael, Fei Wang, Jamal Ismail Kakrasul, Ghaith Abdulrasool, Saif Jawad, Mahdi Al-Naddaf, and Mehari Tesfagabr, undergraduate research assistants, Byron Whitted, Brandon Basgall, Lee Crippen, Zach Brady, Felipe Brandao, and David Rivero, and visiting scholar, Dr. Hongguang Zhang, from The University of Kansas provided great assistance. All the above support and help are greatly appreciated.

Table of Contents

List of Tables

List of Figures

Chapter 1: Introduction

1.1 Background

Shoulders are constructed next to rigid and flexible pavements to provide space for vehicles to stop during an emergency, increase road safety, and provide structural support for the roadway. Shoulders can be paved or unpaved. Unpaved shoulders, including aggregate and turf shoulders, are often constructed along rural two-lane highways for a design traffic volume of 0 to 874 Annual Average Daily Traffic (AADT) according to the Kansas Department of Transportation (KDOT). Typically, aggregate shoulders have a uniform thickness of 150 mm. Turf shoulders are constructed by bringing the grade up to the pavement edge. Unpaved shoulders are often constructed on compacted natural soil of a California Bearing Ratio (CBR) value at 3 to 4% or higher, but sometimes on lime-stabilized subgrade of a CBR value of 5 to 10%.

1.2 Problem Statement

Many two-lane highways with aggregate or turf shoulders require maintenance on a recurring basis. Rutting and edge drop-offs are the most common performance problems associated with granular shoulders as shown in Figure 1.1 (Mekkawy, White, Jahren, & Suleiman, 2010). The maintenance of an unpaved shoulder is typically done by placing more material and compacting it. This practice is considered temporary and does not address the cause of the problem; therefore, the problem often recurs. There have been a few successful projects using geosynthetics for unpaved shoulder construction to improve shoulder performance (for example, Gantenbein, 2006). To provide a good condition for vegetation and maintain sufficient load carrying capacity, Gantenbein used a soil-aggregate mixture for the unpaved shoulder construction. However, the possible effect of geosynthetics on the soil ecological environment and the effect of soil-aggregate mixture and base course cover combination on the structural performance of unpaved shoulders are not well studied.

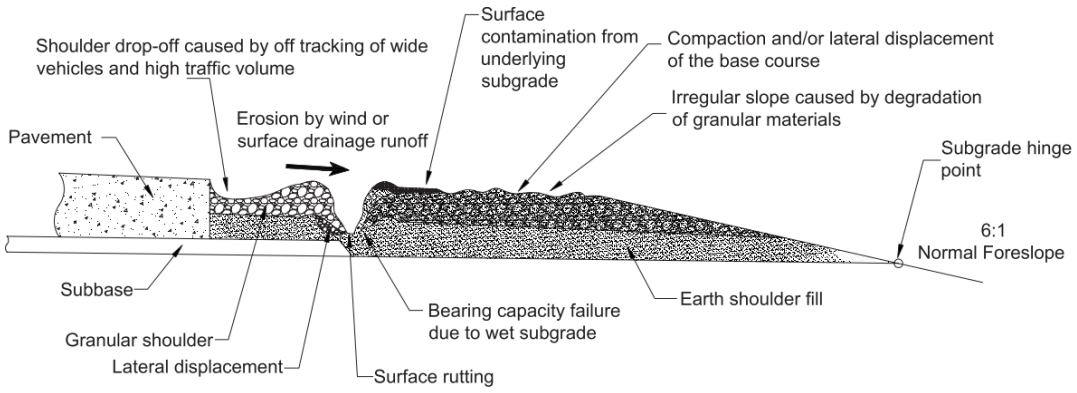

Figure 1.1: Typical Granular Shoulder Performance Problems

Source: Mekkawy et al. (2010)

1.3 Research Objectives

The primary objective of this research was to evaluate geosynthetic-reinforced unpaved shoulders, while the secondary objective was to evaluate geosynthetic-reinforced aggregate shoofly detours. These objectives were achieved by (1) evaluating the effect of geocell or geogrid reinforcements on vegetation and (2) evaluating the base course structural strength improvement provided by the geocell and geogrid reinforcements on moderate and weak subgrade.

1.4 Research Methodology

The possible effect of geocell and geogrid on soil ecological environment was investigated by an outdoor field vegetation test. Geomaterials used in this study included AB-3 aggregate, topsoil, soil mixture containing 50% AB-3 and 50% topsoil, and soil mixture containing 65% AB-3 and 35% topsoil. One control (unreinforced) section and one geosynthetic-reinforced section were constructed in a test section size of 1.5 × 1.5 m each with the following soil and aggregate compositions:

1. 200-mm-thick topsoil (geocell),
2. 200-mm-thick unreinforced 50/50 soil-aggregate mixture (geocell),
3. 50-mm-thick topsoil over 150-mm-thick 50/50 soil-aggregate mixture (geocell),
4. 50-mm-thick aggregate over 150-mm-thick 50/50 soil-aggregate mixture (geocell),
5. 50-mm-thick topsoil over 100-mm-thick aggregate (geogrid),
6. 50-mm-thick topsoil over 100-mm-thick 35/65 soil-aggregate mixture (geogrid),
7. 150-mm-thick 35/65 soil-aggregate mixture (geogrid), and
8. 50-mm-thick topsoil over 100-mm-thick 50/50 soil-aggregate mixture (geogrid).

The effects of geocell and geogrid reinforcements were evaluated by comparing the growth of vegetation on the control and reinforced test sections.

This study also investigated the effectiveness of geocell and geogrid in improving the structural capacity of base courses by comparing the permanent deformations and vertical interface stresses between unreinforced and reinforced test sections.

The effect of geocell reinforcement on unpaved shoulders over moderate subgrade (5% CBR) was studied by conducting large-scale cyclic plate loading tests on the following test sections:

1. 200-mm-thick unreinforced aggregate,
2. 200-mm-thick unreinforced soil-aggregate mixture,
3. 200-mm-thick geocell-reinforced soil-aggregate mixture,
4. 50-mm-thick topsoil over 150-mm-thick geocell-reinforced soil-aggregate mixture,
5. 50-mm-thick aggregate over 150-mm-thick geocell-reinforced soil-aggregate mixture, and
6. 200-mm-thick geocell-reinforced topsoil.

The effect of geogrid reinforcement on unpaved shoulders over weak and moderate subgrade (i.e., 3% and 5% CBR, respectively) was studied by conducting large-scale cyclic plate loading tests on the following test sections:

1. 150-mm-thick unreinforced AB-3 base over 3% CBR subgrade,
2. 150-mm-thick reinforced AB-3 base over 3% CBR subgrade,
3. 150-mm-thick unreinforced AB-3 base over 5% CBR subgrade,
4. 150-mm-thick reinforced AB-3 base over 5% CBR subgrade,
5. 150-mm-thick unreinforced soil-aggregate mixture base over 3% CBR subgrade,
6. 150-mm-thick reinforced soil-aggregate mixture base over 3% CBR subgrade,
7. 150-mm-thick unreinforced soil-aggregate mixture base over 5% CBR subgrade, and
8. 150-mm-thick reinforced soil-aggregate mixture base and 5% CBR subgrade.

1.5 Report Organization

This report consists of six chapters. Chapter 1 introduces unpaved shoulders, problem statements, research objectives, research methodology, and report organization. Chapter 2 presents a literature review of past studies on shoulder vegetation, geocell, and geogrid. Chapter 3 presents the properties of the geomaterials used in this project. Chapter 4 presents the results and discussions of the outdoor vegetation test. Chapter 5 presents the results and discussions of the plate loading tests. Chapter 6 concludes the test results and presents the recommendation based on the test results.

Chapter 2: Literature Review

The literature review presented in this chapter focuses on three topics: (1) past studies on geocell and geogrid reinforced roadways, (2) design methods for geosynthetic reinforced roadways, and (3) functions of shoulder vegetation.

2.1 Past Studies

2.1.1 Geocell Reinforcement

2.1.1.1 Mechanisms

Early studies in the late 1970s investigated the effects of the following factors: (1) geocell geometry, (2) subgrade stiffness, and (3) loading position, as well as identified possible failure modes of geocells (Mitchell, Kao, & Kavazanjian, 1979; Rea & Mitchell, 1978). These studies concluded the optimum ratios of h/d (height to equivalent opening diameter of geocell) was 1.42 to 2.13, and w/d (diameter of loading plate to equivalent opening diameter of geocell) was 1.42. Seven possible failure modes identified in these studies are: (1) geocell penetration into subgrade, (2) cell bursting due to excessive stress from infill material, (3) cell wall buckling due to lack of lateral constraint, (4) bearing capacity failure in subgrade, (5) bending failure in the soil-geocell composite layer, (6) durability failure due to geocell exposure to environment, and (7) excessive rutting.

As demonstrated by Pokharel, Han, Leshchinsky, Parsons, and Halahmi (2010) in Figure 2.1, geocells provide confinement in two ways: (1) the friction between cell wall and soil and (2) the restraint of the infill soil upwards and lateral movement under loading.

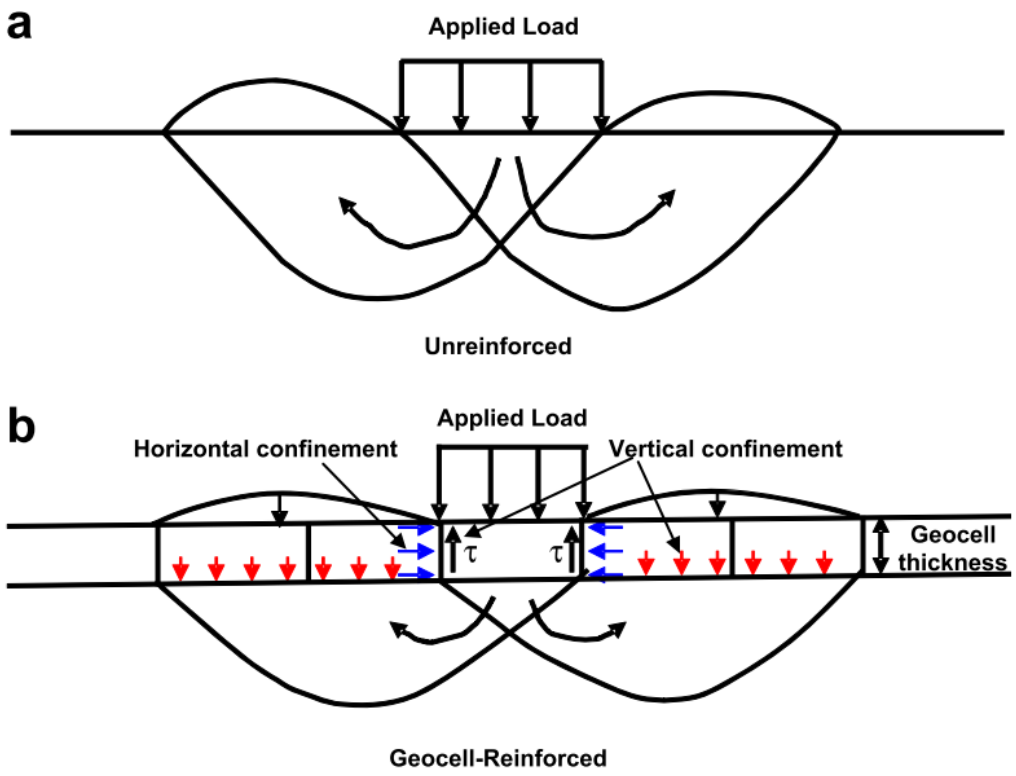

Figure 2.1: Unreinforced and Geocell-Reinforced Soil Behavior
Source: Pokharel et al. (2010)

Bathurst and Karpurapu (1993) conducted a series of large-scale triaxial compression tests and numerical analysis. They proposed that the enhancement of the soil strength from the confinement effect could be expressed in the terms of equivalent cohesion c_r using Equation 2.1 and Figure 2.2. The study by Madhavi Latha, Rajagopal, and Krishnaswamy (2006) verified the equation of the equivalent cohesion.

$$\mathbf{c_r} = \frac{\Delta\boldsymbol{\sigma_3}}{\mathbf{2}}\mathbf{tan}\left(\frac{\boldsymbol{\pi}}{\mathbf{4}} + \frac{\boldsymbol{\varphi}}{\mathbf{2}}\right) \qquad \textbf{Equation 2.1}$$

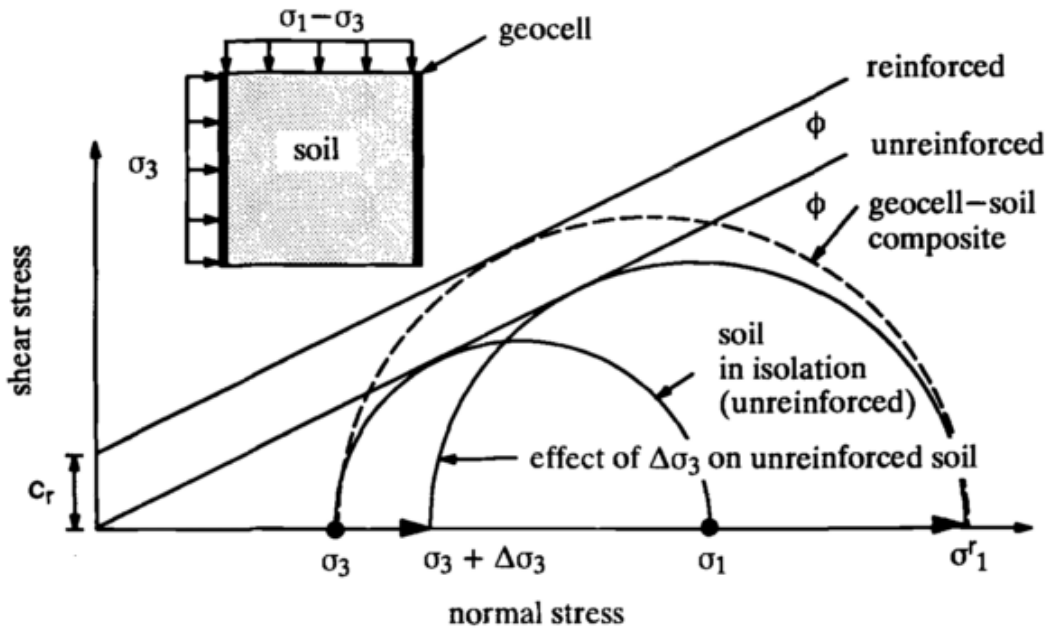

Figure 2.2: Mohr Circle Construction for Estimating Equivalent Cohesion for Geocell-Soil Composites

Source: Bathurst and Karpurapu (1993)

2.1.1.2 Performance Evaluation

The experimental and numerical studies done by Han, Yang, Leshchinsky, and Parsons (2008) showed a 65% increase in the bearing capacity of the sand up to 1.25-mm deformation by geocell reinforcement. Pokharel et al. (2011) showed a 170-mm-thick geocell-reinforced crushed-stone section outperformed a 300-mm-thick crushed-stone section in the accelerated moving-wheel tests. Another accelerated moving-wheel loading test indicated that the inclusion of geocell reinforcement in the 70-mm-thick aggregate (AB-3) base yielded 48-mm rut depth under an 80-kN axle load at 5,000 passes while the unreinforced base at the same thickness could not support one pass (Yang et al., 2012). The experimental studies on the application of geocell with reclaimed asphalt pavement (RAP) material indicated that the inclusion of geocell significantly increased the strength and stiffness of the RAP base, distributed the load to a wider

area, and reduced the permanent deformation under cyclic loading (Thakur, Han, Pokharel, & Parsons, 2012; Thakur, Han, & Parsons, 2013).

2.1.2 Geogrid Reinforcement

2.1.2.1 Mechanisms

Previous studies (Giroud & Noiray, 1981; Perkins & Ismeik, 1997) summarized three potential functions of geosynthetics as: lateral restraint, increased bearing capacity, and tensioned membrane effect. Figure 2.3 shows the primary functions of geogrids in stabilizing unpaved roads.

The confinement of geogrids results in a stiffer base course and a lower dynamic deflection of the pavement/roadbed structure during traffic loading (Giroud & Han, 2004a, 2004b). Geogrid changes the interface condition between weak subgrade and aggregate base. This phenomenon enhances the bearing capacity of the subgrade (Giroud & Noiray, 1981; Giroud & Han, 2004a). When an excessive amount of deformations is accumulated under the applied traffic load, the curved and tensioned reinforcement can develop an upward force to support the load (Giroud & Noiray, 1981; Sharma, Chen, Abu-Farsakh, & Yoon, 2009). In addition to the above mechanisms, the geogrid at the interface between aggregate base and weak subgrade prevents base aggregates from punching into the subgrade and fines in subgrade from migrating into base courses (Tingle & Jersey, 2005). Giroud and Han (2004a) also indicated that the lateral confinement by geogrid reduced the rate of base deterioration.

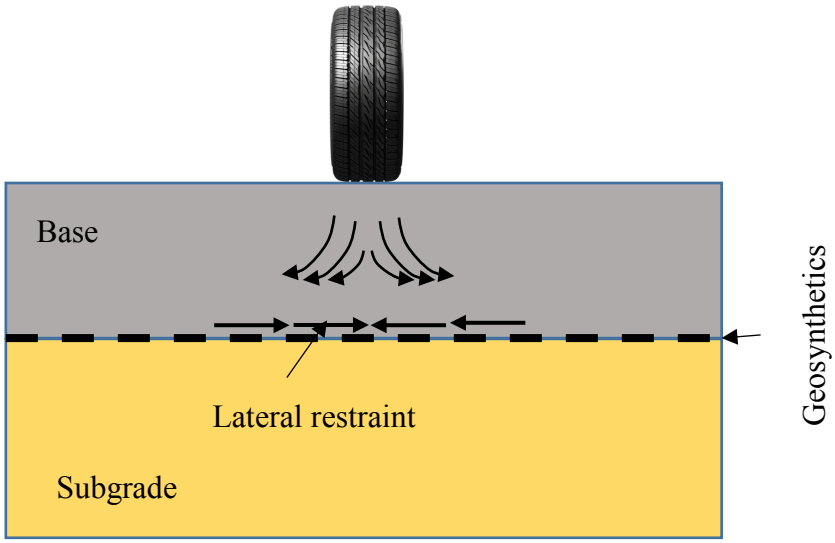

(a)

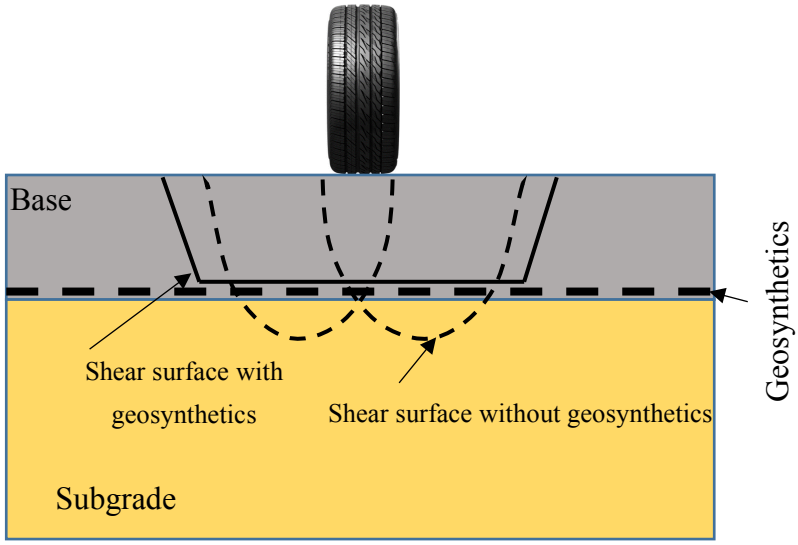

(b)

Figure 2.3: Mechanisms of Geosynthetics in Stabilizing Paved/Unpaved Roads

Source: Giroud and Noiray (1981); Perkins and Ismeik (1997)

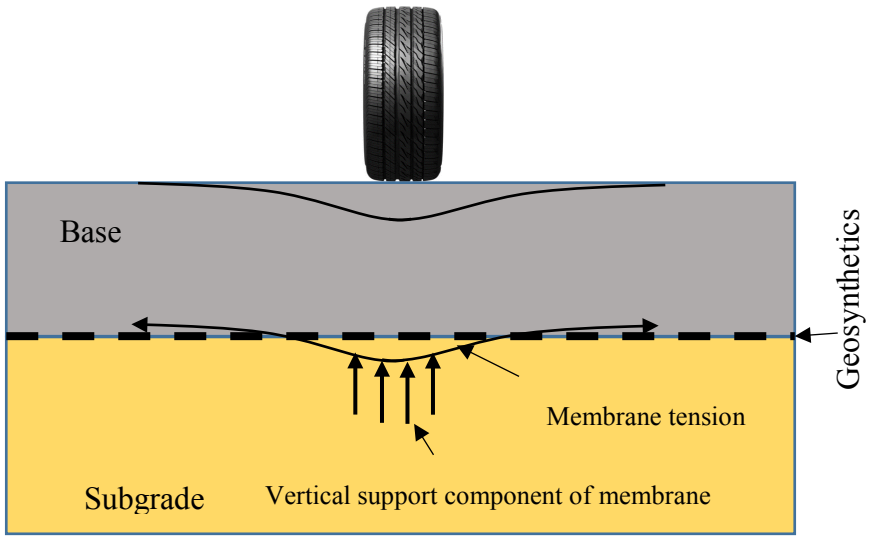

(c)

Figure 2.3: Mechanisms of Geosynthetics in Stabilizing Paved/Unpaved Roads (Continued)

Source: Giroud and Noiray (1981); Perkins and Ismeik (1997)

2.1.2.2 Performance Evaluation

Haas, Walls, and Carroll (1988) performed cyclic plate load tests in a 4.5 × 1.8 × 0.9 m box to investigate the performance of geogrid-reinforced roads. The base course thickness, subgrade strength, and location of geogrid were set as variables in this study. The surface deflection, the vertical stress on the top of subgrade, and the strains in the geogrid were monitored during the tests. The test results indicated that geogrid reinforcement increased the number of load cycles as compared with the unreinforced test sections. Al-Qadi, Brandon, Valentine, Lacina, and Smith (1994) simulated a typical secondary road in Virginia constructed in a box with the dimensions of 3 × 2.1 × 1.8 m under cyclic loading applied through a steel plate with a diameter of 0.305 m. The surface deflections of road sections were monitored by LVDTs. Test results revealed that geogrid considerably reduced the deflections of the pavement sections over weak subgrade. Perkins (1999) performed plate load tests on the road sections constructed in a 2 × 2 × 1.5 m high box. A 40-kN cyclic load was applied on the test sections to simulate traffic loading through a 0.305 m diameter steel plate. Various instruments were used to monitor

the surface deformations, strains of geosynthetics, and stresses in the soils. The test results revealed that the geogrid improved the performance of road sections with a subgrade CBR of 1.5% significantly. However, little improvement was observed for the sections with a subgrade CBR of 20%. Leng and Gabr (2002) conducted cyclic plate load tests on the geogrid-reinforced aggregate over weak subgrade in a 1.5 × 1.5 × 1.35 m high box. The cyclic load was applied through a steel plate with a diameter of 0.305 m and the contact pressure was set at 500 kPa. During the tests, surface deformations and vertical stresses at the interface were measured. The test results showed that geogrid reduced the surface deflection, improved the stress distribution, and mitigated the degradation of the aggregate base.

Tingle and Jersey (2005, 2009) evaluated the performance of geogrid-reinforced aggregate roads in a full-scale model test in terms of the surface deflections, subgrade deflections, and vertical stresses on the top of subgrade, and found both the vertical deflection and vertical stress were reduced by geosynthetics. Chen, Abu-Farsakh, and Tao (2009) also studied the influence of the geogrid-stabilized pavements on subgrade deformation. The tests were conducted inside a test box with dimensions of 2.0 × 2.0 × 1.7 m^3 and a 40-kN cyclic load at a frequency of 0.77 Hz was applied on the test sections through a 0.305 m diameter steel plate. The test results showed that the mechanically stabilized base course distributed the applied load to a wider area than the unstabilized control sections and reduced the permanent deformation of the subgrade. Indraratna, Hussaini, and Vinod (2013) studied the lateral displacement response of geogrid-reinforced ballast under cyclic loading in a smaller 0.8 × 0.6 × 0.65 m^3 box. In this study, one side-wall was replaced by a setup of five independent movable plates along the depth to measure the lateral displacement. The test results revealed that both the vertical and lateral deformations were influenced by the geogrid type and its placement location. The test results also demonstrated the ability of geogrid in arresting lateral displacement of ballast and reducing vertical settlement.

The resilient behavior of the geosynthetic-stabilized bases has not been well understood yet. Previous research shows some inconsistencies. Rahman, Arulrajah, Piratheepan, Bo, and Imteaz (2014) investigated the resilient moduli and permanent deformation characteristics of construction and demolition (C&D) materials stabilized with biaxial and triaxial geogrids.

Repeated load triaxial (RLT) equipment was used to determine resilient modulus of the mechanically stabilized C&D specimens. The resilient modulus values of the geogrid-stabilized C&D materials were found to be higher than that of the respective unreinforced material. The permanent deformations of the geogrid-stabilized C&D materials were smaller than that of the respective unstabilized material. Abu-Farsakh, Nazzal, and Mohammad (2007) performed a series of laboratory triaxial tests and evaluated the effects of the geogrid properties, location, and number of layers on the resilient and permanent deformations of these samples under cyclic load. The test results demonstrated that neither the geogrid type nor the geogrid arrangement had a significant effect on the resilient strain values. Yang and Han (2013) proposed an analytical model to predict the resilient modulus and the permanent deformation of geosynthetic-stabilized unbound granular materials under an RLT test. Both the test and the analytical results showed that the permanent strains of the geosynthetic stabilized samples were reduced significantly even though the resilient moduli of the samples were slightly increased.

Qian, Han, Pokharel, and Parsons (2011) investigated the triangular-aperture geogrid-stabilized base courses over weak subgrade using cyclic plate load tests. The results showed that the vertical stresses at the interface between the base and the subgrade increased with the increase of the number of load cycles due to the deterioration of the base course and the inclusion of the geogrids reduced the rate of the deterioration.

2.2 Design Methods for Geosynthetic-Reinforced Unpaved Roads

Giroud and Noiray (1981) developed a design method considering the tensioned membrane effect of a geotextile based on both empirical formula and theoretical analysis. Two beneficial effects identified in the study are: (1) confinement of the subgrade soil between and beyond the wheels areas and (2) reduction of the pressure applied by the wheels on the subgrade soil.

Giroud and Han (2004a, 2004b) developed a design method for geogrid-reinforced unpaved roads. In their design method, the thickness of the geogrid-reinforced base course h is given in Equation 2.2:

$$\mathbf{h} = \frac{\mathbf{1+klogN}}{tan\alpha_0[\mathbf{1+0.204}(R_E-\mathbf{1})]} \times \left\{ \sqrt{\frac{P}{\pi r^2\left(\frac{s}{f_s}\right)\left\{\mathbf{1}-\xi\exp\left[-\omega\left(\frac{r}{h}\right)^n\right]\right\}N_c c_u}} - \mathbf{1} \right\} r \quad \textbf{Equation 2.2}$$

Where:

k = constant depending on base course thickness and reinforcement

N = number passes

α_0 = reference stress distribution angle in degree

R_E = modulus ratio of base course to subgrade

r = radius of tire contact area in meter

s = allowable rut depth in millimeter

f_s = failure rut depth (typically 75 mm)

P = wheel load in kN

N_c = bearing capacity factor

c_u = undrained shear strength of subgrade soil in kPa

ξ, ω, and n are constants.

This equation considers the following parameters: magnitude of traffic loading, geometry of unpaved road structure, rut depth, properties of base course and subgrade, properties of geogrid, and serviceability.

Pokharel (2010) calibrated the constant k in Equation 2.2 for geocell-reinforced unpaved roads using laboratory large-scale cyclic plate loading tests and accelerated moving-wheel test data.

2.3 Function of Shoulder Vegetation

The above review was focused on the use of geocell or geogrid for unpaved roads. The research results and design methods for geosynthetic-reinforced unpaved roads should be applicable to unpaved shoulders in terms of their structural capacities. Geocells have been proven to reduce rutting on unpaved shoulders effectively in limited tests and projects (for

example, Gantenbein, 2006). However, no study has been reported on the geosynthetic impact on vegetation. Many studies showed that vegetation can effectively reduce the wind speed on the ground surface; thus, shoulder vegetation presents two main benefits: (1) reduction of dust emission, and (2) erosion control (Udo & Takewaka, 2007; Munson, Belnap, Okin, & Schlesinger, 2011).

Chow et al. (1992) pointed out agricultural vehicle movements along unpaved roads and along unpaved shoulders are believed to be one of the main contributors to PM_{10} (particles with a diameter of 10 micrometer or less suspended in air). Moosmüller et al. (1998) concluded that large turbulence events resulted in significant dust entrainment. Such events were caused by vehicles with a large size or poor aerodynamics traveling at high speeds (80 to 104 km/hr). Van de Ven, Fryrear, and Spaan (1989) conducted wind tunnel simulation and found even sparsely standing vegetation can significantly reduce soil loss. Udo & Takewaka (2007) found the complex interaction among the turbulence, the mean wind velocity field, and the vibration of the leaves reduce the sand-transport rate considerably. Munson et al. (2011) conducted long-term monitoring of climate and vegetation in national parks. Their study indicated a decline in the dominant vegetation cover due to increased temperature leading to exponential increase in wind erosion. Leenders, van Boxel, and Sterk (2007) showed that shrubs have the ability to reduce the wind speed and its low hanging branches can trap sediment.

Chapter 3: Materials and Properties

This chapter presents the materials used in the following tests to investigate the performance of geosynthetic-reinforced unpaved shoulders through: (1) cyclic plate loading tests and (2) outdoor vegetation tests. The materials include AB-3 aggregate, topsoil, soil-aggregate mixture, fine-grained soil subgrade, geocell, geogrid, and seeds. The properties of these materials were also determined in this study.

3.1 AB-3 Aggregate

AB-3 aggregate is commonly used in Kansas as a coarse material in road construction. The grain size distribution is shown in Figure 3.1. The compaction curve was obtained based on ASTM D1557 (2012) modified Proctor tests as shown in Figure 3.2. The well-graded aggregate contained approximately 10% fines. The optimum moisture content of this aggregate was approximately 11.5% and its corresponding maximum dry density was 2,050 kg/m^3.

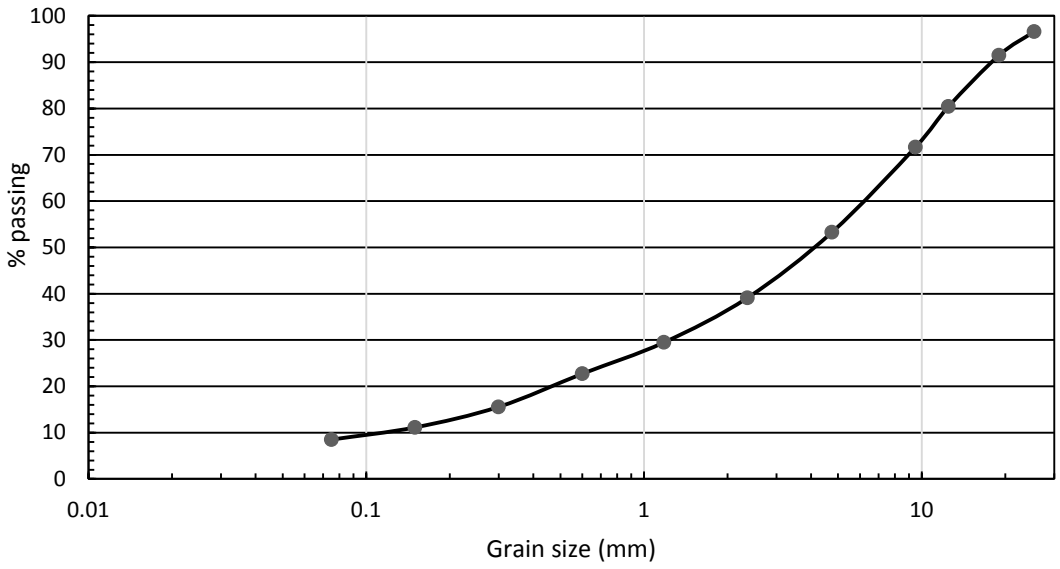

Figure 3.1: Grain Size Distribution of the AB-3 Aggregate

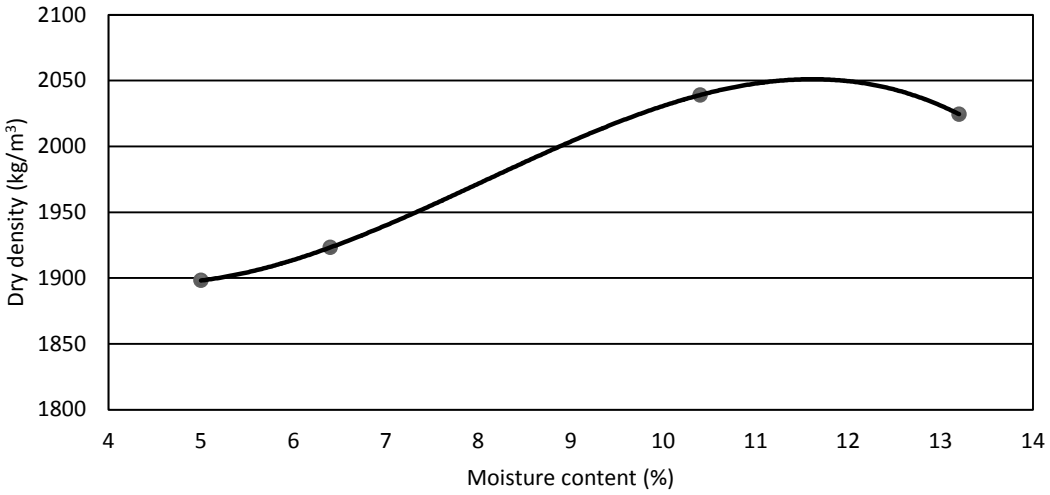

Figure 3.2: Modified Proctor Compaction Curve of the AB-3 Aggregate

3.2 Topsoil

The topsoil was obtained from the outdoor vegetation test area on the University of Kansas West Campus. The native grass was removed prior to the excavation to avoid contamination as shown in Figure 3.3.

Figure 3.3: Topsoil Source Area

The topsoil is classified as organic silt, which appears black in color with traces of light brown. The plastic limit of the topsoil was 34 and the plasticity index was 15. The organic content of soil was 19% following ASTM D2974 (2014). The modified Proctor compaction

curve of the topsoil is shown in Figure 3.4. The compaction curve indicates the optimum moisture content of the topsoil was approximately 21% and the maximum dry density was approximately 1,570 kg/m^3.

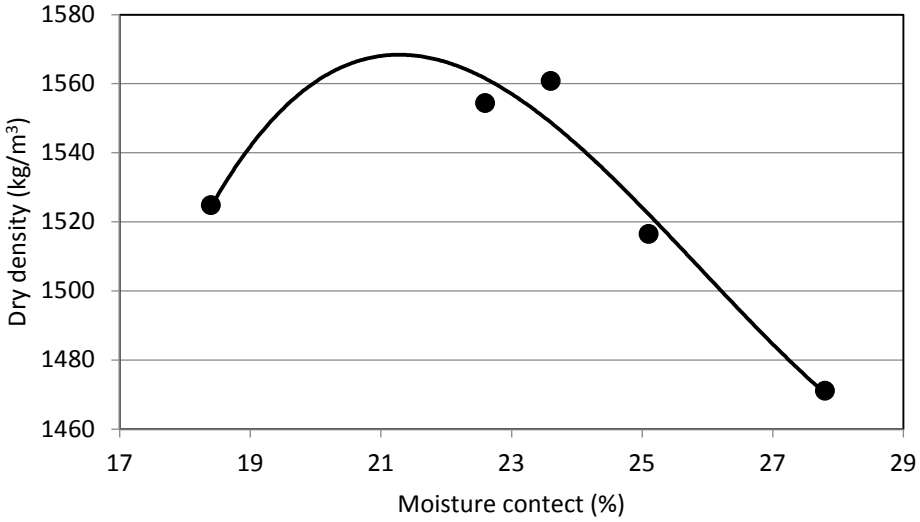

Figure 3.4: Modified Proctor Compaction Curve of Topsoil

3.3 Soil-Aggregate Mixture

The first soil-aggregate mixture consisted of 50% AB-3 aggregate and 50% topsoil by dry weight. This material is referred to as the 50/50 mixture in the current and following chapters. The modified Proctor compaction curves of the mixture are shown in Figure 3.5. The compaction curve indicates the optimum moisture content was approximately 15% and the maximum dry density was approximately 1,830 kg/m^3.

The second soil-aggregate mixture consisted of 65% AB-3 aggregate and 35% topsoil by dry weight. This material is referred to as the 65/35 mixture in the current and following chapters. The modified Proctor compaction curve of the mixture is shown in Figure 3.6. The compaction curve indicates the optimum moisture content was approximately 12% and the maximum dry density was approximately 1,915 kg/m^3.

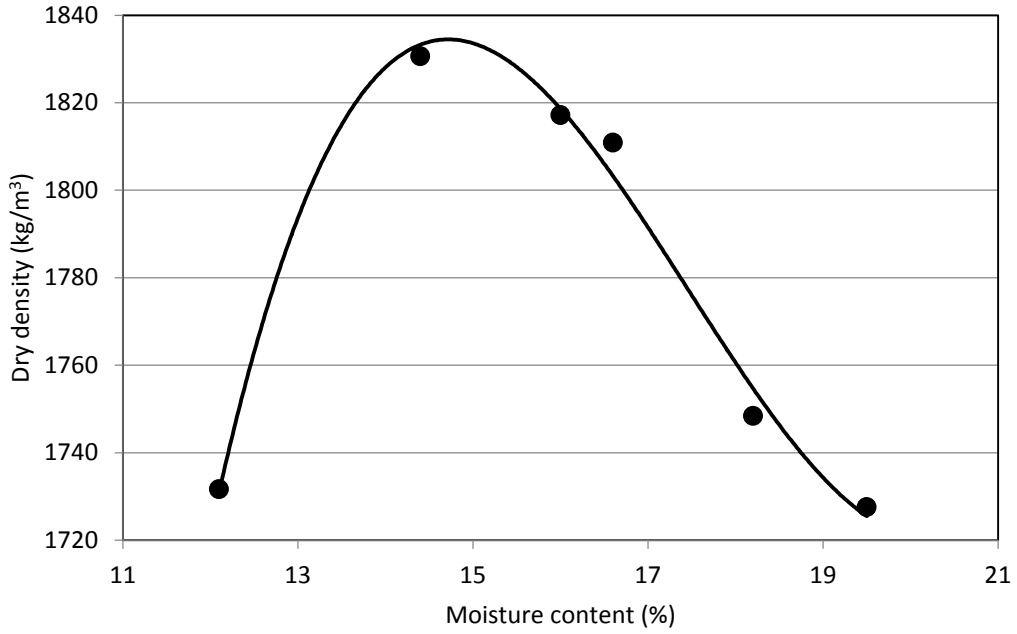

Figure 3.5: Modified Proctor Compaction Curve of 50/50 Soil-Aggregate Mixture

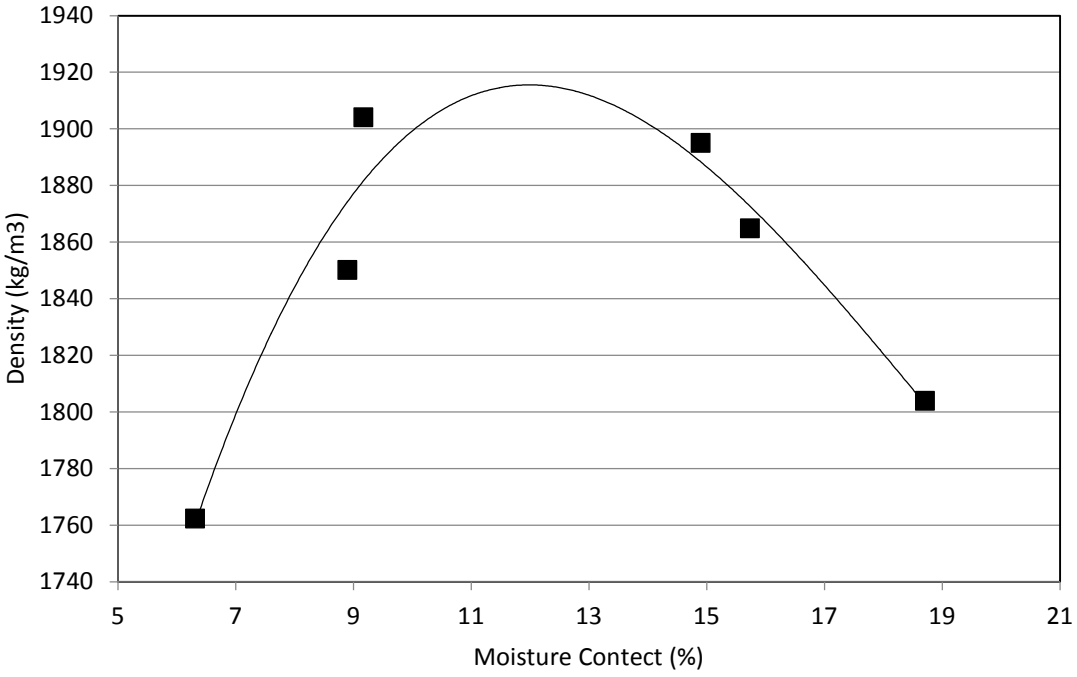

Figure 3.6: Modified Proctor Compaction Curve of 65/35 Soil-Aggregate Mixture

3.4 Subgrade

Two types of subgrade soil were used in this study. The subgrade soil for the cyclic plate loading tests was a mixture of 25% kaolin and 75% Kansas River sand (by dry weight). Previous tests by Pokharel (2010) on this subgrade soil showed that the maximum dry density was 2,010 kg/m^3 at 10.8% moisture content by the standard Proctor method. In the field vegetation test, the topsoil was used as the subgrade.

3.5 Geocell

Presto Geosystems supplied the geocells used for this study. The geocell is made of polyethylene with a density of 0.935-0.965 g/cm^3. The height of the cell was 150 mm. The cell seam strength of this geocell was 2,130 N. Figure 3.7 presents the detailed schematic of the geocell including holes on the cell wall.

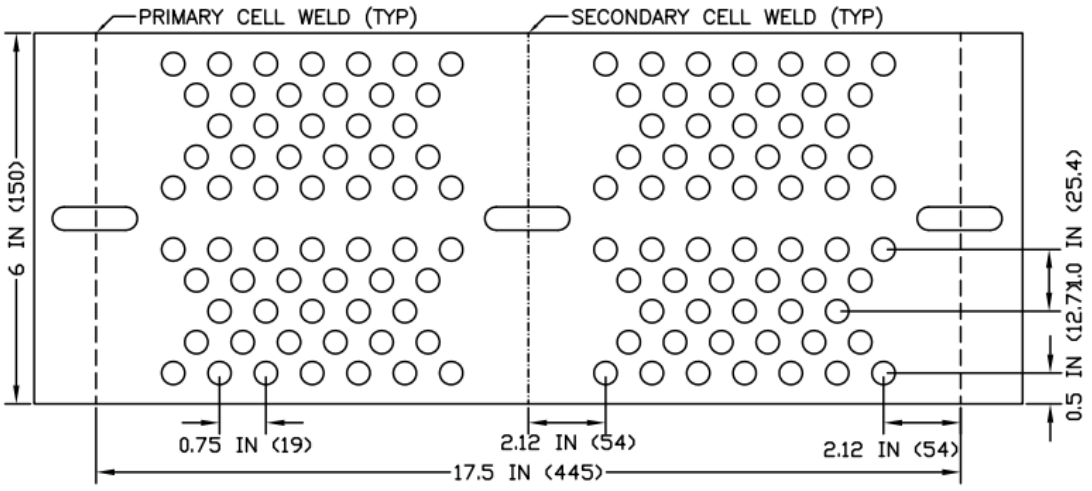

Figure 3.7: Geocell Dimension and Hole Pattern

Source: Presto Geosystems (2011)

3.6 Geogrid

The geogrid used in this study was a triaxial geogrid provided by Tensar International as shown in Figure 3.8. The geogrid is made of polypropylene. The radial stiffness of the geogrid was 270 kN/m at 0.5% strain. The rib pitches, both longitudinal and diagonal, were 40 mm.

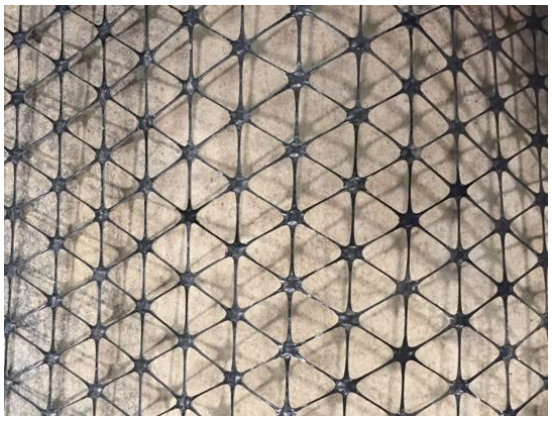

Figure 3.8: Picture of Triaxial Geogrid

3.7 Seeds

The seed mixture for the vegetation test followed the standard by KDOT (2013) as shown in Table 3.1.

Table 3.1 shows that two primary species are perennial ryegrass and tall fescue. According to the U.S. Department of Agriculture (USDA), perennial ryegrass cannot survive severe weathers, such as heat and dry in the summer and low temperatures in the winter (USDA Natural Resources Conservation Service Plant Materials Program, 2002a). Tall fescue is more robust than perennial ryegrass and can survive for a long time period under different weather conditions. Tall fescue's roots can reach a deeper depth as compared with perennial ryegrass. Tall fescue grass also tends to grow on soil surfaces with large clumps (Gibson & Newman, 2001). Dunnett, Willis, Hunt, and Grime (1998) indicated that tall fescue often becomes a locally dominant species. For decades, Kentucky-31 type of tall fescue has been planted widely for forage and erosion control due to its easy establishment and long life cycle under harsh conditions and tolerance to mistreatment (Henson, 2001). Raeside, Friend, Behrendt, Lawson, and Clark (2012) concluded that tall fescue is more tolerable to heat and more responsive to precipitation in the summer, and has deeper roots than perennial ryegrass.

For both species, the seeding rates (weight of seed per m^2) recommended by KDOT for permanent seed mixes are significantly higher than those recommended by the USDA (USDA Natural Resources Conservation Service Plant Materials Program, 2002a, 2002b).

Table 3.1: Seed Mixture

Species Name	Amount
	g/m^2
Fertilizer (12-12-12)	23.15
Blue Grama Grass Seed (Lovington)	0.04
Buffalograss Seed (Treated)	0.53
Perennial Ryegrass	5.2
Prairie Junegrass	0.31
Side Oats Grama Grass Seed (El Reno)	0.71
Tall Fescue (Endophyte Free)	5.2
Western Wheatgrass Seed (Barton)	0.71

Chapter 4: Outdoor Vegetation Test

The goal of the outdoor field vegetation test was to investigate possible effect of the following two factors on vegetation growth: (1) base course composition and (2) geosynthetics reinforcement. The test was continued for a period of 13 months. To minimize interference, human activities were restricted as much as possible and the nearby trees were taken down. The test sections were not mowed over the test period. The grass leaf blade length, root length, and vegetation density were measured as the indicators of vegetation growth. Biomasses were collected at the end of the test. Soil volumetric moisture contents were monitored during the test.

4.1 Test Setup and Preparation

The outdoor vegetation test was conducted on the University of Kansas West Campus. The location of the test site is noted with a white box in Figure 4.1.

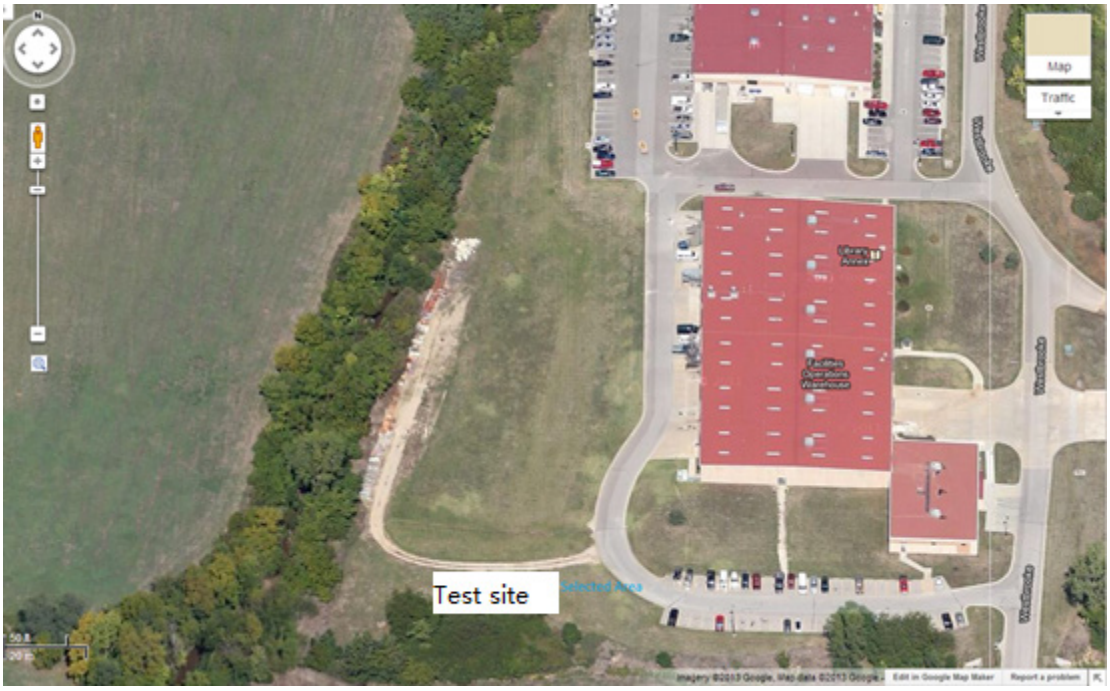

Figure 4.1: Location of the Test Site

Source: Google Maps (2015)

A total of 16 test sections were constructed in this study, which are divided into eight groups (numbered from 1 to 8). Four groups were designated for the investigation on geocell and the other four groups were designated for the investigation on geogrid. The base combinations of sections are listed in Table 4.1. Each test section size was 1.5 × 1.5 m. Two sections in each group were constructed with identical base course and soil cover materials at identical thickness and received the same amount of seeds. Each group consisted of a control (unreinforced) section (noted with C followed by the group number), in which no geosynthetic reinforcement was installed, and a reinforced section (noted with R followed by the group number) was installed with the geocell or geogrid. All the groups were arranged in a line with all control sections placed on the north side and the reinforced sections on the south side. Each test section was constructed with a transverse slope to simulate the slope of the shoulder. According to the KDOT (2014) Road Design Manual, a 1.6% slope was used for both the subgrade and the base course and a 4.2% slope was used for the top surface. A longitudinal slope along the centerline of the groups was created in place to provide drainage of each section. The group arrangement and the cross section of each group are shown in Figure 4.2.

Table 4.1: List of Base Course Combinations

Base Course Combination	Section Label		Geosynthetic
	Control	Reinforce	
200-mm topsoil	1C	1R	Geocell
200-mm 50/50 mixture	2C	2R	Geocell
50-mm topsoil over 150-mm 50/50 mixture	3C	3R	Geocell
50-mm AB-3 over 150-mm 50/50 mixture	4C	4R	Geocell
50-mm topsoil over 100-mm AB-3	5C	5R	Geogrid
50-mm topsoil over 100-mm 65/35 mixture	6C	6R	Geogrid
150-mm 65/35 mixture	7C	7R	Geogrid
50-mm topsoil over 100-mm 50/50 mixture	8C	8R	Geogrid

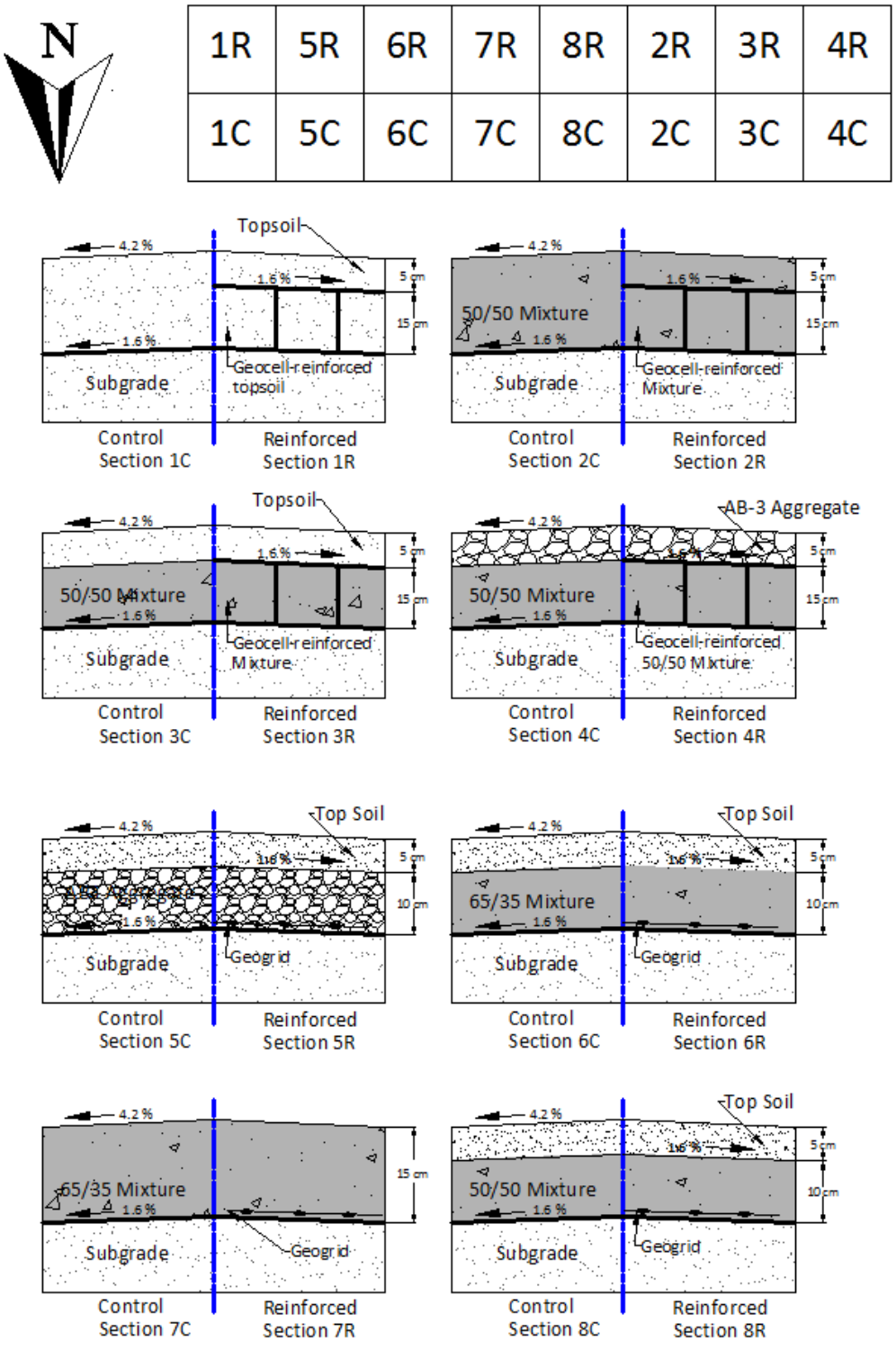

Figure 4.2: Test Section Arrangement and Cross Sections

Native grass was trimmed off in a 4 × 10 m area. Then a 3.5 × 10 m test area was excavated to a depth of 170 mm, as shown in Figure 4.3.

Figure 4.3: Area for the Vegetation Test

After the excavation, leveling equipment and a compactor were brought in to create the desirable depth and slope of the subgrade. In order to maintain the desired size and depth of each section and minimize the influence by adjacent sections, plywood frames were assembled on the site, as shown in Figure 4.4 (a). Instead of setting the plywood frames directly on the subgrade, they were elevated with small pieces of wood block leaving a gap of approximately 50 mm between the frames and the subgrade to allow the drainage of water and prevent excessive water trapped in each test section. According to the KDOT (2014) Road Design Manual, a 1.6% slope was constructed on the native soil shown in Figure 4.4 (b).

To provide a drainage condition similar to that for actual unpaved shoulders, a 20-mm-thick layer of geotextile-wrapped ballast (not shown in figure) was placed between the fill material and the plywood board along each side allowing water flow to the drainage trench. The drainage trench then led water to a water storing hole (not shown) at the far end in Figure 4.5.

(a) Plywood frame

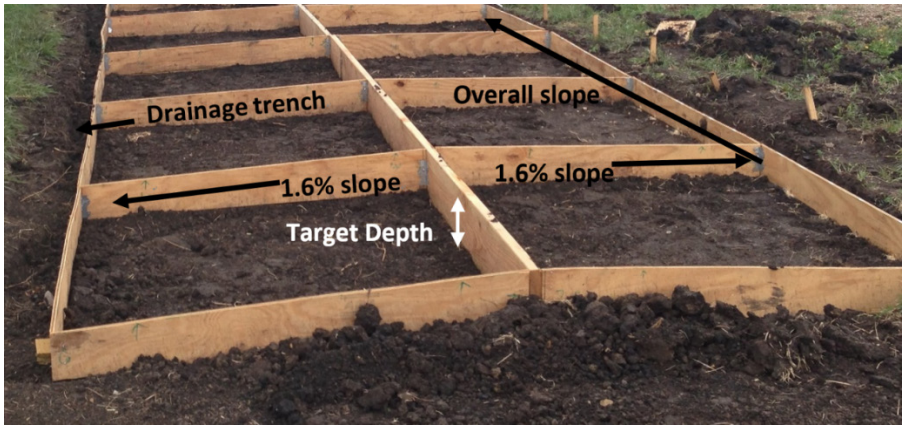

(b) Slopes of sections

Figure 4.4: Test Sections with Plywood Frame and Slopes

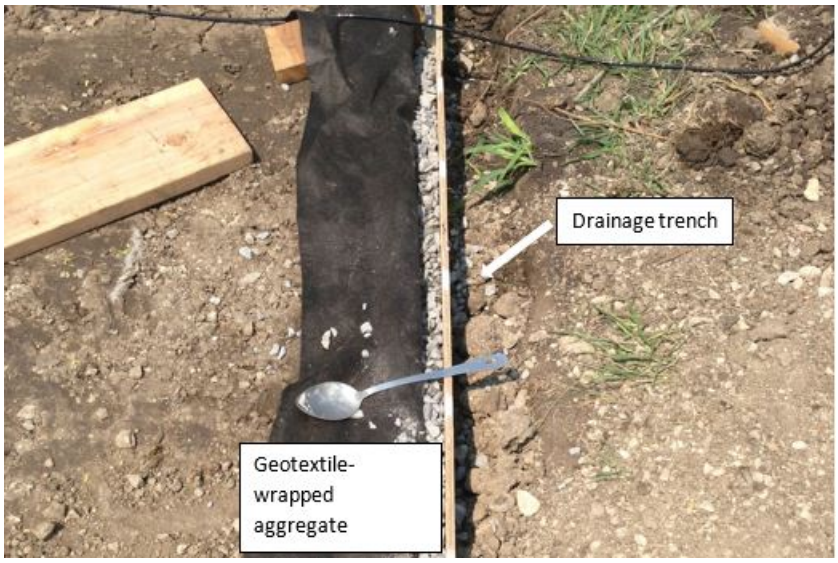

Figure 4.5: Drainage System

During the backfill, a diesel vibratory compactor was used to compact the soil to approximately 90% relative compaction based on the maximum dry density determined by the modified Proctor method. To achieve 90% compaction, the materials were compacted in three to four layers. The degree of compaction in each section was verified with sand cone tests. Sand cone tests showed the degrees of relative compaction for all sections ranged from 87.2% to 90.5%. Figure 4.6 (a) shows the placement of geocell while Figure 4.6 (b) shows the placement of geogrid.

(a) Geocell

(b) Geogrid

Figure 4.6: Placement of Geocell and Geogrid

Two types of moisture sensors produced by Campbell Scientific, CS-655 and CS-616L, were installed horizontally at a depth of 75 mm below the surface in the center of each test section. The CS-655 sensors had a rod length of 120 mm and were capable of measuring both temperature and volumetric water content. The CS-655 sensors were installed in test sections 1C, 1R, 2R, 4R, 6R, and 7C. The CS-616L sensors had a rod length of 300 mm and could only measure water content. The CS-616L sensors were installed in all other sections. The volumetric moisture sensors could only detect water in a liquid form, thus the data collected in the winter was not representative. The CS-616L sensor installed in section 3R could not fit in a single geocell pocket, thus the sensor was placed in two pockets with rods through the opening of the geocell wall, as shown in Figure 4.7 (a). The sensors were connected to a data logger, as shown in Figure 4.7 (b), and the volumetric water contents were recorded every hour.

Preparation for seeding started after all sections were filled and compacted to the desired thickness. For each section to receive an equal amount of seeds of each species, seeds were weighted and mixed for each section separately. The amount of seed needed for each vegetation species was first calculated accurately to 100^{th} of a gram based on the area of one test section, as shown in Table 4.2. The seeds of different vegetation species weighed with a high precision scale (accurate to 100^{th} of a gram) based on the calculation were then mixed and kept in individual containers.

The surface of each section was gently loosened so that the seeds would not be directly exposed to sunlight. Then the test sections were watered for the equal amount of time prior to spreading seeds to provide the water that the seeds needed in the planting process. Then seeds were spread evenly on each section by hand. At the end, a thin layer of red mulch was placed over all the sections to further protect the seeds from overheating and to maintain moisture. Figure 4.8 shows the section after sowing.

(a) CS-616L in Section 3C

(b) Data logger

Figure 4.7: Sensors and Data Logger for Volumetric Moisture Content Measurements

Table 4.2: Amount of Seed for One Section

Item	Amount (g/section)
Fertilizer (12-12-12)	10.41
Blue Grama Grass Seed (Lovington)	0.03
Buffalograss Seed (Treated)	0.23
Perennial Ryegrass	2.34
Prairie Junegrass	0.14
Side Oats Grama Grass Seed (El Reno)	0.33
Tall Fescue (Endophyte Free)	2.34
Western Wheatgrass Seed (Barton)	0.31

Figure 4.8: Sections After Sowing

4.2 Results and Discussion

4.2.1 Weather Records

Based on the field observations and recorded data, the vegetation growth can be divided into three periods or stages. The first period started from the initial establishment in the fall of 2013, and ranged from Day 0 (i.e., the sowing day, August 2nd, 2013) to Day 89 (i.e., mostly during the fall season). During this period, the average daily temperature gradually decreased with the highest temperature of 20^{o}C and lowest temperature of 6^{o}C while a few major rainfalls were recorded. The average temperature during this period was 13.3^{o}C and the accumulated precipitation was 295.5 mm according to the National Climatic Data Center record. The second period was the dormancy stage, ranging from Day 90 to Day 220 (i.e., mostly during the winter season). During this period, a portion of the vegetation died and vegetation growth was seized. Temperature fluctuated largely during this period with the highest temperature of 18^{o}C and the lowest temperature of -18^{o}C. The average temperature in this period was 0^{o}C and 83 mm precipitation was accumulated in the forms of rainfall and snow. The third time period was mostly within the spring and summer seasons of 2014, i.e., from Day 221 to Day 360. During this period, the temperature increased with an average temperature of 16^{o}C and the vegetation recovered and grew again. Some heavy rainfalls were recorded between Day 300 and Day 330 and the accumulated precipitation during this period was 431 mm. The weather data records obtained from the National Climatic Data Center between Day 0 and Day 400 are plotted in Figure 4.9, in which the average daily temperature is presented.

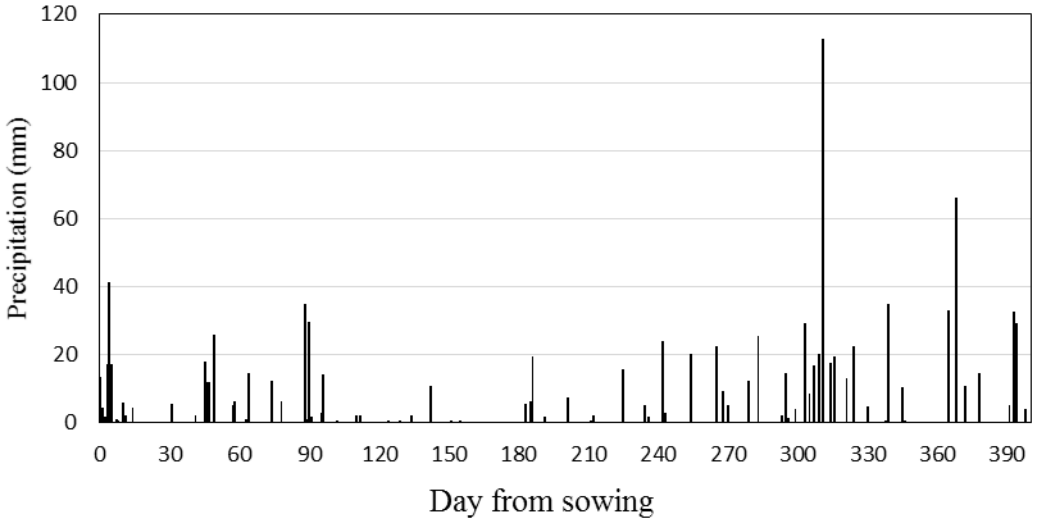

(a) Precipitation

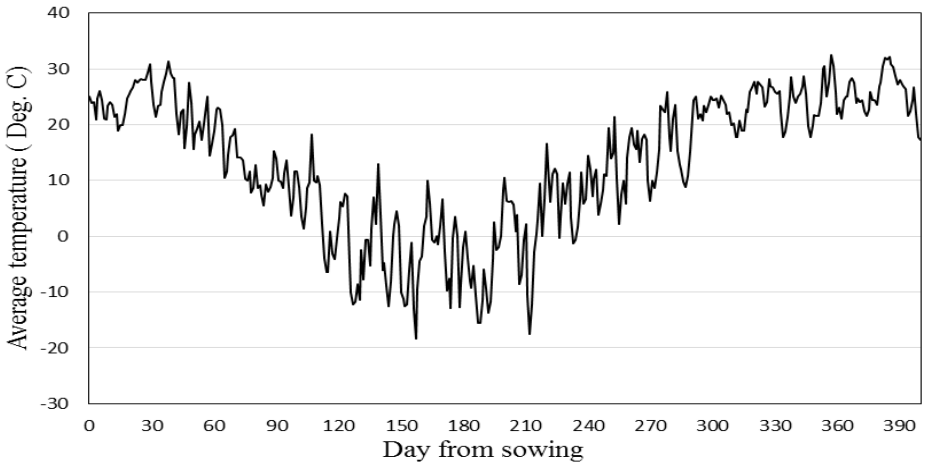

(b) Average daily temperature

Figure 4.9: Daily Weather Record

The average soil temperature measured by six CS-655 sensors was averaged and the soil temperatures at 5:00 and 15:00 were plotted with the air temperature in Figure 4.10. The soil temperature showed a similar overall trend to the air temperature. However the soil temperatures fluctuated less than the air temperature. In the winter, the soil temperatures were kept around 0^{o}C possibly due to the freeze and thaw of water in soil. In the spring, the summer, and the fall, the soil temperatures at 15:00 were higher than those at 5:00.

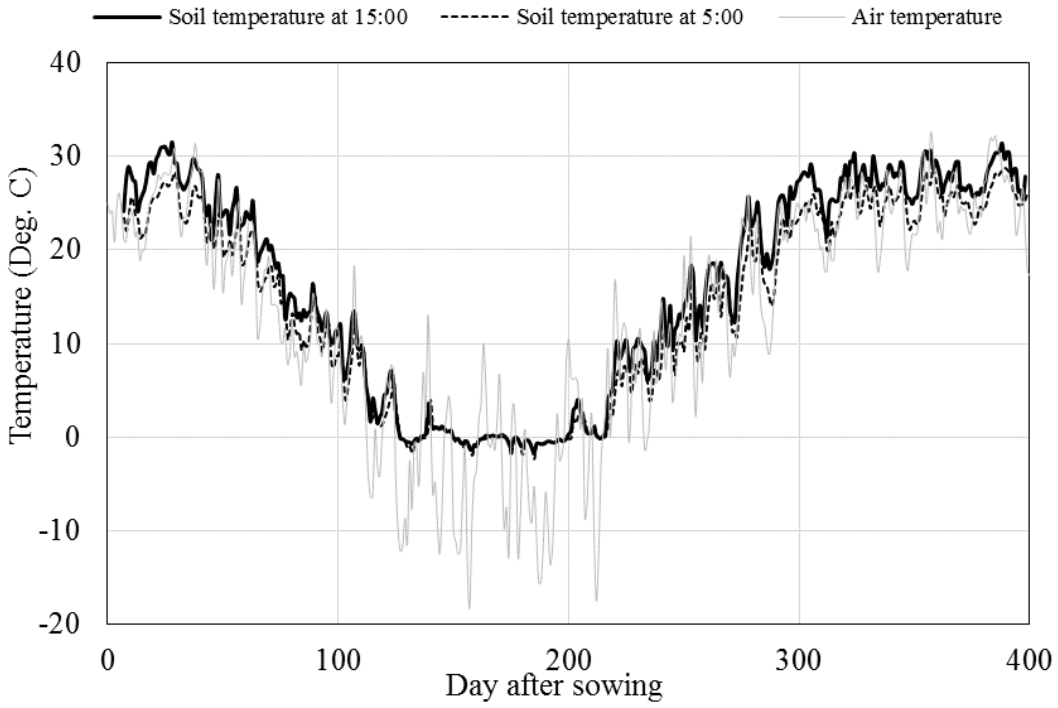

Figure 4.10: Soil and Air Temperatures

4.2.2 Soil Volumetric Moisture Content

Figure 4.11 presents the soil volumetric moisture content comparisons between the control and reinforced sections in all groups. Water contents for Groups 1, 4, 6, and 8 were close to each other throughout the entire test period. In Group 2, the control section presented significantly higher water content than the reinforced section at the beginning. The difference in the water content gradually decreased in the first 90 days. Between Day 250 and Day 400, the control section showed approximately 6% more volumetric water content than the reinforced section. In Group 3, the reinforced section showed higher water content than the control section throughout the entire test. The difference between two sections gradually decreased. The difference between control and reinforced sections was most likely caused by the placement of the water content sensor in Section 3R. In Group 4, the control section showed higher water content in the first 50 days than the reinforced section. Both sections showed the similar amount of water content in the period between Day 220 and Day 400. In Group 5, the volumetric moisture content in the control section was constantly lower than that of the reinforced section

significantly. The most plausible explanation is the sensor in the control section was installed in the aggregate and was damaged during compaction. Excavation after the vegetation test revealed the steel rod on the sensor was bent. Thus the control section volumetric moisture content was not plotted. In Group 7, the reinforced section presented significantly higher water content than the control section at the beginning. The difference in the water content gradually decreased in the first 90 days. Between Day 250 and Day 400, the control section showed approximately 4% less volumetric water content than the reinforced section. The measured volumetric water contents in all the sections showed a similar trend with precipitation. The volumetric water content decreased in dry days and increased sharply after heavy rain. For example, volumetric moisture content data of all sections reached peaks on Day 339 and Day 369. High precipitations were recorded on both days based on the weather data. Based on the volumetric moisture content comparisons between the control and reinforced sections in most groups, it is suggested that although there was slight difference, the control and reinforced section showed similar moisture content over the test period. Thus, no definitive evidence of geosynthetic altering the soil moisture content was found.

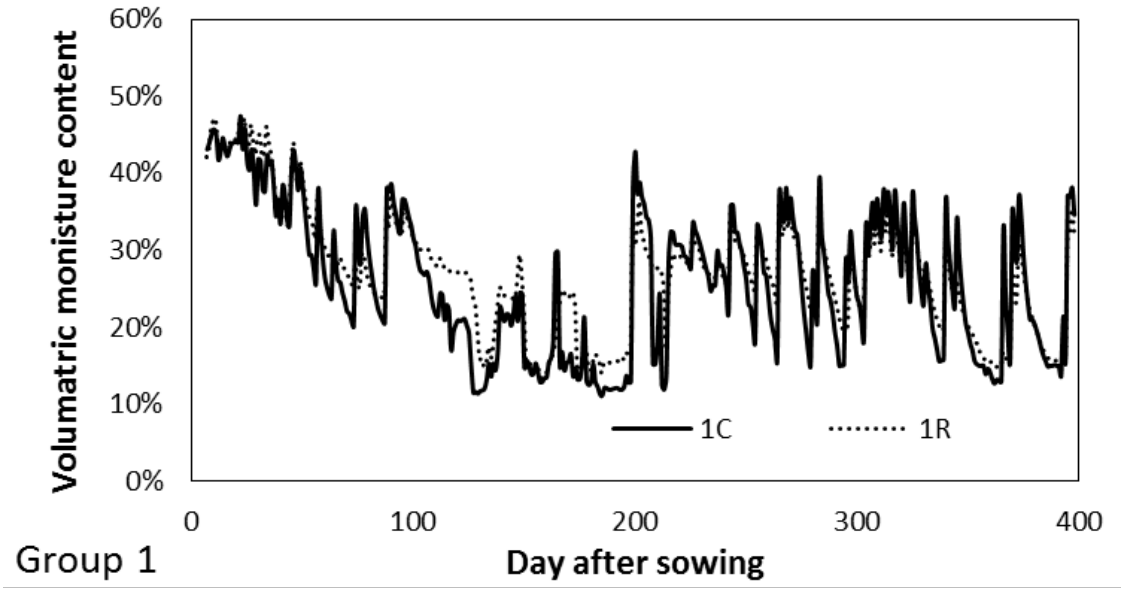

(a)

Figure 4.11: Volumetric Moisture Content Comparisons

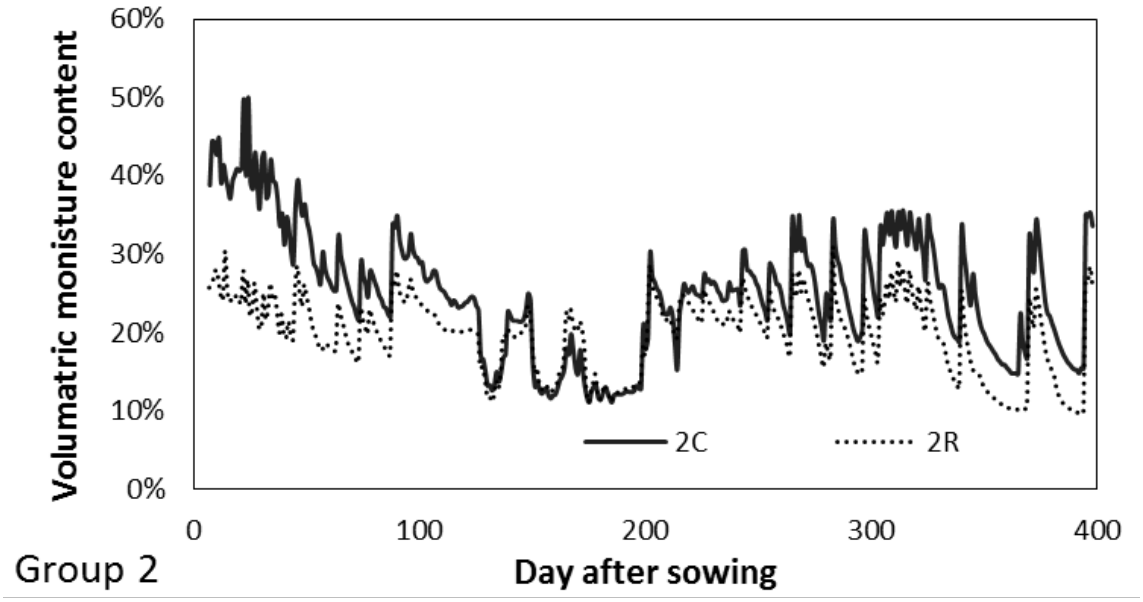

(b)

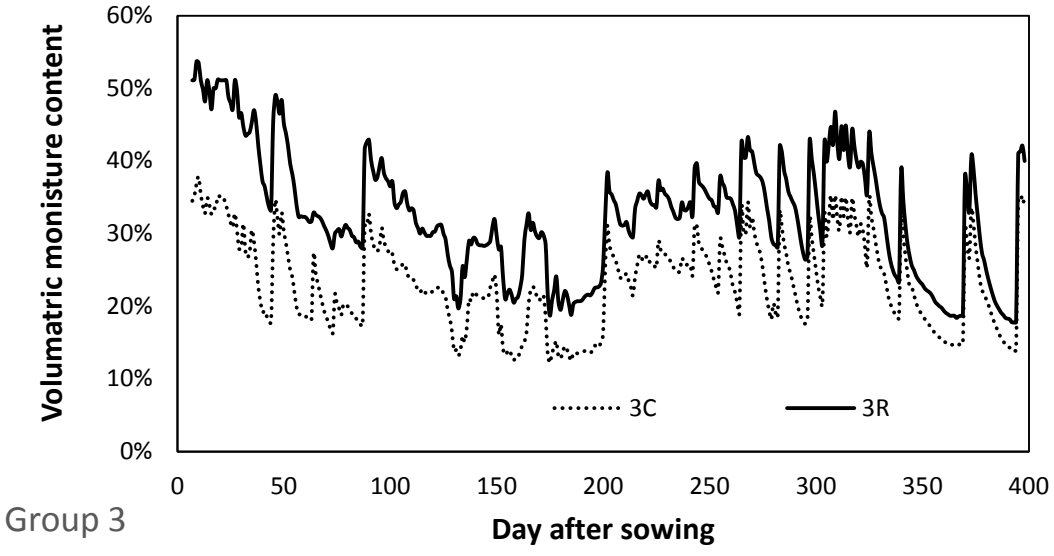

(c)

Figure 4.11: Volumetric Moisture Content Comparisons (Continued)

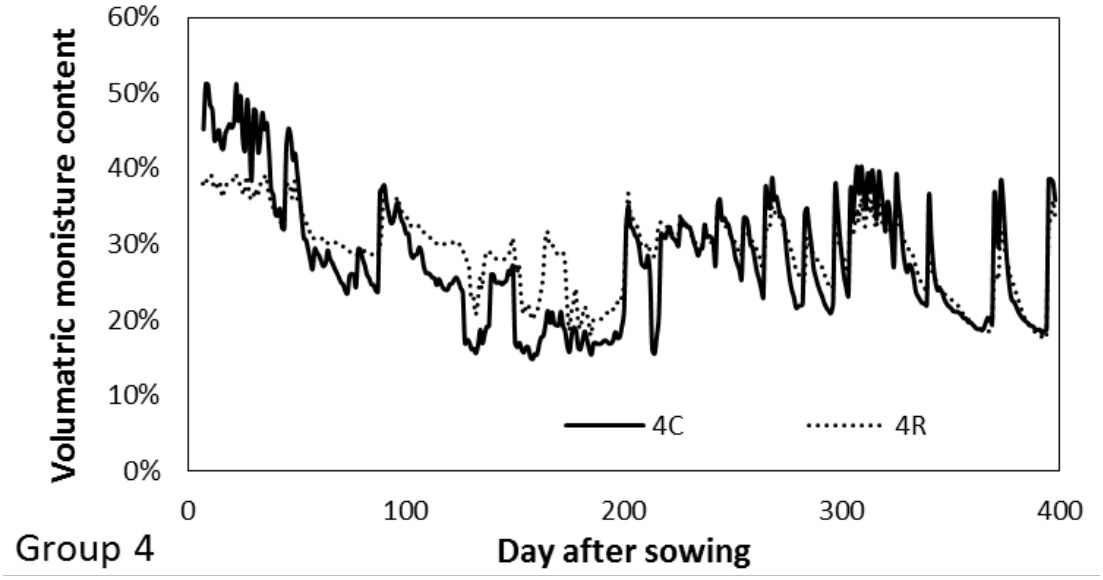

(d)

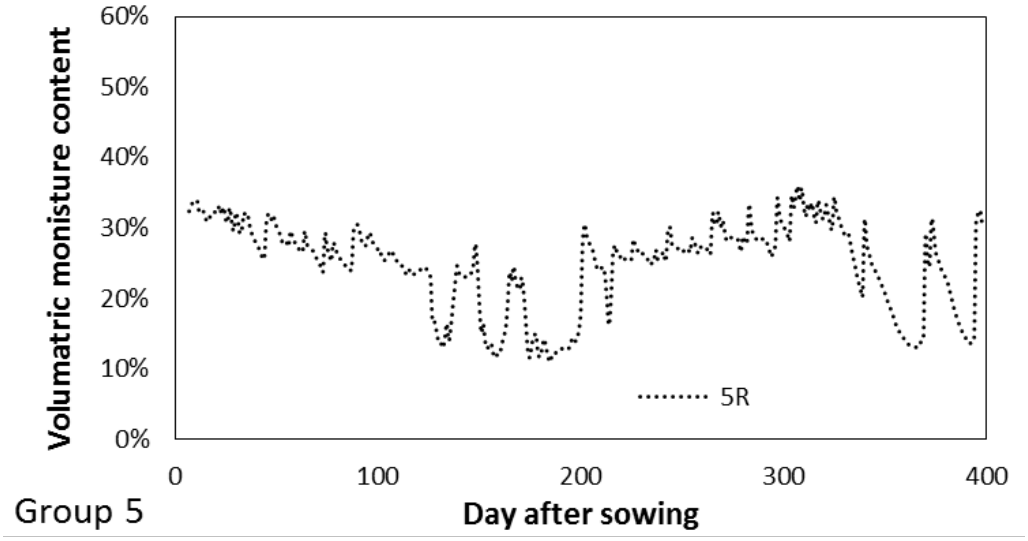

(e)

Figure 4.11: Volumetric Moisture Content Comparisons (Continued)

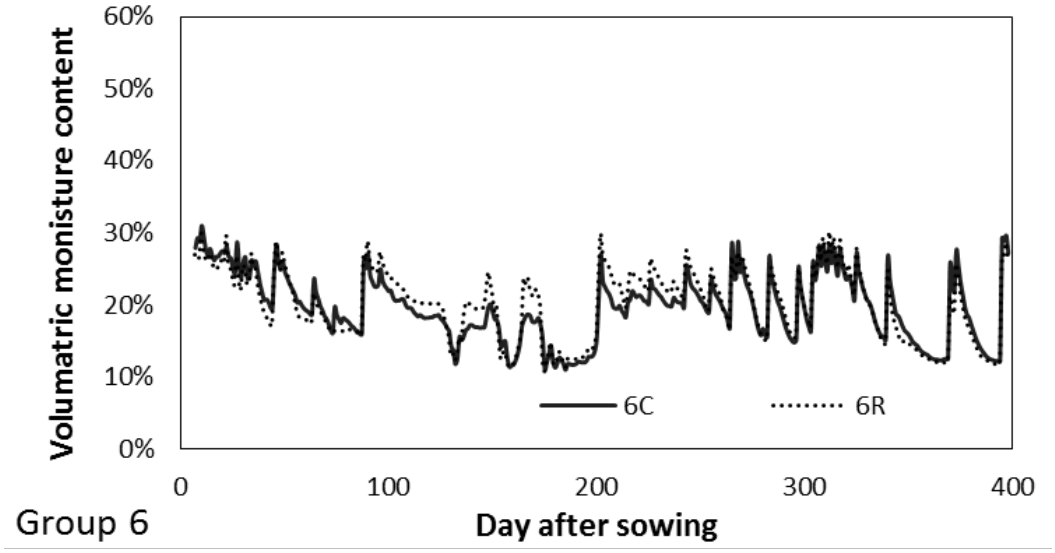

(f)

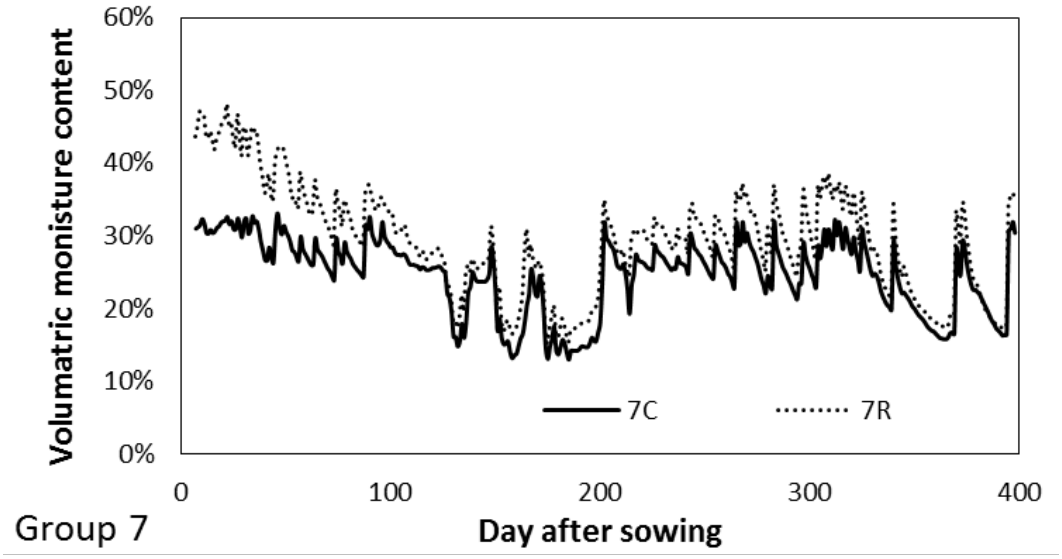

(g)

Figure 4.11: Volumetric Moisture Content Comparisons (Continued)

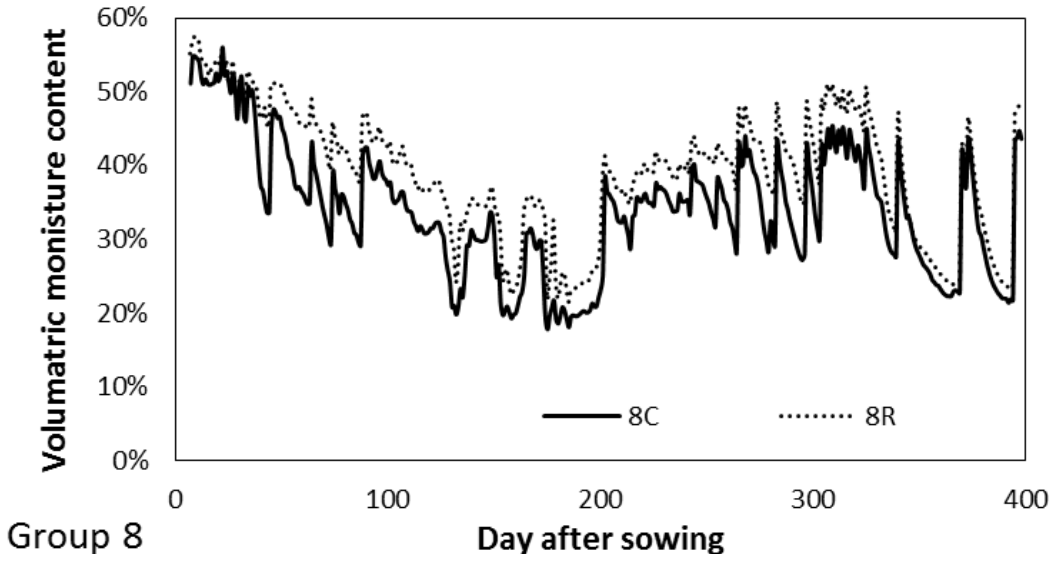

(h)

Figure 4.11: Volumetric Moisture Content Comparisons (Continued)

4.2.3 Grass Leaf Blade Length

Five to eight individual plants, regardless of the species, were chosen randomly from each section as the sample of population. A limited number of plants were sampled considering the total number of plants available in each section at that time. The longest green leaf on each individual plant was measured and the average length was used to represent the blade length of the section. Figure 4.12 presents a picture taken during the blade length measurement.

The comparison of average leaf blade length between the control and reinforced sections in each group was used to identify whether the inclusion of geosynthetic material altered the growth pattern of the vegetation. The first buds appeared on Day 2 in all sections. Due to the blade length in the establishment stage differing significantly from the later stages, the comparisons of blade lengths of all groups are presented separately in Figures 4.13 and 4.14, where Figure 4.13 presents the blade length comparison between Day 0 to Day 89 and Figure 4.14 presents the blade length comparison between Day 89 to Day 333.

Figure 4.12: Measuring Blade Length

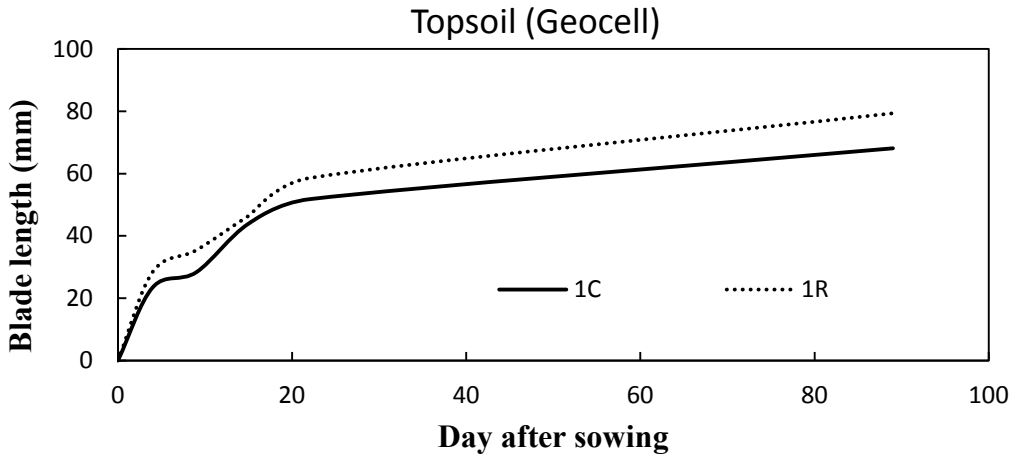

(a)

Figure 4.13: Average Leaf Blade Length Comparison from Day 0 to Day 89 of All Groups

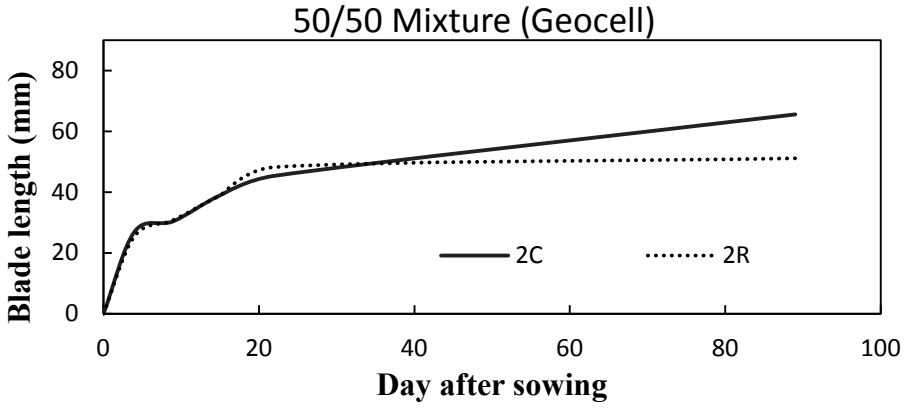

(b)

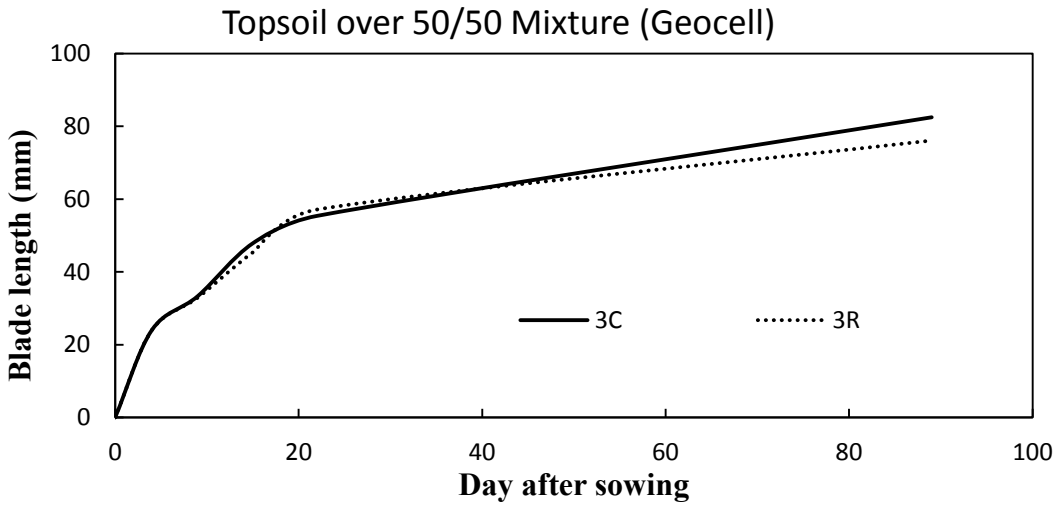

(c)

Figure 4.13: Average Leaf Blade Length Comparison from Day 0 to Day 89 of All Groups (Continued)

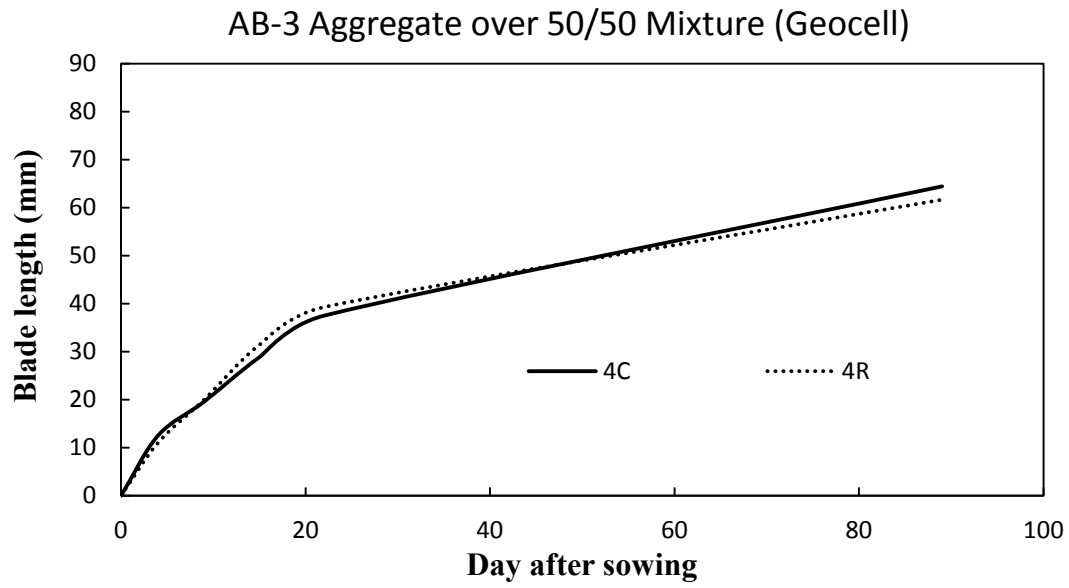

(d)

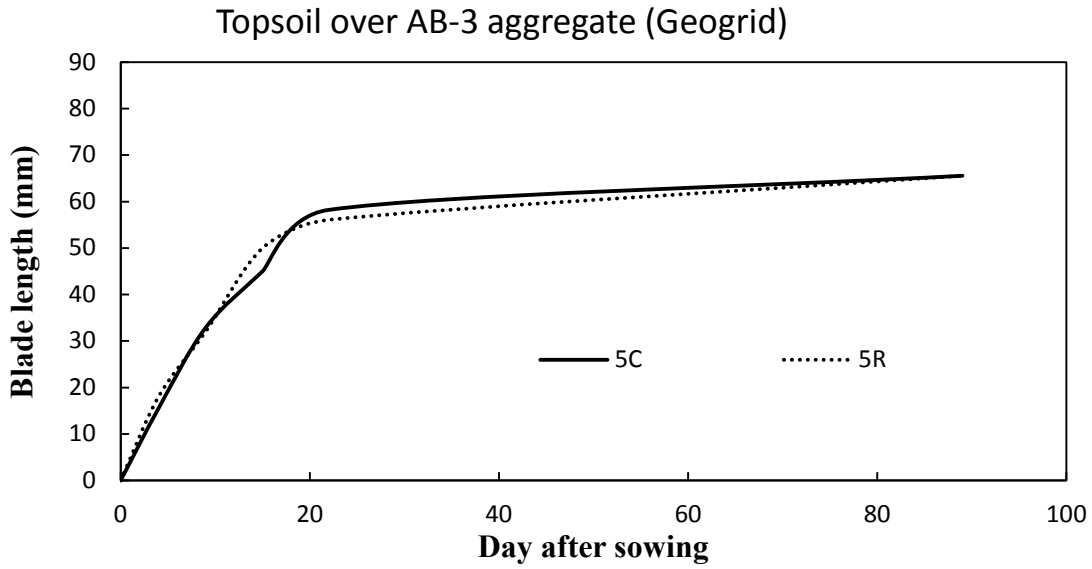

(e)

Figure 4.13: Average Leaf Blade Length Comparison from Day 0 to Day 89 of All Groups (Continued)

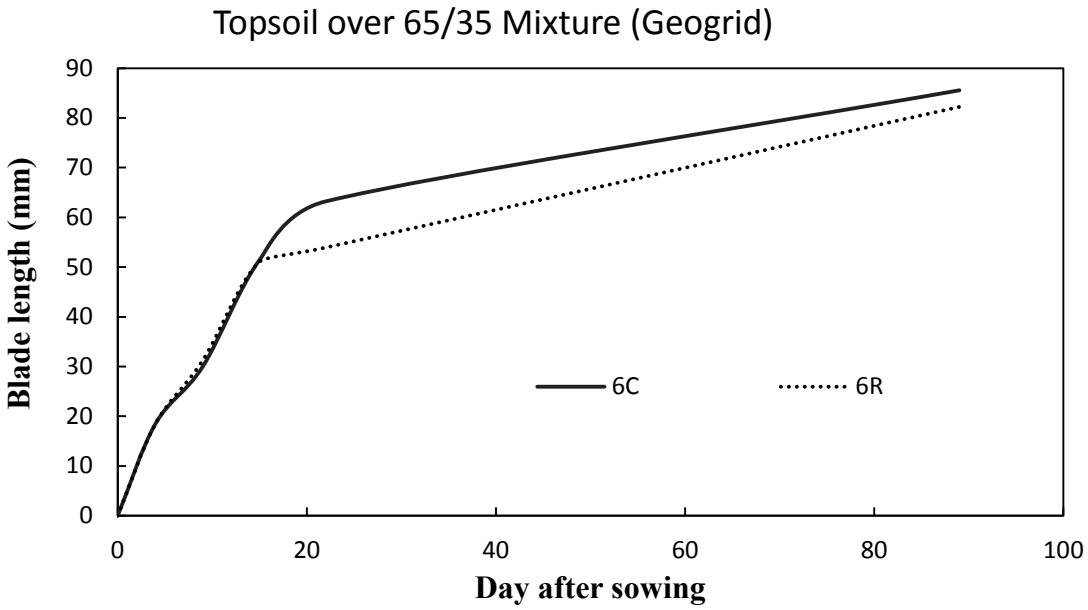

(f)

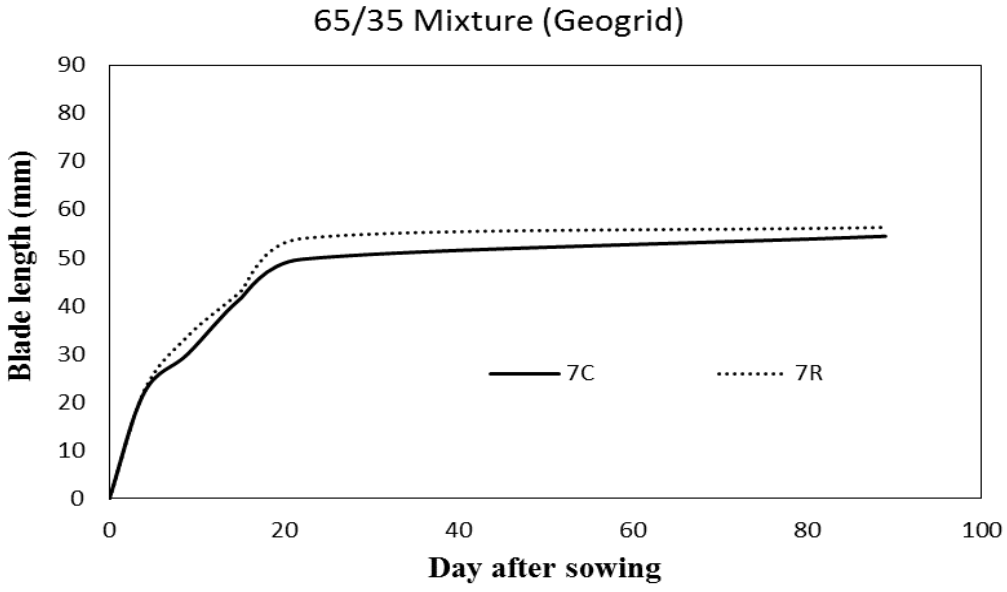

(g)

Figure 4.13: Average Leaf Blade Length Comparison from Day 0 to Day 89 of All Groups (Continued)

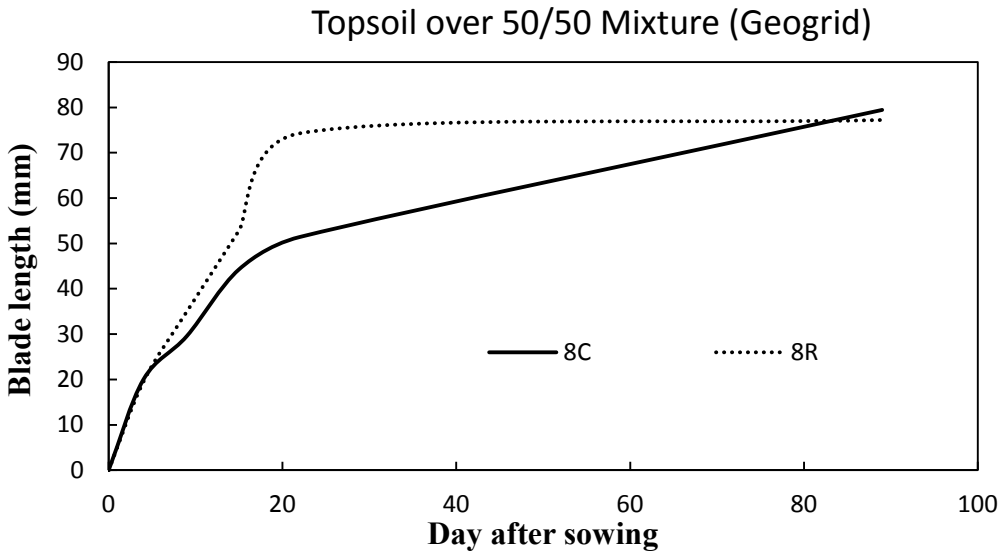

(h)

Figure 4.13: Average Leaf Blade Length Comparison from Day 0 to Day 89 of All Groups (Continued)

Figure 4.13 presents the average leaf blade length comparison results from Day 0 to Day 89 of all groups, which were obtained in the fall of 2013. The comparisons of the results between the reinforced and control sections indicate that the geocell and geogrid reinforcement had a minor or no effect on the vegetation at the establishment stage. For all the test sections, grass grew rapidly in the first 22 days, then the growth rate slowed down from Day 22 to Day 89. The blade length and the trend of vegetation growth from Day 0 to Day 22 were almost identical between the control and reinforced sections in all groups except Group 8. In Group 8, on Day 22, the blade length of the reinforced section was significantly higher than the control section. However, the difference between the control and reinforced sections narrowed down to approximately 3 mm on Day 89. In Group 6, the average blade length on the control section was 10 mm more than that of the reinforced section. On Day 89, the difference between the control and reinforced sections decreased to approximately 3 mm. On Day 89, the sections in Groups 1 and 2 started to show some difference in the blade length. In Group 2 the control section out-grew the reinforced section by 15 mm in average while the standard deviation of the samples from both sections was around 14 mm. The reinforced section in Group 1 grew 10 mm longer in

average than the control section, while the standard deviations of these two sections were 13 mm and 19 mm, respectively. Sections in Groups 2, 4, 5, and 7 had the similar blade length. The blade length comparison by the establishment stage indicates that the geosynthetic reinforcement had no significant impact on the vegetation establishment.

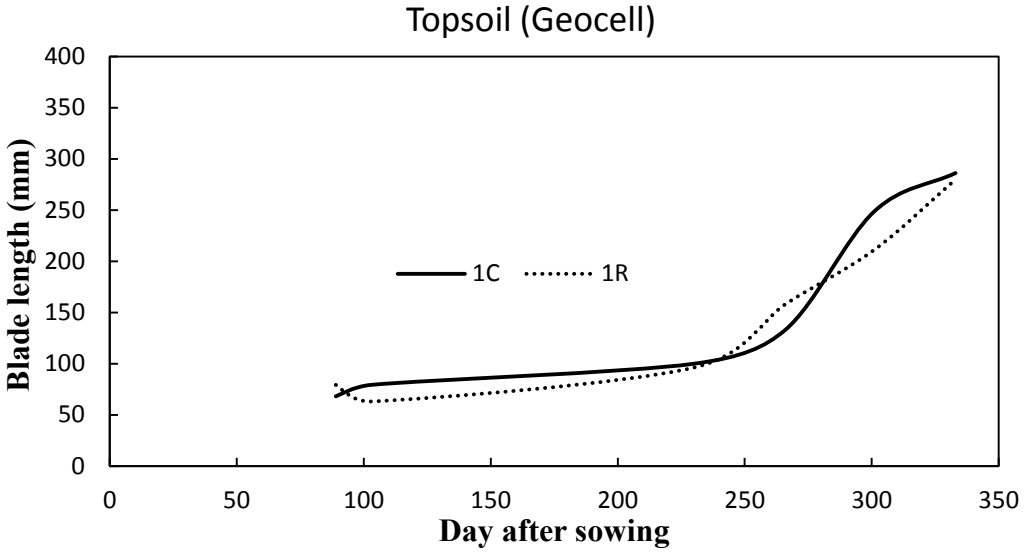

(a)

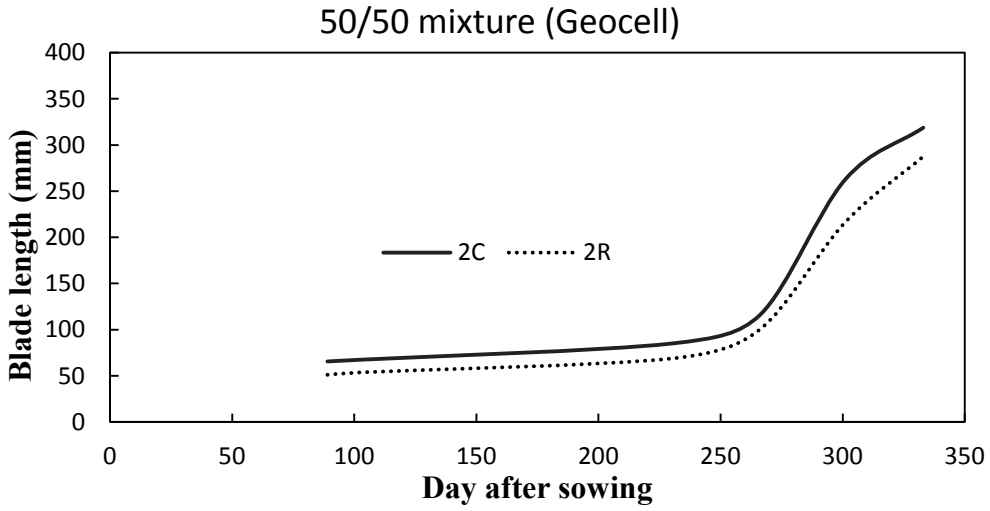

(b)

Figure 4.14: Average Leaf Blade Length Comparison from Day 89 to Day 333 of All Groups

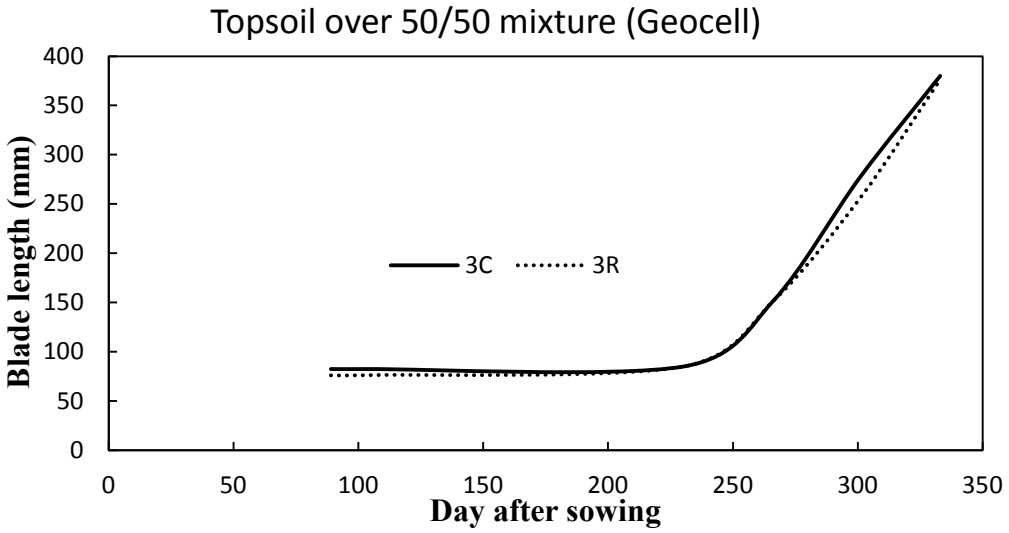

(c)

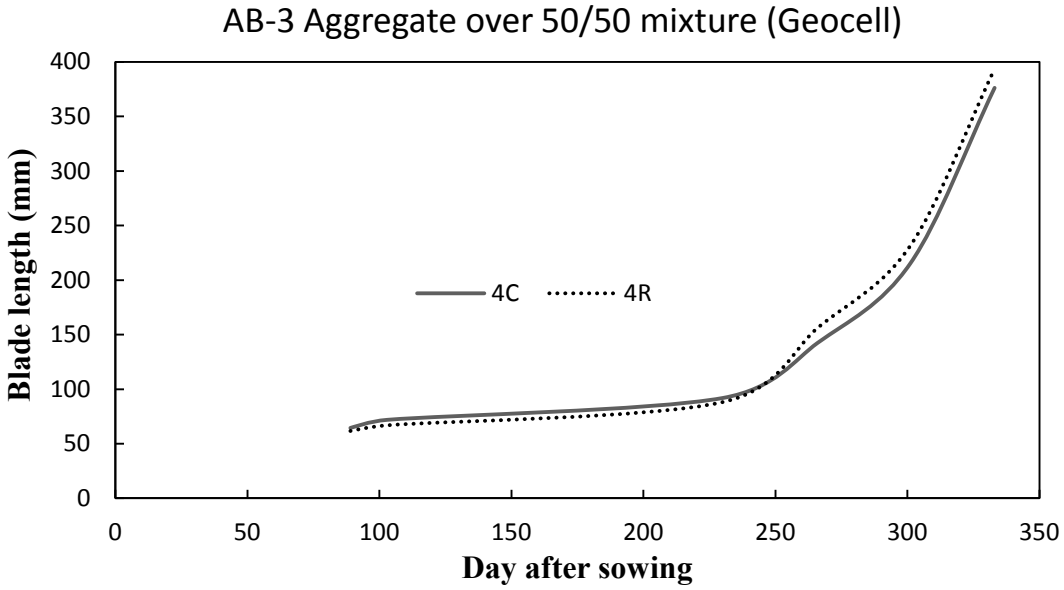

(d)

Figure 4.14: Average Leaf Blade Length Comparison from Day 89 to Day 333 of All Groups (Continued)

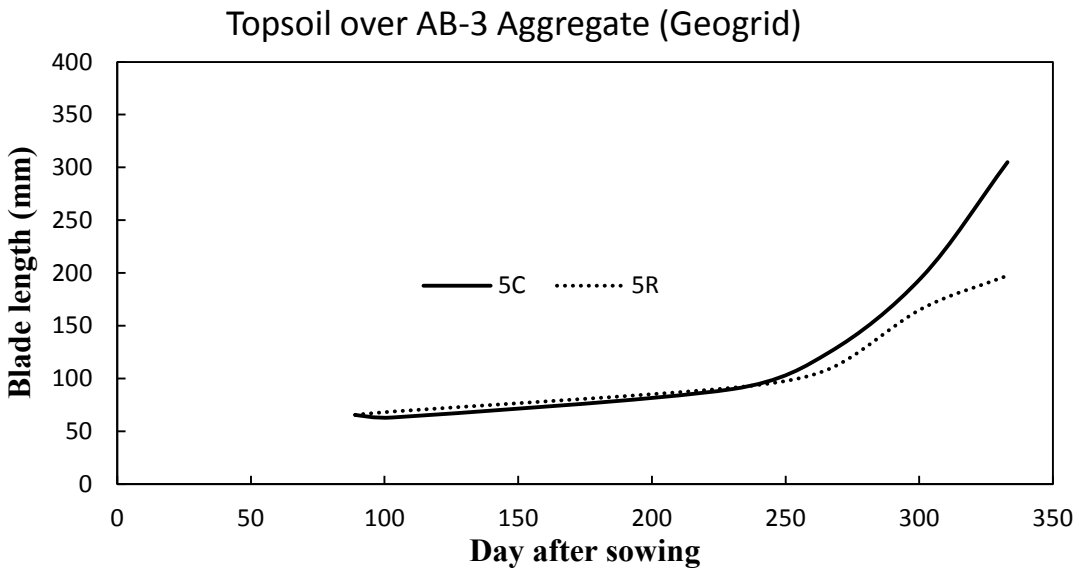

(e)

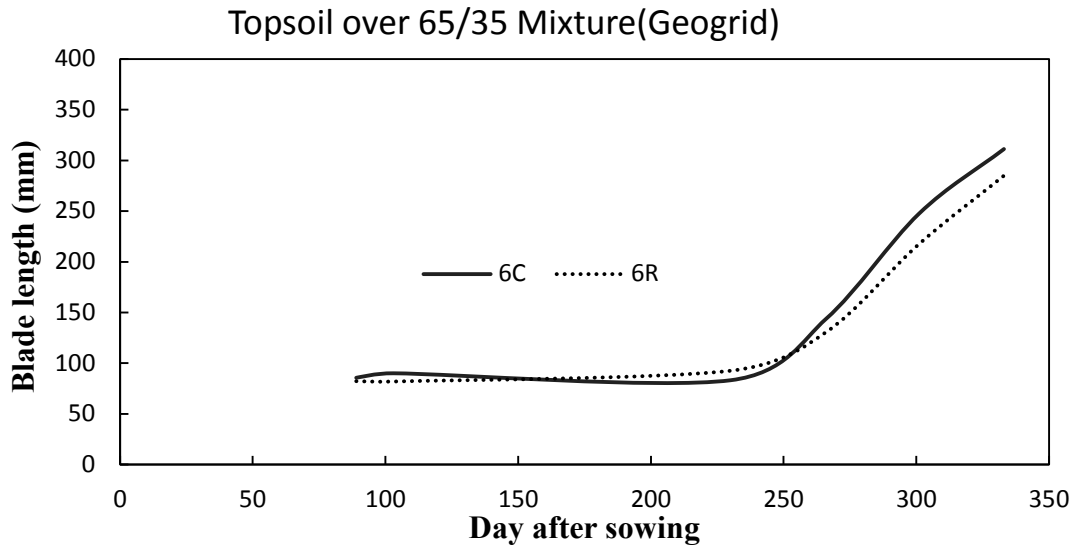

(f)

Figure 4.14: Average Leaf Blade Length Comparison from Day 89 to Day 333 of All Groups (Continued)

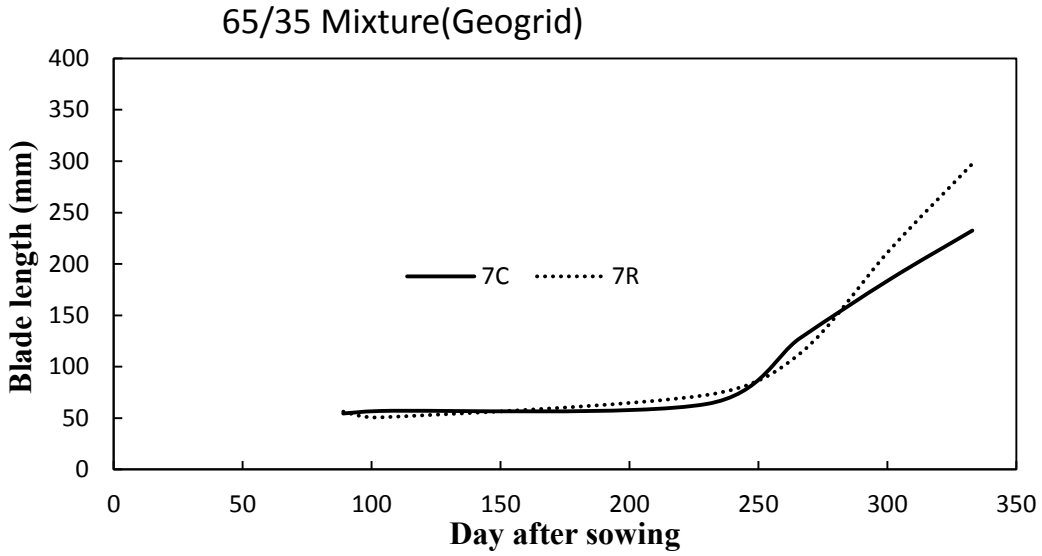

(g)

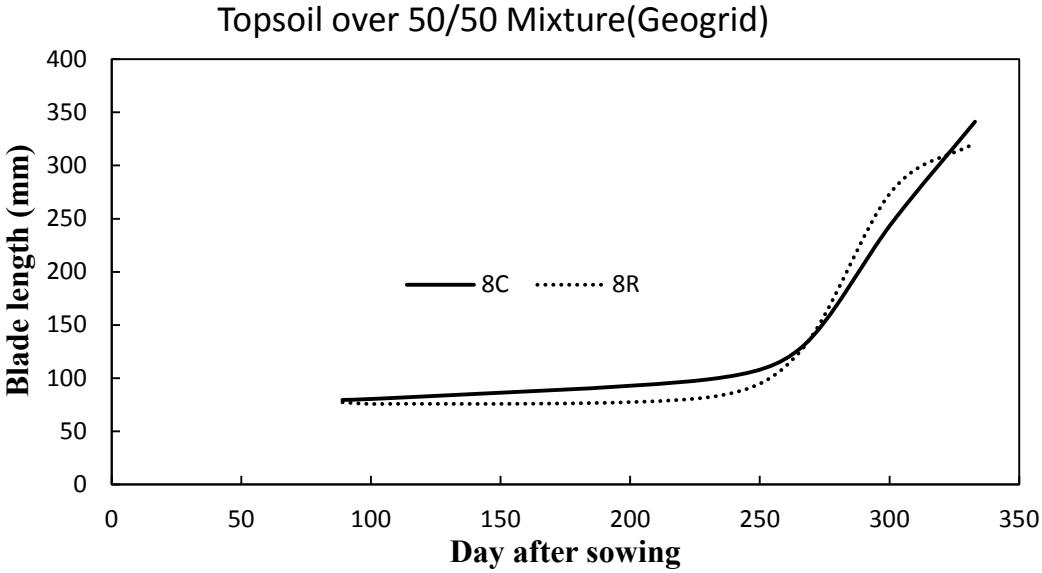

(h)

Figure 4.14: Average Leaf Blade Length Comparison from Day 89 to Day 333 of All Groups (Continued)

Figure 4.14 presents the blade lengths from Day 89 to Day 333, which were obtained in the winter of 2013 and the spring and the summer of 2014. Leaf blade length from Day 89 to Day 230 showed little growth because it was in the winter. The lowest temperature recorded over the winter was -24.4°C and there were 66 days in this winter with the average temperature lower than 0°C. After Day 230, most sections started to show an increase in the blade length. By Day 333, the longest average blade length was 393 mm on Section 4R. In Groups 1, 2, 3, 4, 6, and 8 the average blade length from the reinforced section showed no significant difference from that of the control section throughout the test period. In Group 5, the average blade length in control and reinforced sections started to show difference on Day 266. By Day 333, the blade length from the reinforced section was almost 100 mm higher than the control section. In Group 7, the average blade length in control and reinforced sections started to show difference on Day 301. By Day 333, the blade length from the reinforced section was approximately 60 mm less than the control section. The differences between control and reinforced section were also confirmed by visual inspection as shown in Figure 4.15. In Figure 4.15, Section 5R showed obviously shorter leaf blades. Based on the visual observation on Sections 5R and 7C, the alive leaves on plants were less than plants from other sections. The cause of such phenomenon was unknown, however, it was observed on one reinforced section and one control section, thus it is reasonable to deduct that the decrease in alive leaves on plants was likely not caused by geosynthetic reinforcement.

The comparisons of the control and reinforced sections showed no definitive evidence of the inclusion of geosynthetic altering the vegetation leaf blade length.

In order to investigate the impact of base course soil combination on the development of vegetation, the blade lengths of control and reinforced sections from each group were averaged and plotted in Figures 4.16 and 4.17. The groups designated for geocell had a thicker base course than those designated for the geogrid; thus, the results for geocell and geogrid groups are plotted separately.

Figure 4.16 (a) shows the average blade length of each group from Day 0 to Day 89 of geocell groups. In the first 22 days, Group 4 with the AB-3 aggregate over the soil-aggregate mixture grew the slowest. On Day 22, the average blade length of Group 4 was 38 mm. The

vegetation in Group 2 grew the second slowest with an average blade length of 47 mm on Day 22. The vegetation growths in Groups 1 and 3 were similar with an average blade length around 55 mm. Figure 4.16 (b) shows the average blade length of each group from Day 0 to Day 89 of geogrid groups. Group 7 showed the slowest growth in blade length on Day 22 and the blade length increased the least from Day 22 to Day 89, almost remaining the same. On Day 22, the blade length of Group 5 was slightly more than that of Group 1. However, on Day 89, the blade length of Group 1 surpassed that of Group 5. Group 8 had the longest blade length among the geogrid groups on Day 22 at 63 mm. On Day 89, Group 6 had the longest blade length at 84 mm. Such vegetation growth shows a correlation with the type of the soil cover. Overall, from Day 0 to Day 22, Groups 1, 3, 5, 6, 7, and 8 that consisted of a topsoil cover showed the similar fast blade growth. Group 2 with a 50/50 soil-aggregate mixture had a medium blade growth rate. Group 4 with an AB-3 aggregate cover resulted in the slowest blade growth.

Figure 4.15: Picture of Test Sections on Day 292

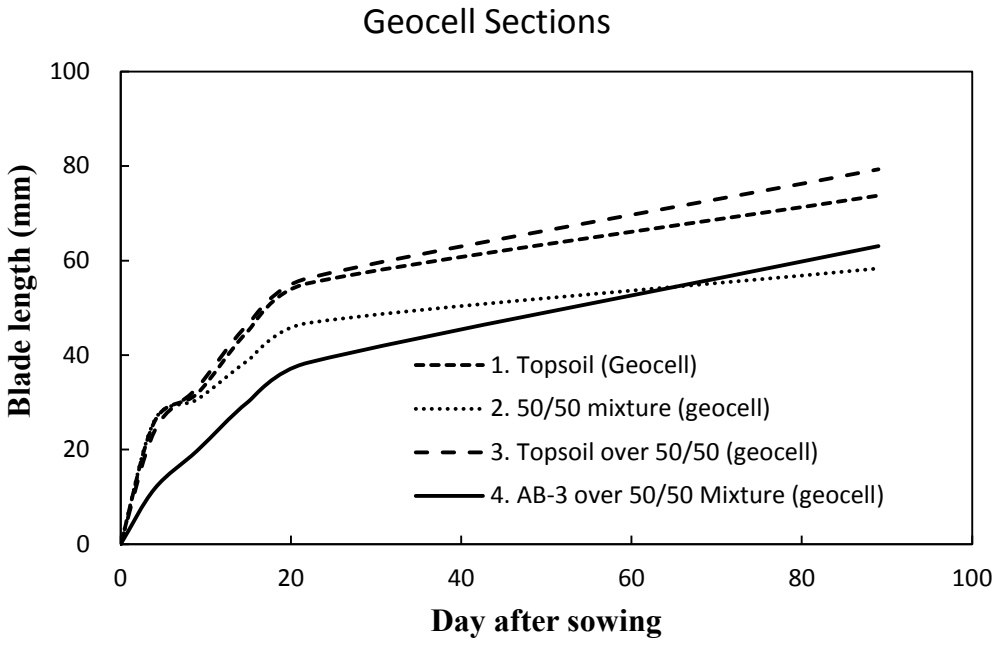

(a)

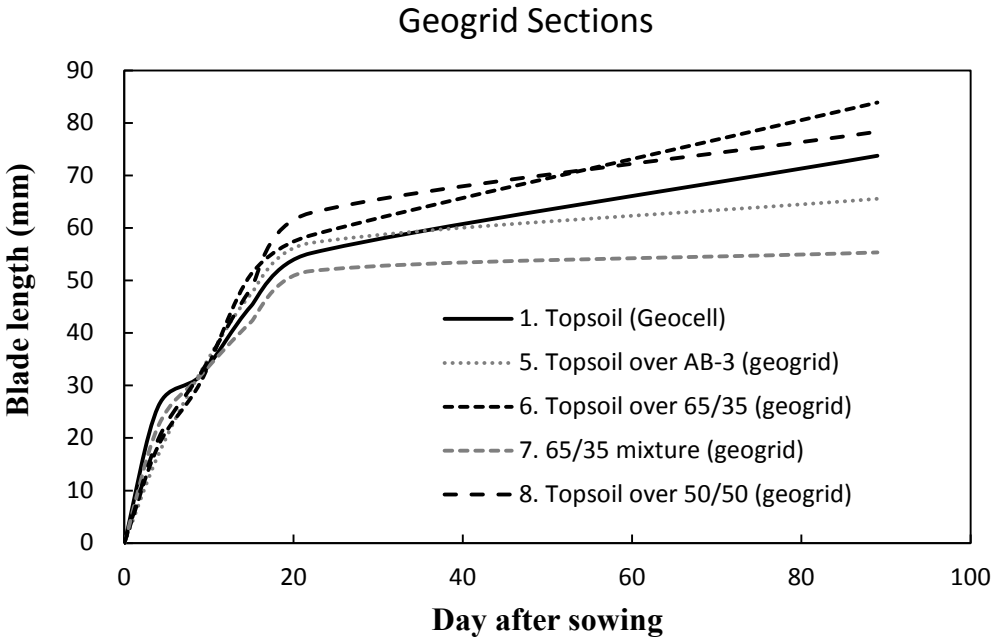

(b)

Figure 4.16: Group Average Blade Length from Day 0 to Day 89

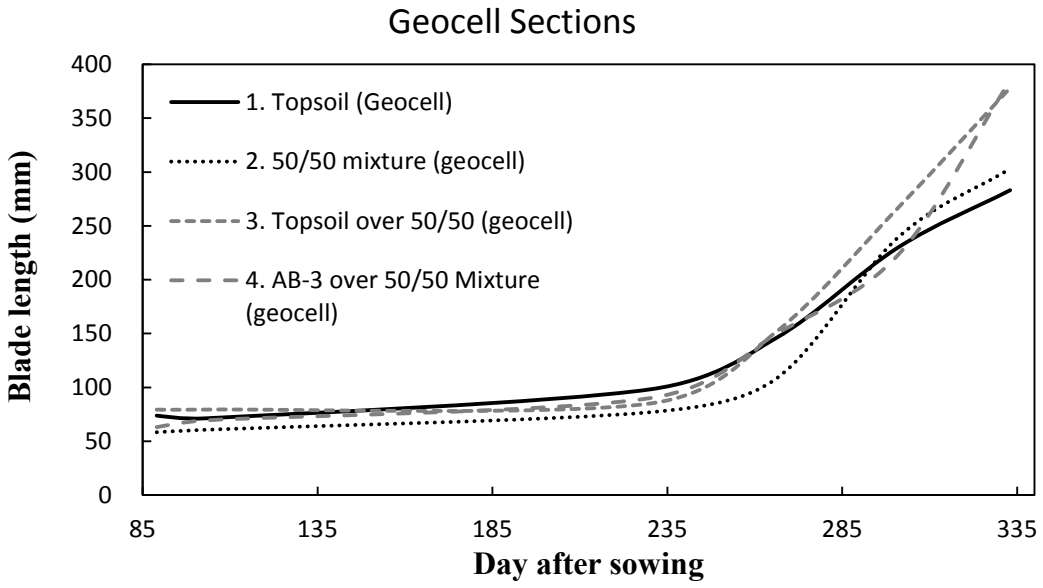

(a)

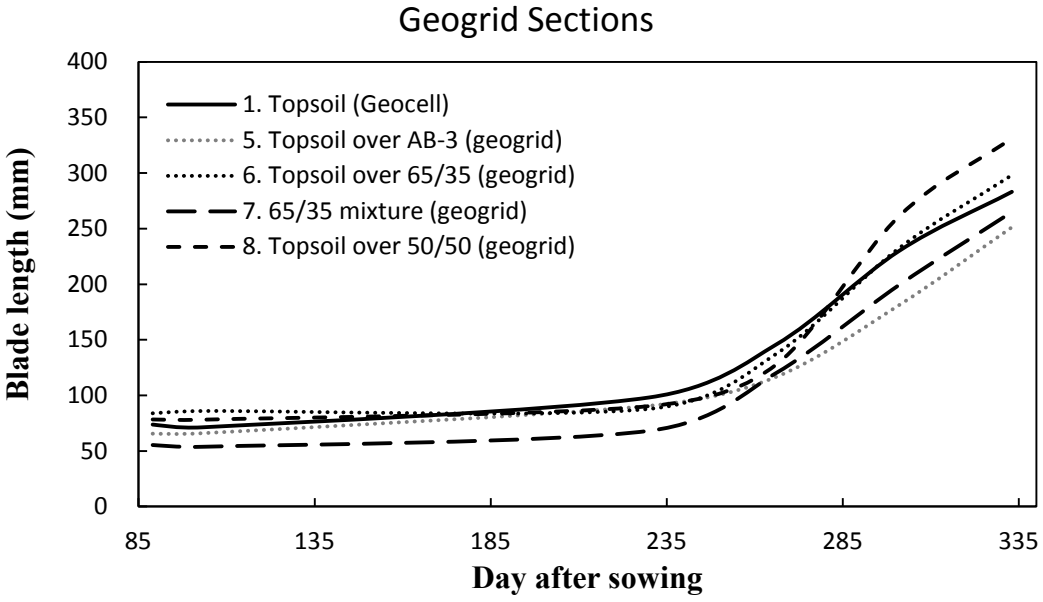

(b)

Figure 4.17: Group Average Blade Length from Day 89 to Day 333

Figure 4.17 shows the average blade length of each group from Day 89 to Day 333. The blade lengths of all groups were similar on Day 230. Among the geocell groups, from Day 230 to Day 266, Groups 1, 3, and 4 had a similar growth rate. From Day 266 to Day 333, the leaf growth in Group 1 slowed down while those in Groups 2, 3, and 4 increased. On Day 333, Groups 3 and 4 showed the longest blade length at 385 mm. Group 2 had a longer blade length than Group 1. Among the geogrid groups, Groups 5, 6, and 8 showed similar blade length, while the blade length from Group 7 was less than other groups. On Day 333, Group 8 showed the longest blade length at 331 mm. Group 6 showed similar blade length as Group 1 at around 290 mm. Group 5 showed the least blade length at 250 mm. These results suggested that the 50/50 soil mixture allowed the already established vegetation to grow faster in the spring and the early summer. The 65/35 soil mixture showed evidence of limiting the growth of vegetation, while the AB-3 aggregate was the least favorable soil for the growth of vegetation.

According to the above comparisons, it can be concluded that the type of soil cover had an obvious effect on the vegetation growth in the first stage geocell. However, it had a minor effect on the development of the already established vegetation. The reason for less effect of the type of soil cover in this stage than that in the initial establishment is related to the root development of vegetation. As the root system of vegetation developed through the cover layer, the effect of the cover layer on vegetation became less important.

4.2.4 Vegetation Density

To measure the population density of vegetation, a 600 × 600 mm frame was placed on each section randomly. The area surrounded by the frame was considered as the measurement area. The total number of alive individual plants, regardless of species, in the measurement area was counted and used to compute the grass population density of the measured section. Figure 4.18 displays the measuring equipment. The grass density comparisons between sections and groups are plotted in Figures 4.19 and 4.20, respectively.

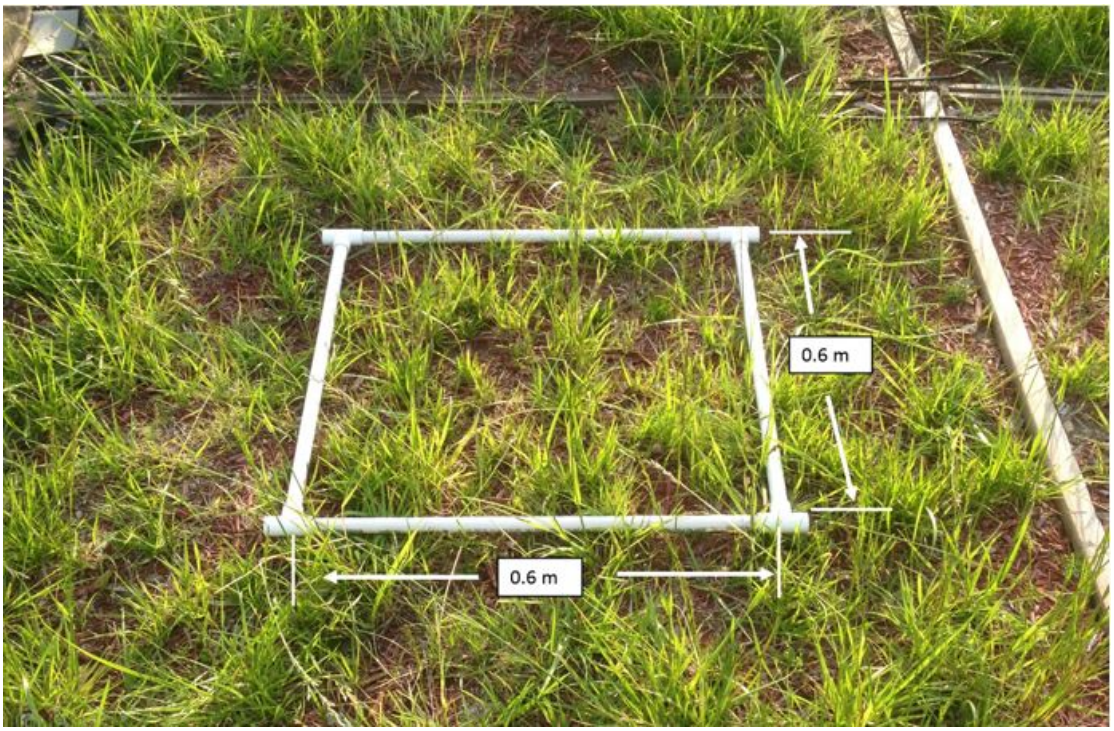

Figure 4.18: Frame for Vegetation Density Measurement

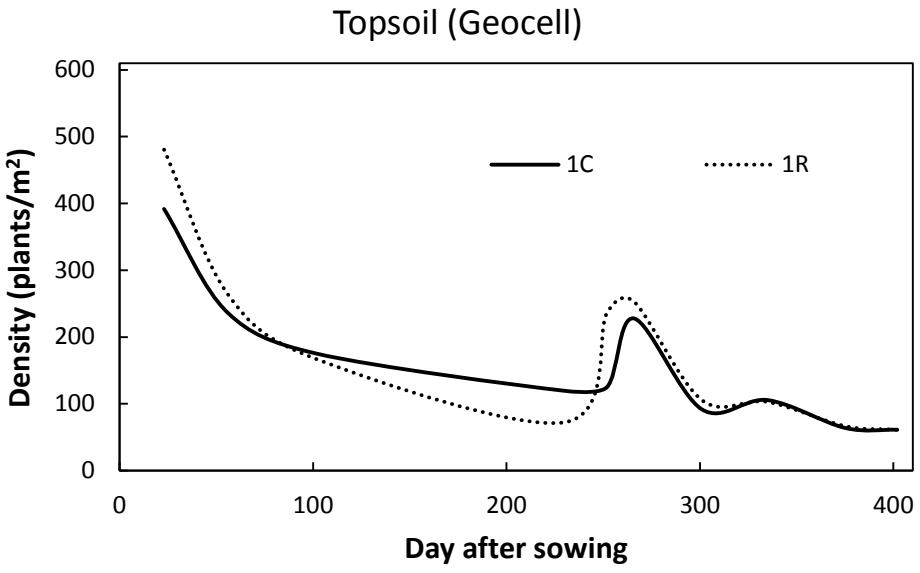

(a)

Figure 4.19: Grass Population Density Comparison of All Groups

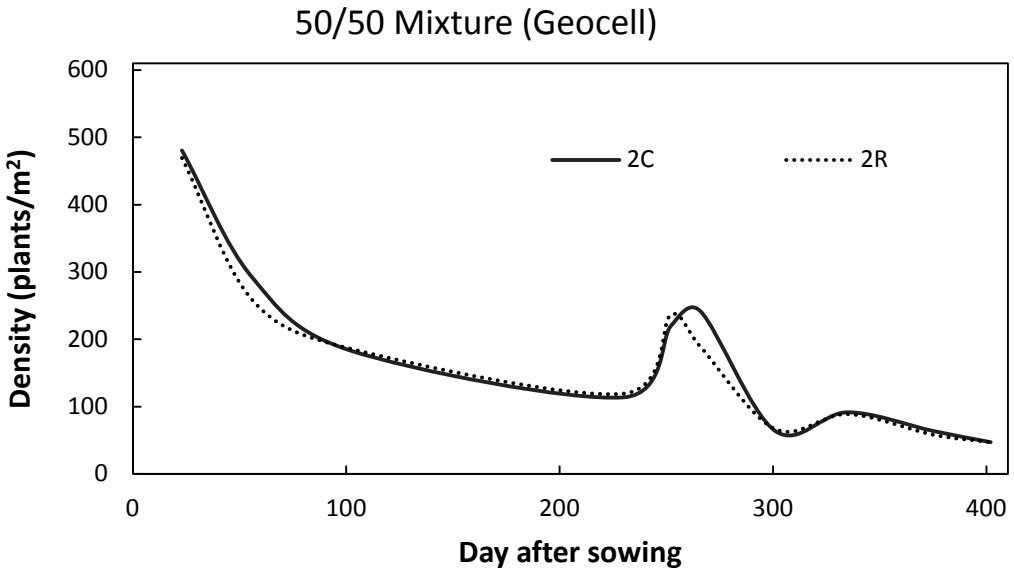

(b)

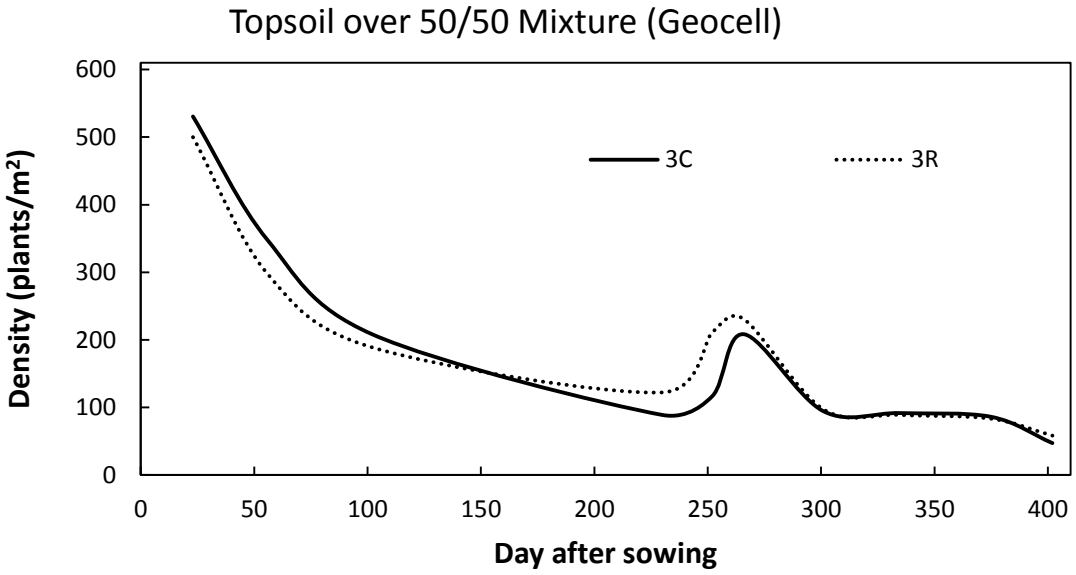

(c)

Figure 4.19: Grass Population Density Comparison of All Groups (Continued)

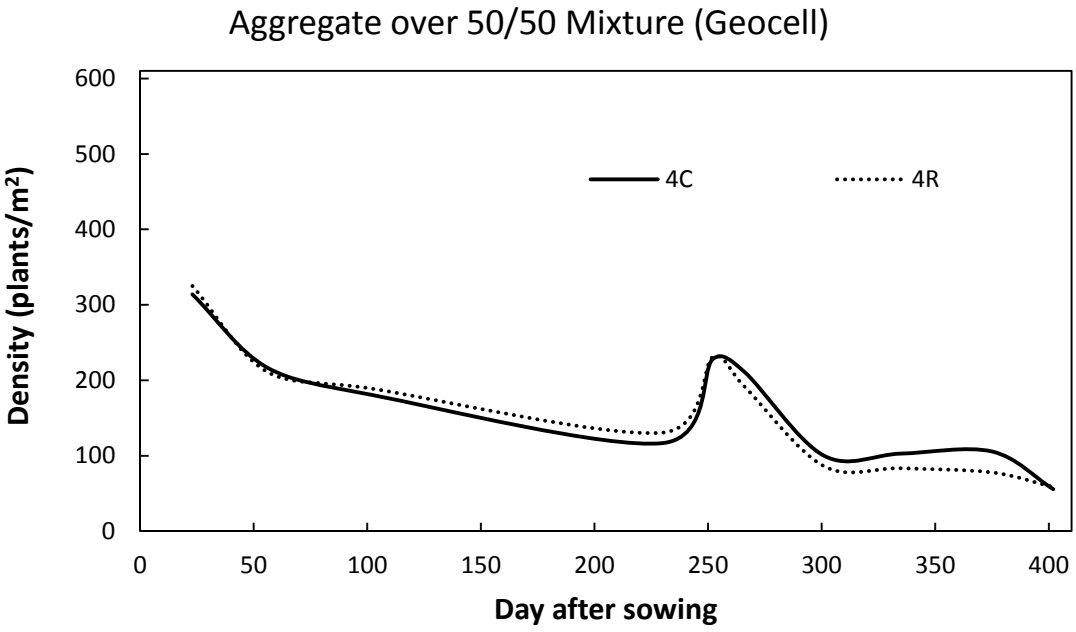

(d)

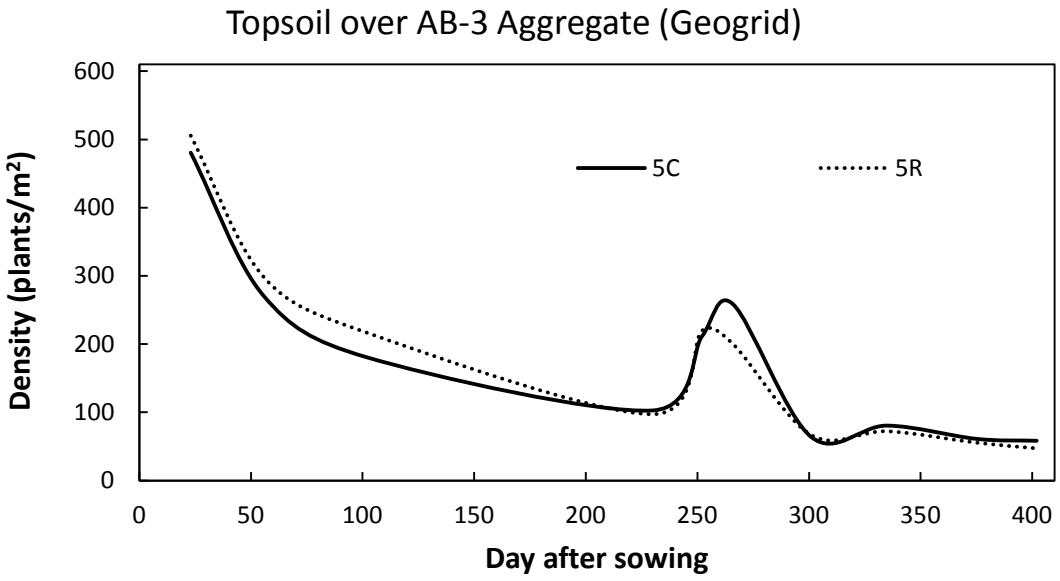

(e)

Figure 4.19: Grass Population Density Comparison of All Groups (Continued)

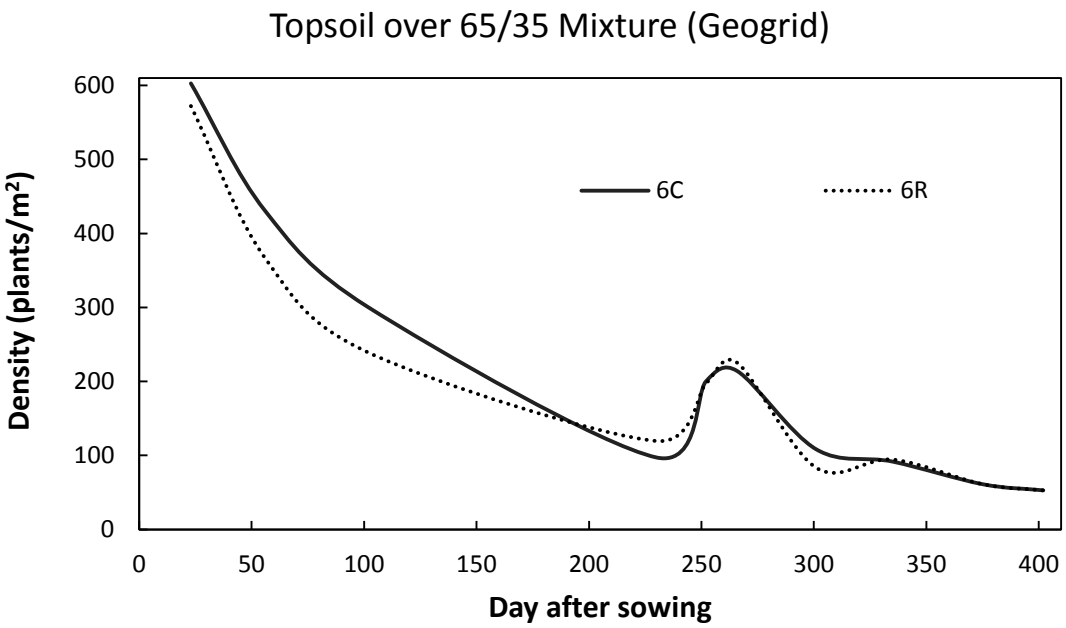

(f)

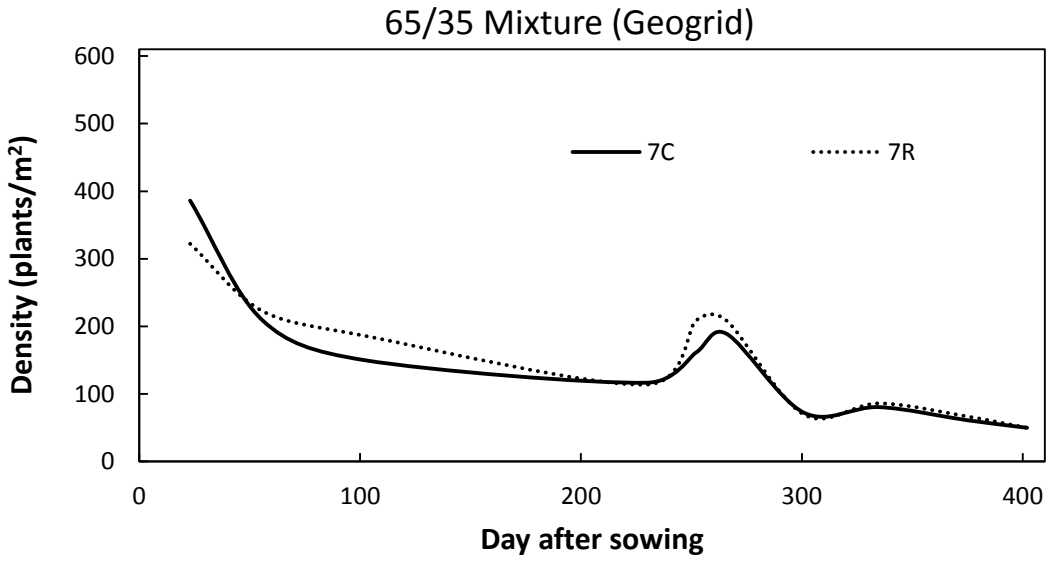

(g)

Figure 4.19: Grass Population Density Comparison of All Groups (Continued)

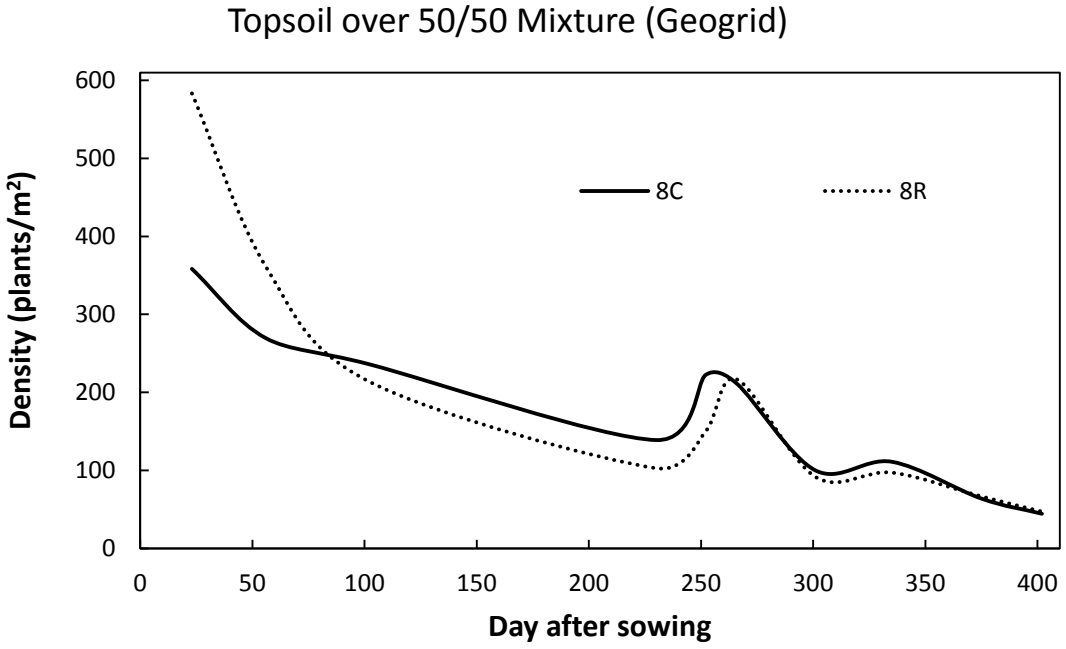

(h)

Figure 4.19: Grass Population Density Comparison of All Groups (Continued)

All 16 test sections showed a similar trend in the population density. The maximum densities in all sections were recorded on Day 23 (i.e., the first data point in Figure 4.19). The high densities of vegetation at the first data point were the result of seed germination. The population densities then decreased rapidly from Day 23 to Day 102 as the season transitioned from the fall to the winter. An increase in the densities was observed from Day 230 to Day 250 during the spring of 2014. Then the densities decreased again after Day 266 during the summer of 2014. The densities declined from Day 300 to Day 400. The peak densities in the spring were contributed to by the revival of the already established grass and the newborn grass.

In Groups 2, 4, and 5, the vegetation density in the control and reinforced sections were similar. In Group 1, the vegetation density on the control section was 100 plants/m^2 less than that of the reinforced section. However, on Day 89, the vegetation densities on both sections were the same. The control section had almost twice the density as the reinforced section on Day 230. Then a rapid increase in the density was observed on the reinforced section between Day 230 and

Day 252. By Day 266, the density difference between these two sections was small. A similar phenomenon was also observed on Group 3. The density of the reinforced section increased faster than that of the control section. However, the peak densities of these two sections were similar on Day 266. In Group 6, the vegetation density on the control section was slightly lower than that of the reinforced section in the fall and winter (i.e., from Day 23 to Day 230). Then in the spring and summer of the next year, the densities of both sections showed no significant difference. In Group 7 on Day 23, the control section had a higher vegetation density. Then the density of the control section decreased sharply and was lower than the reinforced section. Both sections from Group 7 had similar vegetation density in the spring and summer. In Group 8, the vegetation density from the control section was significantly lower than the reinforced section before Day 102. On Day 23, the vegetation density on the control was 358 plants/m^2 while the reinforced section had a density of 583 plants/m^2. The 225 plants/m^2 difference between the control and reinforced sections in Group 8 was the largest vegetation density difference observed between control and reinforced sections throughout the test period. However, the difference between the control and reinforced sections of Group 8 decreased to 90 plants/m^2 on Day 56. As of the beginning of spring (i.e., Day 230), the vegetation density of the control section was lower than the reinforced section and the density differences between the control and reinforced section in the spring and summer remained small.

The section comparisons suggest that the inclusion of geosynthetic in base courses did not influence the vegetation density.

Similar to the leaf blade length comparisons, the vegetation densities of control and reinforced sections from each group were averaged and are plotted in Figure 4.20 to investigate the influence of base course soil combination on vegetation growth. The groups designated for geocell had a thicker base course than those designated for the geogrid, thus the geocell and geogrid groups are plotted separately.

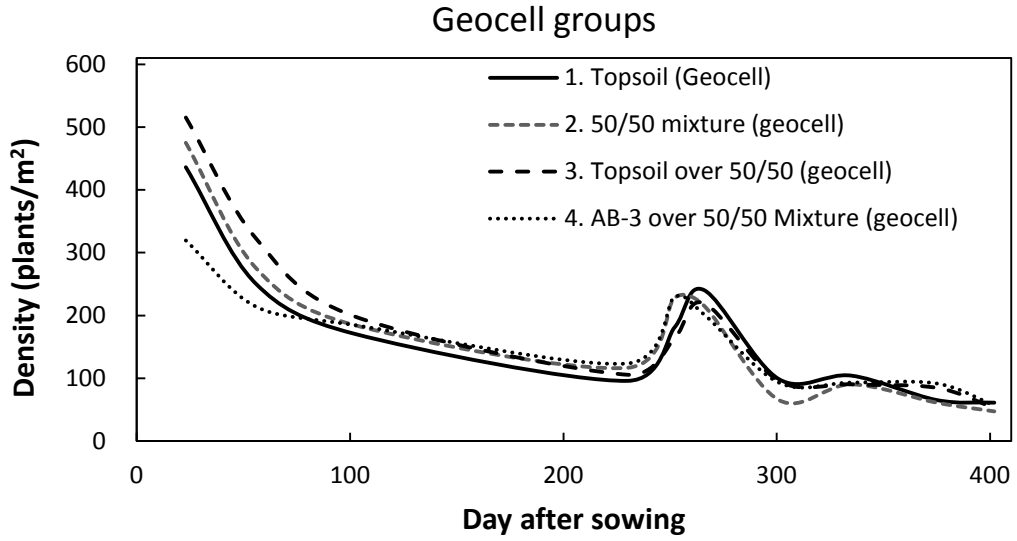

(a)

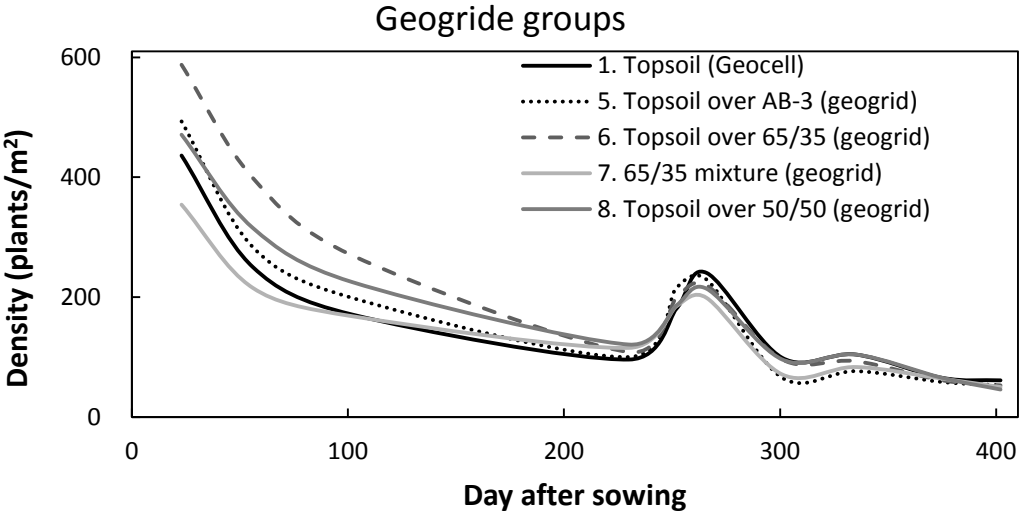

(b)

Figure 4.20: Vegetation Density Comparison of Groups

Figure 4.20 (a) shows the group average densities of the control and reinforced sections in all geocell groups. In the initial establishment stage, Group 3 had the maximum density at 517 plants/m^2. Groups 1 and 2 had 436 and 475 plants/m^2, respectively. Group 4 with the AB-3 aggregate top layer had a significantly lower density of 115 plants/m^2 than other groups. On Day 50, the differences between the sections decreased. By the early winter on Day 102, the densities

of all the groups were between 167 and 194 individual plants/m^2 and small differences among the groups were observed. The vegetation densities in the spring showed some differences. The densities in Groups 2 and 4 increased faster than Groups 1 and 3 from Day 230 to Day 252. However, Group 1 yielded the maximum density of 242 plants/m^2 in the spring period. By Day 400, all groups showed similar vegetation densities. Figure 4.20 (b) shows the group average densities of the control and reinforced sections in all geogrid groups. On Day 23, Group 6 showed the highest density among all groups at 588 plants/m^2. Groups 5 and 8 showed similar vegetation densities at 493 and 471 plants/m^2, respectively. Group 7 showed the least vegetation density at 215 plants/m^2. On Day 102, Group 6 still presented the highest density of vegetation. The vegetation density of Group 8 surpassed that of Group 5. On Day 230, the vegetation densities of all geogrid groups were similar, ranging from 100 to 121 plants/m^2. In the spring and summer of the consequent year (i.e., Day 230 to Day 400), the vegetation densities of all geogrid groups were similar.

The group comparisons indicate that in the long term (i.e., more than one year), the base course combination showed no significant impact on the vegetation density. However, the vegetation density on Day 23 of Groups 4 and 7 showed a high aggregate-content soil cover layer (i.e., AB-3 aggregate and 65/35 mixture) would limit the germination at the vegetation establishment stage. The 50/50 mixture on the other hand showed an equal fertility as the topsoil.

4.2.5 Dry Biomass

Dry biomass is defined here as the mass of oven dried collected vegetation structure. The oven drying process reduced the impact on specimen masses by moisture which may not be part of the vegetation structure such as condensation. Dry biomass is a more comprehensive, however destructive, measurement to evaluate vegetation. The grass was first trimmed and collected in this study. The collected biomass was then oven dried at 105^oC for a period of 24 hours according to ASTM E1756 (2008). Due to the destructive nature, this evaluation was conducted toward the end of the testing period. Two biomass collections were conducted. First, the grass in each section was cut off at 150 mm from the ground surface on Day 339. Figure 4.21 shows the biomass collecting process on Day 339. The wood frame had a height of 150 mm and was used

as a ruler. Then on Day 421, the grass was cut off at the ground surface and all the vegetation parts above ground surface were collected. Figure 4.22 shows the dry biomass amounts from each section on both Day 339 and Day 421.

Figure 4.21: 150-mm-Tall Reference Frame and Biomass Collection

The biomass collected on Day 339 included seeds, stems, and leaves above 150 mm from the ground. The dry biomass from Day 339 indicates the reinforced sections from Groups 1, 3, 4, and 7 produced more biomass than the control sections. The control section produced more biomass than the reinforced section in Group 2, 5, 6 and 8. The biomass production between the control and reinforced sections in all groups differed within 10 g/m^2 except for Groups 5 and 8. In Group 5, the control section biomass production was almost twice that of the reinforced section. In Group 8, the control section produced 27% more biomass than the reinforced section. The average dry biomass in Group 1 was the highest of 77 gram/m^2. Productions from Groups 3 and 4 (i.e., 70 and 68 gram/m^2, respectively) were similar. During the biomass collection, it was noticed that the biomass from Group 2, both the control and reinforced sections, contained less seeds and stems than those in other groups. Thus, dry biomass from Group 2 was significantly less than those from other groups.

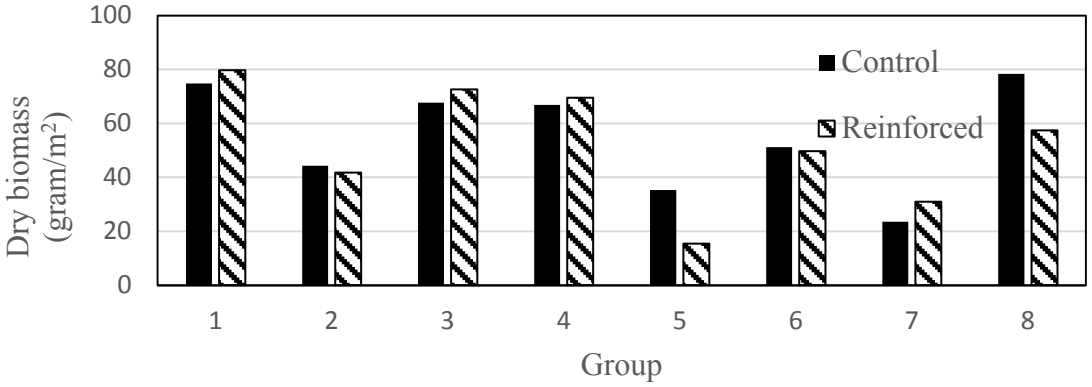

(a)

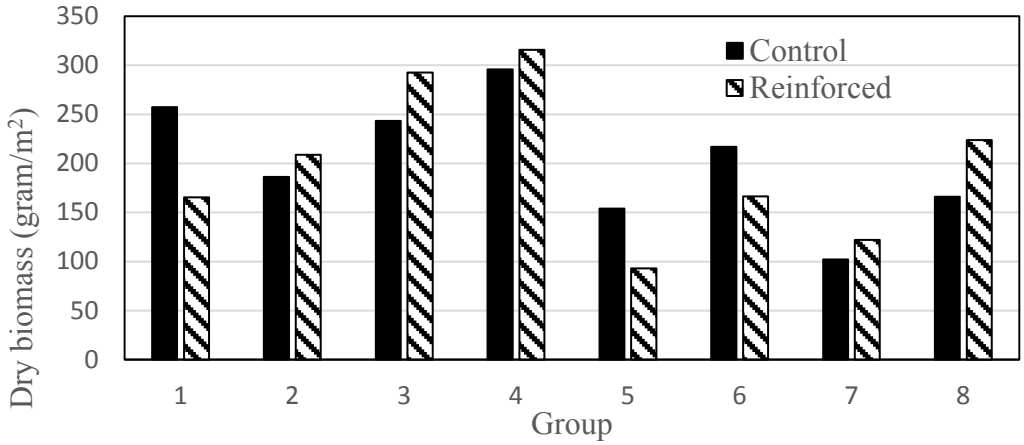

(b)

Figure 4.22: Dry Biomass Comparison on (a) Day 339 and (b) Day 421

The biomass collected on Day 421 included all the vegetation parts above the ground surface. The collection on Day 339 trimmed off most of the stems and seeds, thus little stems and seeds were collected on Day 421 and the biomass collected on Day 421 contained mainly of leaves. Based on Figure 4.22 (b), only the control section from Group 1 produced more biomass than the reinforced section. The reinforced sections in Groups 2, 3, 4, and 8 produced 12%, 20%, 7%, and 25% more biomass than the control sections, respectively. Compared with Section 1C, the reinforced section from Group 3 and both sections from Group 4 produced more biomass. The control section from Group 3 produced slightly less biomass. Group 4 produced the greatest amount of biomass among all groups (i.e., average production = 305.8 g/m^2). Group 3 had an

average production of 267.9 g/m^2, which was similar to Section 1C (257.3 g/m^2 production). Groups 5 and 7 produced the least amount of biomass.

The dry biomass of vegetation comparisons indicated no evidence of geocell or geogrid reinforcement limiting the growth of vegetation. The biomass production difference between groups indicated the 50/50 mixture presented similar ability to sustain vegetation as the topsoil; however, the 65/35 mixture and the AB-3 aggregate limited the biomass production of vegetation.

4.3 Summary

To investigate the effect of geocell reinforcement on vegetation, eight test groups with different base courses and soil cover layers to represent unpaved shoulders were constructed. Each group consisted of a control section and a geocell or geogrid-reinforced section. Two primary species (tall fescue and ryegrass) were planted on all the test sections. Blade length, grass population density, and biomass were measured for all test sections. Based on the test data, the following conclusions can be drawn from this study:

1. Throughout the one-year test period, no definite evidence of geocell or geogrid reinforcement limiting vegetation growth in unpaved shoulders was found.
2. The type of soil cover had a significant effect on the vegetation growth at the initial establishment stage. The soil cover containing a high percentage of aggregate retarded the establishment of vegetation while the soil cover containing a high percentage of fines promoted the establishment of vegetation.
3. The 50/50 soil-aggregate mixture showed no significant difference from the native topsoil on the ability to sustain the already established vegetation. The AB-3 aggregate and 65/35 soil-aggregate mixture did limit the biomass production of vegetation, and thus is not recommended for the application of vegetated shoulders.

Chapter 5: Cyclic Plate Loading Tests

This chapter presents the cyclic plate loading tests on unreinforced and geocell or geogrid-reinforced unpaved roads on moderate or weak subgrade. A total of 14 cyclic plate loading tests were conducted in the large-scale geotechnical box to investigate the performance improvement provided by the inclusion of geocell or geogrid. Based on the vegetation study, the 50/50 soil-aggregate mixture was selected over the 65/35 soil-aggregate mixture for base course material and is referred to as the mixture in this chapter.

5.1 Equipment and Test Setups

5.1.1 Large-Scale Geotechnical Box

The large-scale geotechnical testing box, shown in Figure 5.1, has a dimension of 2.2 × 2 × 2 m (L × B × H). The loading system produces cyclic loading in a trapezoidal wave form as shown in Figure 5.2. The maximum load was 40 kN and the minimum load was 0.5 kN. The loading was transferred to a test section via a 304-mm diameter steel plate with a 12.5-mm-thick rubber base. At the peak load of 40 kN, the loading plate generated an average contact pressure of 552 kPa or 80 psi to simulate a wheel load of heavy vehicles.

The box was filled up to 1 meter with the subgrade material (the Kansas River sand and kaolin mixture), which was prepared at a target CBR value of 5% (moderate subgrade) or 3% (weak subgrade). Four earth pressure cells were installed at the interface between subgrade and base course with the sensitive side of the pressure cell towards the subgrade. In the geocell tests, the pressure cells were installed at the center of loading plate, and at the distances of 150, 300, and 600 mm from the center; in the geogrid tests, the pressure cells were installed at the center, and at the distance of 180, 250, and 280 mm from the center. After the construction of the base course, three displacement transducers, which were suspended from a reference beam across the top of the box, were positioned at 300, 450, and 600 mm away from the center of the loading plate for the geocell studies and 250 mm, 500 mm, and 1 m away from the center for the geogrid studies to measure the base surface deformations. Both data acquisition systems were set at 10

Hz frequency to record the data from the earth pressure cells and displacement transducers. An overall schematic drawing of the test setup is presented in Figure 5.3.

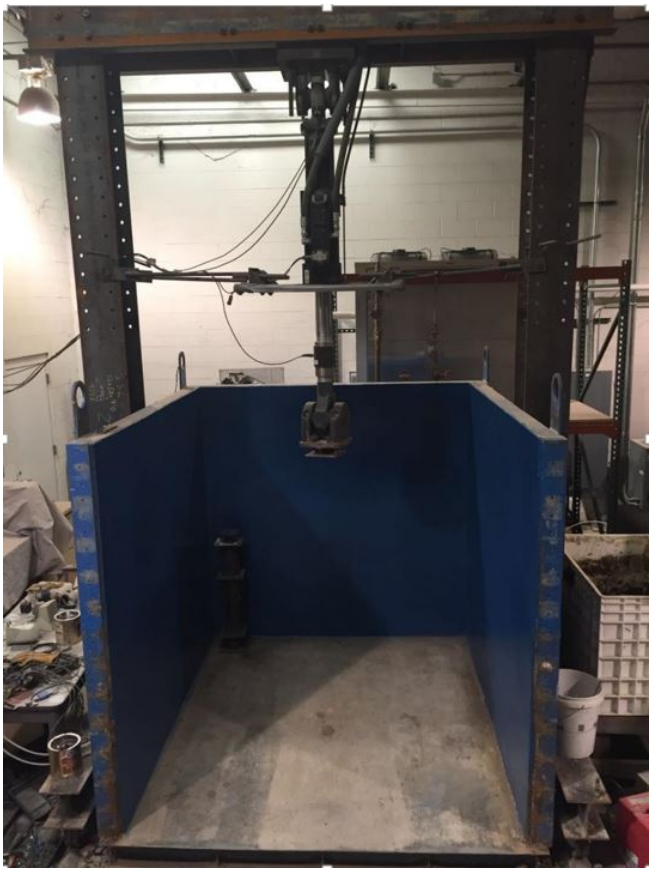

Figure 5.1: Picture of the Large-Scale Geotechnical Box

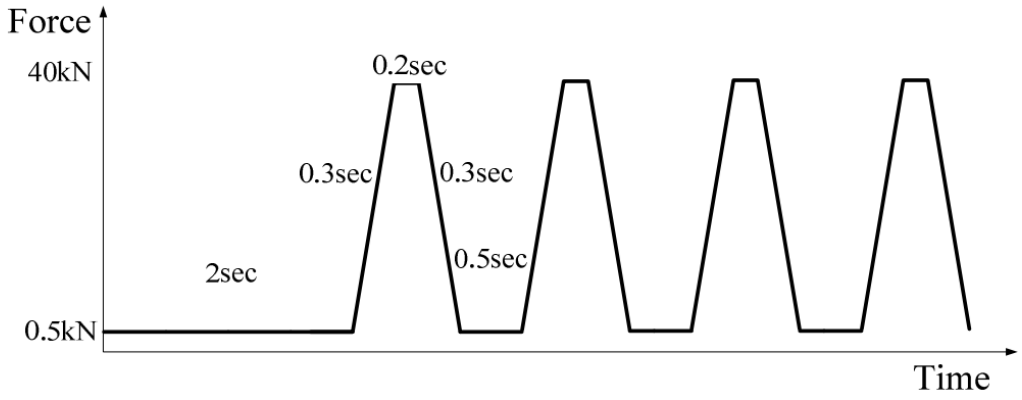

Figure 5.2: Cyclic Loading Wave Form

Source: Pokharel (2010)

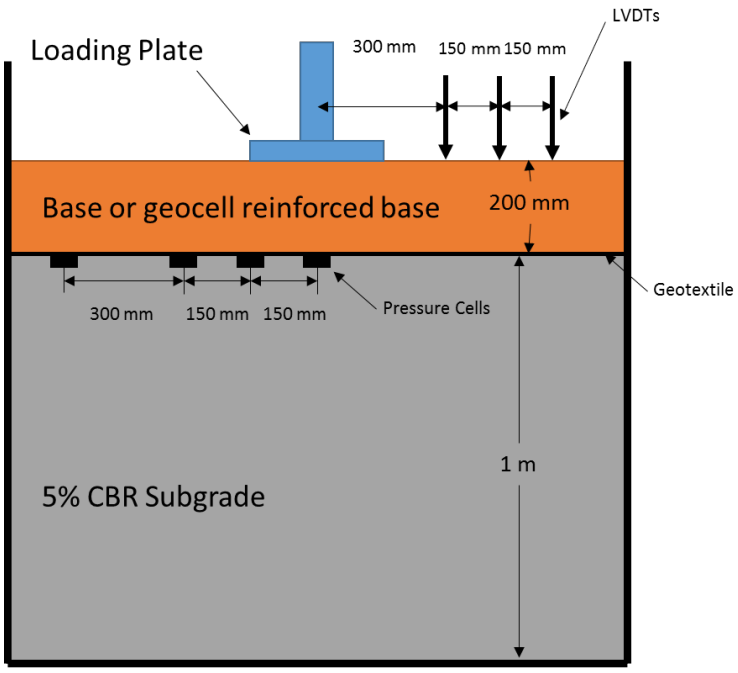

(a) Geocell test section

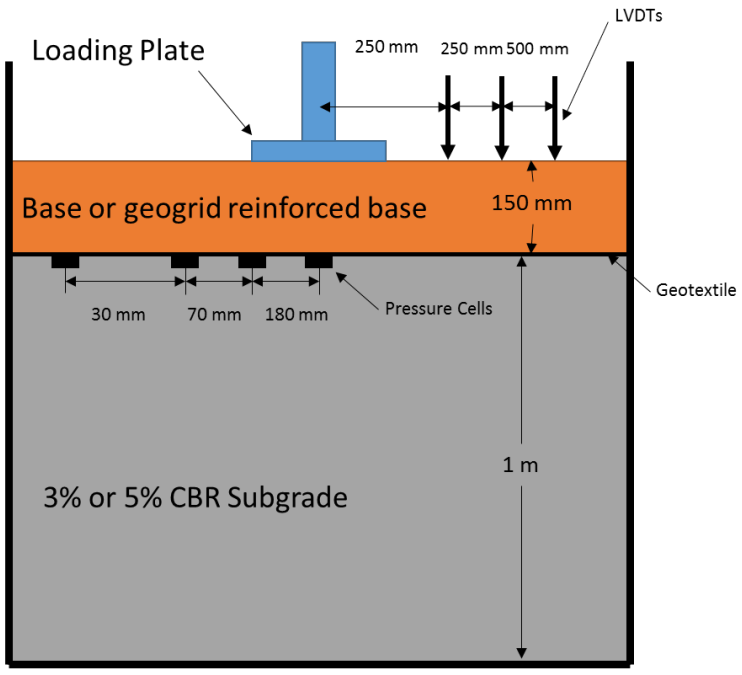

(b) Geogrid test section

Figure 5.3: Schematic Drawing of Test Sections (Not to Scale, All Units in mm)

5.1.2 Test Preparation

The subgrade material was placed in the box in 150-mm lifts, leveled, and then compacted with an electrical vibratory compactor as shown in Figure 5.4. Five vane shear tests were conducted after the compaction of the subgrade on each lift with a hand held vane shear machine at depths of 100, 175, and 250 mm. The subgrade CBR and undrain shear strength correlation was developed by Pokharel (2010) shown in Equation 5.1.

$$\mathbf{CBR}(\%) = \frac{\boldsymbol{C_u}}{\mathbf{20}} \qquad \textbf{Equation 5.1}$$

Where:

c_u = measured undrained shear strength in kPa

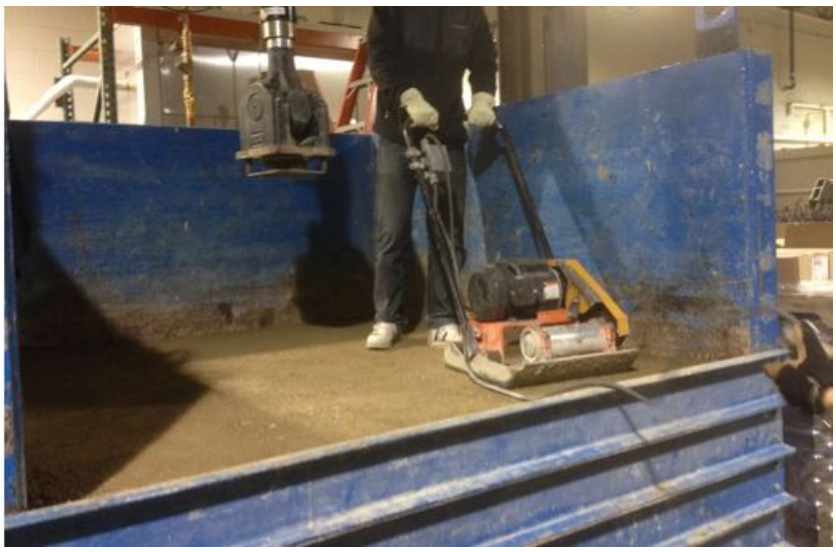

Figure 5.4: Compaction with the Electric Vibratory Compactor

After the box was filled to the target height with the subgrade material, earth pressure cells were installed. To protect earth pressure cells during the compaction and testing, trenches were dug for pressure cells and wires. A level was used to adjust the pressure cell position to be horizontal, as shown in Figure 5.5.

The quality of the base course was controlled via adjusting the moisture content to the optimum moisture content. For the geocell tests, the 200-mm-thick base courses were

constructed in 2 or 3 lifts. The reinforced base consisted of a 150-mm-thick geocell-reinforced layer and a 50-mm-thick cover layer. The vibratory compactor was used for the unreinforced sections. For the geocell-reinforced bases, the geocell was first placed over the subgrade with each edge fixed with rebar as shown in Figure 5.6. The first lift was compacted in each cell individually with an air-driven compactor operating at 550 kPa (80 psi), as shown in Figure 5.7. The air compactor has a 130-mm diameter plate. The second lift was compacted with the vibration compactor when the cover layer consisted of the same geomaterial as the first lift. Under the circumstance of the cover layer with different geomaterial, the second lift was also compacted with the air compactor and the cover layer was compacted with the vibratory compactor. For the geogrid tests, the base was compacted with the same electric vibration compactor in two lifts.

Figure 5.5: Installation of Earth Pressure Cell

Figure 5.6: Placement of Geocell

Figure 5.7: Air-Driven Compacter

Three LWD (light weight deflectometer) tests and four DCP (dynamic cone penetrometer) tests were conducted prior to the plate loading test. The CBR value of the geomaterial was calculated from the DCP tests based on Equation 5.2 from ASTM D6951 (2015).

$$\mathbf{CBR}(\%) = \frac{\mathbf{292}}{\boldsymbol{DCP}^{\mathbf{1.12}}} \qquad \textbf{Equation 5.2}$$

Where:

DCP = measured in mm/blow

5.2 Test Results and Discussions

The test results and discussions will be presented separately in this chapter, as the base thicknesses were different for the geocell and geogrid tests.

5.2.1 Geocell Reinforced Bases

Six test sections under cyclic plate loading tests were evaluated in this study. The base was constructed over approximately 5% CBR subgrade. Table 5.1 presents a summary of these tests with different base combinations.

Table 5.1: Summary of Base Combinations for Geocell Test Sections

Test/Section No.	Base Course	
	Cover layer (50 mm)	Sub layer (150 mm)
1*	AB-3	AB-3
2*	Mixture	Mixture
3	Mixture	Geocell-reinforced mixture
4	AB-3	Geocell-reinforced mixture
5	Topsoil	Geocell-reinforced mixture
6	Topsoil	Geocell-reinforced topsoil

5.2.1.1 Test 1: 200-mm Aggregate Base

The control test consisted of a 200-mm-thick AB-3 aggregate base over 5% CBR subgrade. The subgrade strength was at 4.1% CBR based on the vane shear correlation, while the DCP data indicated a subgrade strength of 6.1% CBR. The base course CBR was 11% based on DCP.

Figure 5.8 presents the surface permanent and rebound deformations of the loading plate with the number of cycles. Figure 5.9 presents the interface pressures at different pressure cell locations. Surface permanent deformations at 300 and 450 mm from the center of the plate are presented in Figure 5.10, in which the positive value indicates settlement.

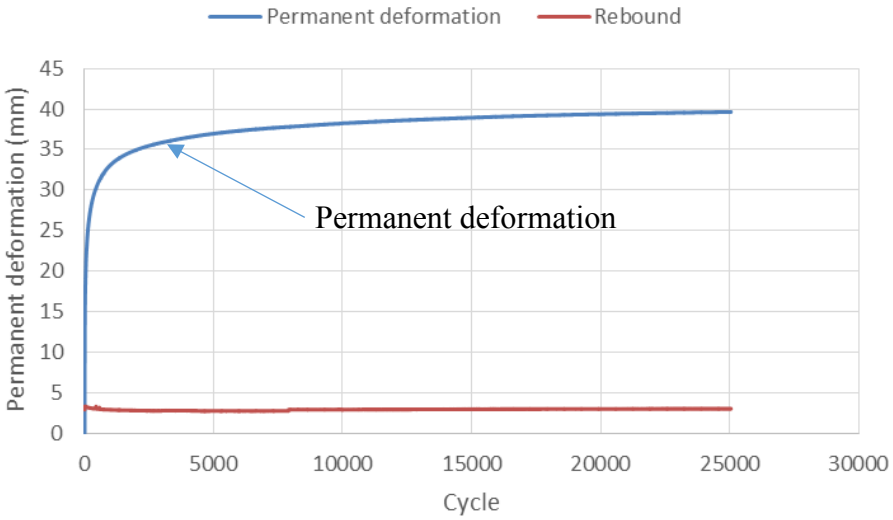

Figure 5.8: Permanent and Elastic Rebound Deformations of the Loading Plate in Test 1

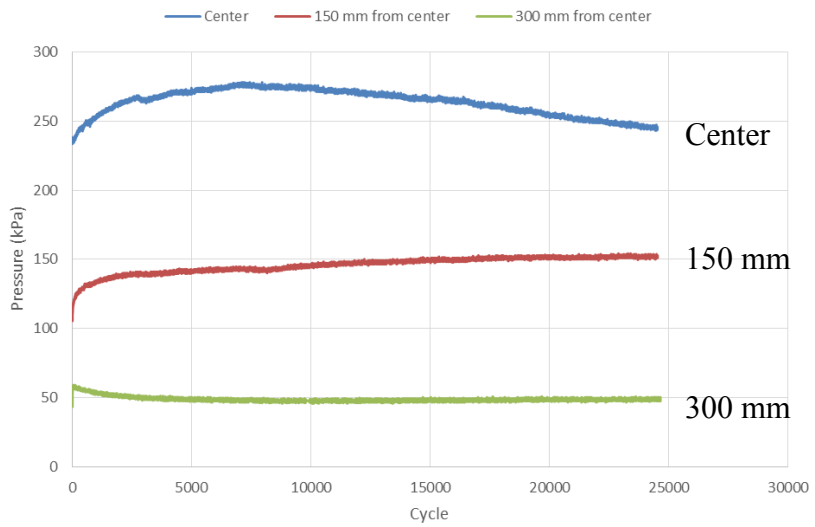

Figure 5.9: Interface Pressures at Various Locations in Test 1

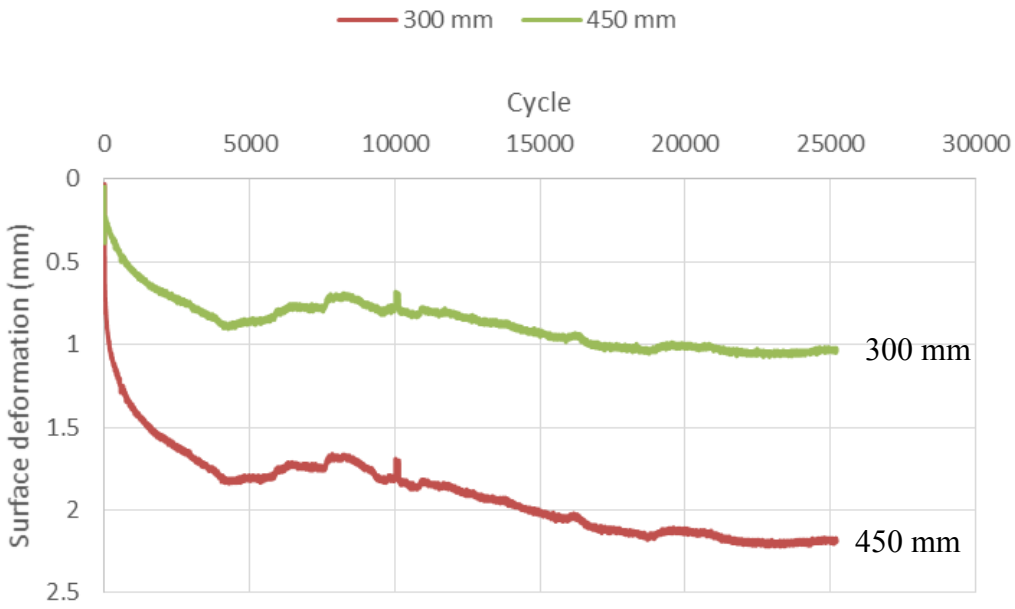

Figure 5.10: Surface Permanent Deformations at Distances from the Center in Test 1

The test was interrupted several times due to the overheating of the oil pump. The test was terminated at the pre-set maximum number of cycles (i.e., 25,000 cycles) before reaching the failure criterion of 75 mm. The permanent deformation at 25,000 cycles was approximately 39.6 mm. The average elastic rebound deformation was 2.9 mm. The interface pressure at the center of the loading plate first increased then decreased. The highest pressure recorded on the

center pressure cell was 278 kPa. The interface pressure at 150 mm from the center of the loading plate increased rapidly in the first 100 cycles from 105 to 121 kPa. Then the pressure continued to increase at a slower rate, and at 25,000 cycles, the pressure was at 154 kPa. The interface pressure at 300 mm from the center gradually decreased from 57 to 49 kPa. The earth pressure cell at 600 mm from the center did not record any pressure significant enough to be distinguished from the noise; thus, it was not presented. Figure 5.10 shows that the surface permanent deformations away from the plate were small.

5.2.1.2 Test 2: 200-mm Soil-Aggregate Mixture Base

The vane shear test data indicated the subgrade had a CBR of 5.1%. The DCP test indicated a 4.9% CBR of the base and 7.5% CBR of the subgrade. The LWD test showed an average elastic modulus of the base course at 29.1 MPa. The lower CBR value of the base course as compared with that in Test 1 was because of the existence of the topsoil in the mixture and the higher moisture content in the preparation.

Figure 5.11 presents the permanent and rebound deformations of the loading plate with the number of cycles. Figure 5.12 presents the interface pressure at different pressure cell locations. Surface permanent deformations at the distances of 300, 450, and 600 mm from the center of the plate are presented in Figure 5.13, in which the positive value indicates settlement and the negative value indicates heave.

The 200-mm-thick soil-aggregate mixture base did not reach the 75-mm permanent deformation failure criterion; thus the test was terminated at 25,000 cycles. The final permanent deformation under the loading plate was approximately 65 mm. The average elastic deformation under the loading plate was 2.9 mm. Figure 5.13 indicates that the surface around the loading plate first heaved then settled. The surface permanent deformations indicated the settlements (but less than 0.6 mm) at 300 and 600 mm and heave at 450 mm from the center. The earth pressure cell at 150 mm from the center was damaged at the 26^{th} loading cycle. Within the first 26 cycles, the interface pressure at 150 mm increased from 143 to 212 kPa rapidly. The interface pressure at the center increased from 257 kPa at the first loading cycle to a peak value of 323 kPa at approximately 300 cycles then remained relatively constant. The interface pressure at 300 mm

from the center decreased from 40 to 27 kPa within the first 5,000 cycles and then remained constant. The earth pressure cell at 600 mm from the center did not record any pressure significant enough to be distinguished from the noise; thus, it was not presented.

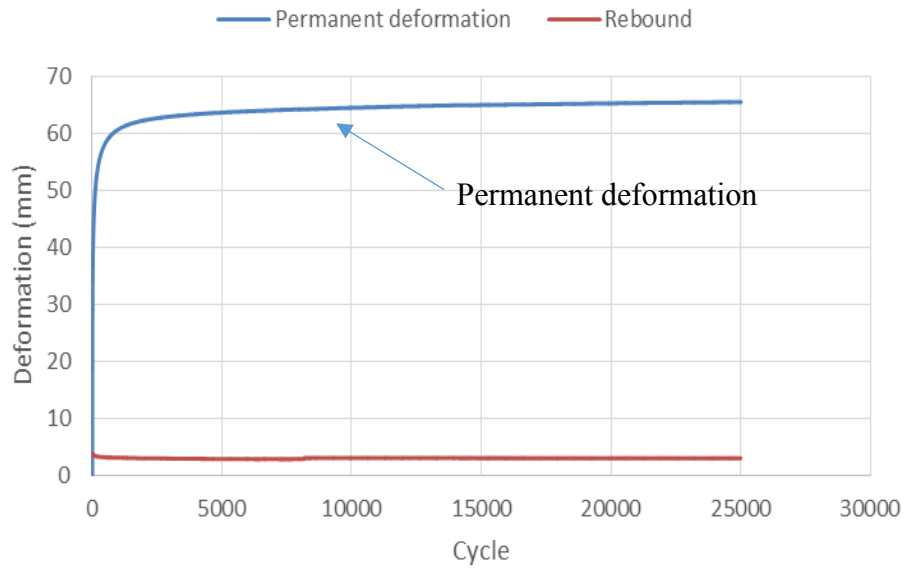

Figure 5.11: Permanent and Elastic Rebound Deformations of the Loading Plate in Test 2

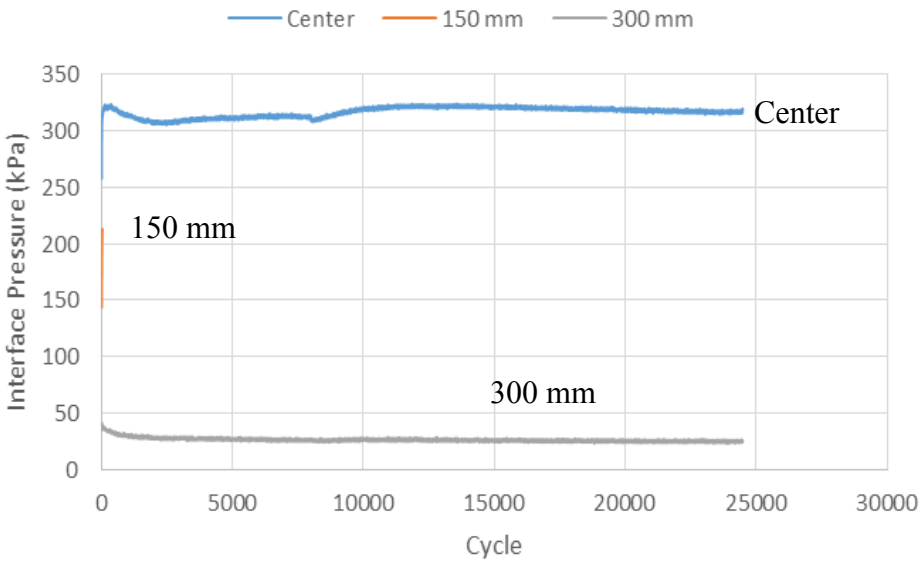

Figure 5.12: Interface Pressures at Various Locations in Test 2

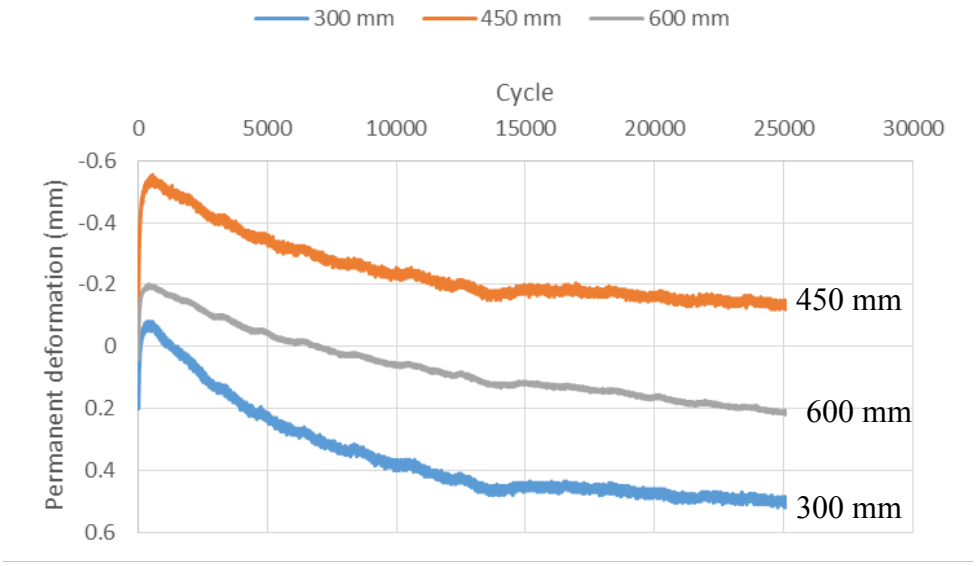

Figure 5.13: Surface Permanent Deformations at Distances from the Center in Test 2

5.2.1.3 Test 3: 200-mm Geocell-Reinforced Soil-Aggregate Mixture Base

The vane shear tests indicated a 4.7% CBR for the subgrade. The DCP tests showed 8% CBR for the base course and 6.1% CBR for the subgrade. The LWD test indicated the elastic modulus of the base course was 34.2 MPa.

Figure 5.14 presents the permanent and elastic rebound deformations with the number of cycles. Figure 5.15 presents the interface pressures at different pressure cell locations. The surface permanent deformations at distances of 300, 450, and 600 mm are presented in Figure 5.16.

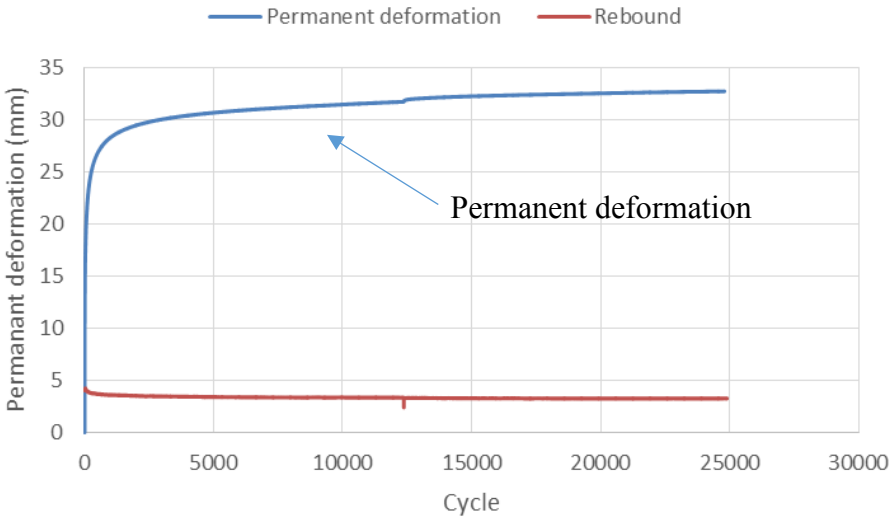

Figure 5.14: Permanent and Elastic Rebound Deformations of the Loading Plate in Test 3

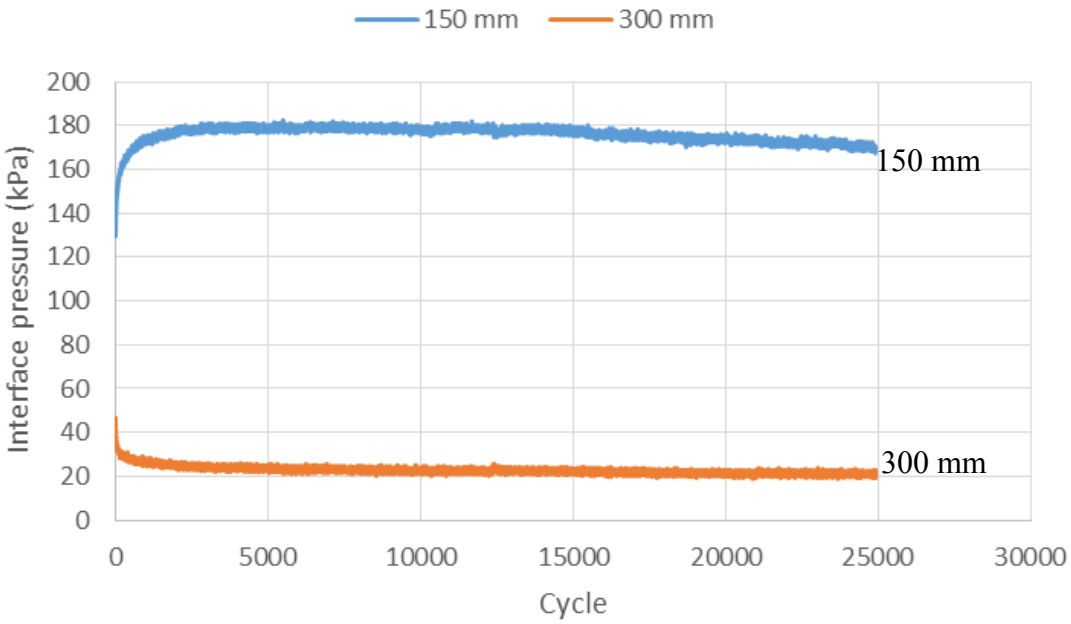

Figure 5.15: Interface Pressures at Various Locations in Test 3

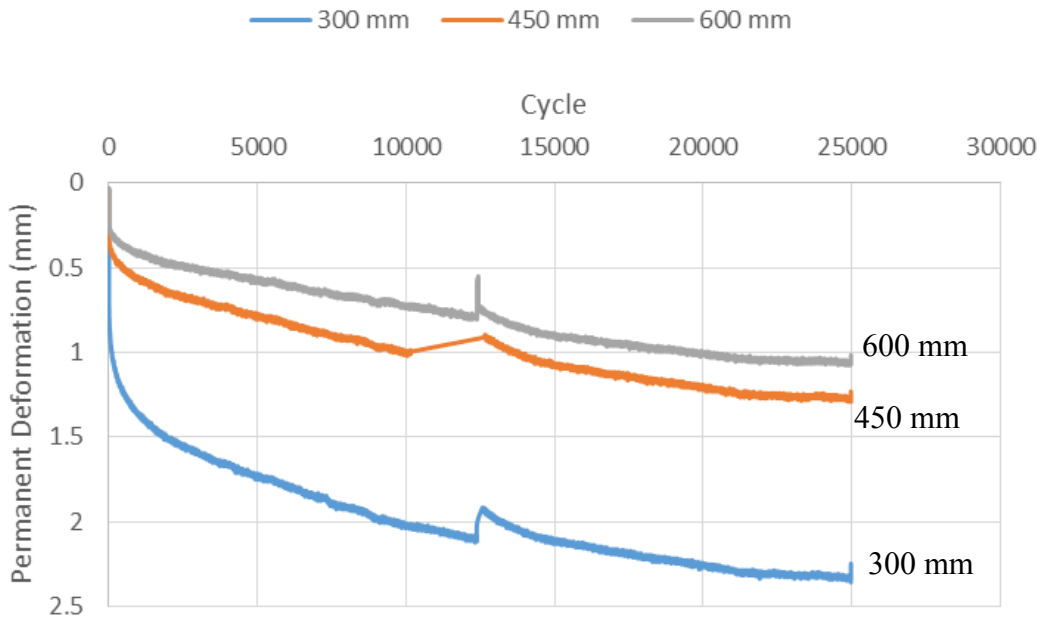

Figure 5.16: Surface Permanent Deformations at Distances from the Center in Test 3

Test 3 was paused at around 12,000 cycles due to the overheating of the oil pump. The test was terminated at 25,000 cycles and the final permanent deformation was 32.7 mm. The average elastic deformation under the loading plate was 3.4 mm. The pressure cell at the center was damaged during installation. The interface pressure at 150 mm from the center increased rapidly from 130 to 180 kPa in the first 2,500 cycles and then decreased slightly after 15,000 cycles. The interface pressure at 300 mm from the center decreased from 40 kPa to approximately 20 kPa. The earth pressure cell at 600 mm from the center did not record any pressure significant enough to be distinguished from the noise; thus, it was not presented. The surface of the test section settled over the process of the test at all three measured locations. At 300 mm from the center, the final permanent deformation was 2.4 mm.

5.2.1.4 Test 4: 50-mm-Thick AB-3 over 150-mm Geocell-Reinforced Soil-Aggregate Mixture

The vane shear tests showed a 4.4% CBR subgrade. The DCP tests indicated the base course CBR at 8.2% and the subgrade CBR at 6.0%. The LWD tests indicated the base elastic modulus was 34.3 MPa.

Figure 5.17 presents the permanent and elastic rebound deformations of the loading plate. Figure 5.18 presents the interface pressures at different pressure cell locations. The surface permanent deformations at distances of 300, 450, and 600 mm are presented in Figure 5.19.

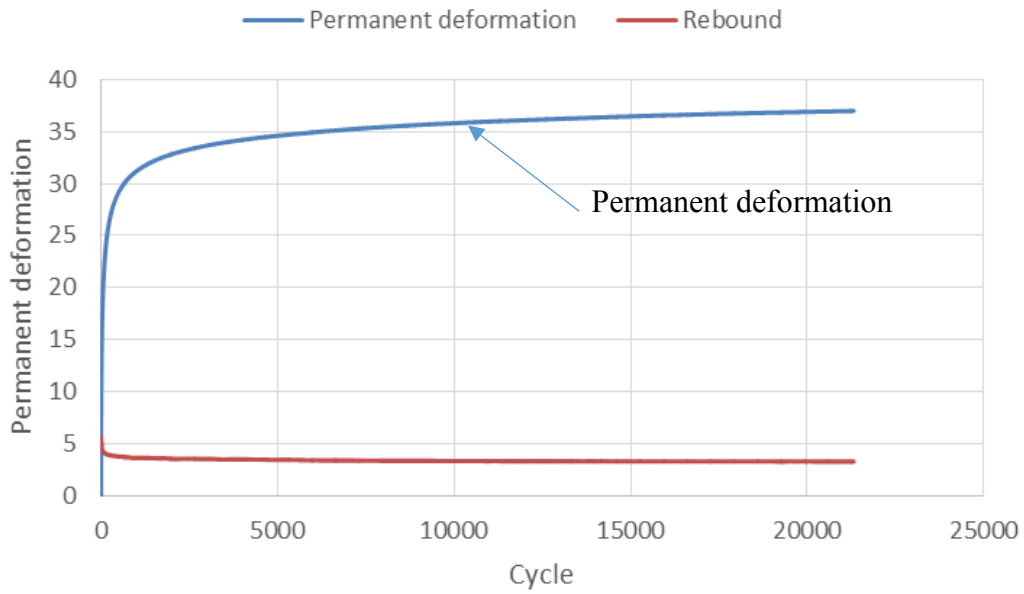

Figure 5.17: Permanent and Elastic Rebound Deformations of the Loading Plate in Test 4

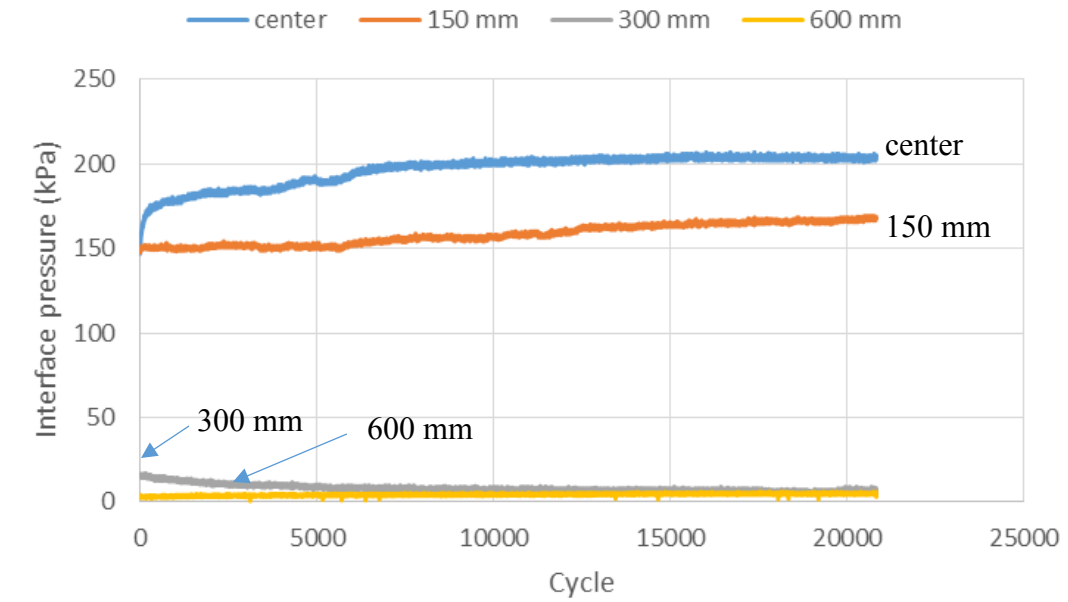

Figure 5.18: Interface Pressures at Various Locations in Test 4

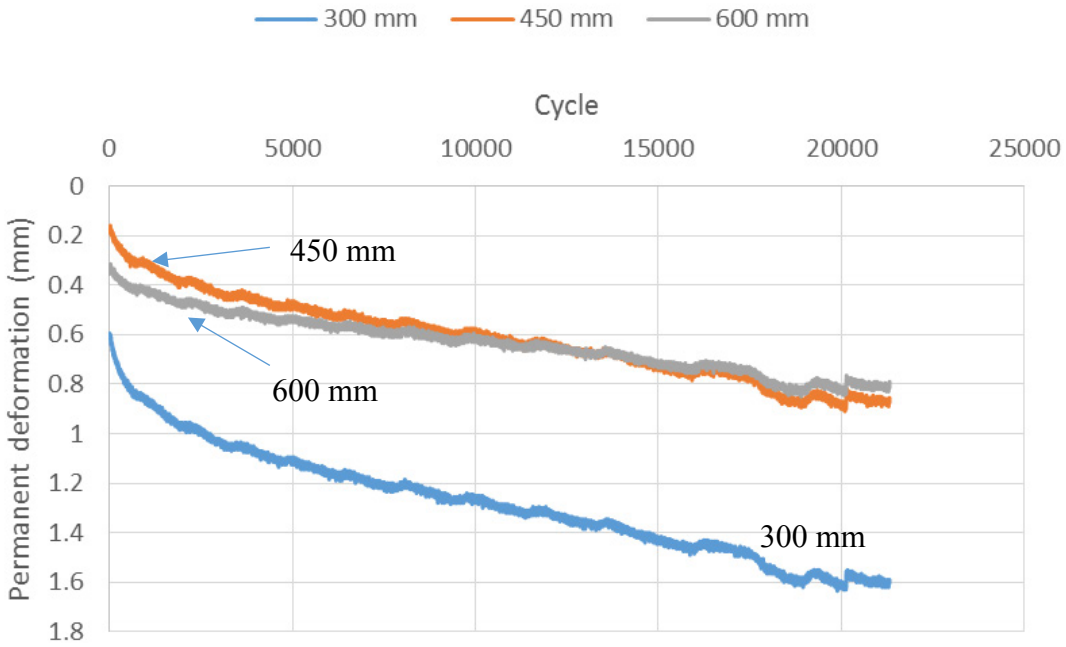

Figure 5.19: Surface Permanent Deformations at Distances from the Center in Test 4

The test was terminated at 22,000 cycles. The test section had a final permanent deformation of 37 mm. The average elastic deformation was 3.4 mm. The center interface pressure increased from 150 to 200 kPa within the first 7,500 cycles and increased slightly in the rest of the test. The interface pressure at 150 mm from the center remained constant in the first 5,500 cycles and then started to increase and reached a maximum value of 170 kPa. The interface pressure at 300 mm from the center decreased from 16 to 7 kPa gradually over the test period. The interface pressure at 600 mm from the center started from 3 kPa and reached 5 kPa at the end of the test. The surface of the test section settled as the test progressed. At 300 mm from the center, the surface settled 1.6 mm at the end of the test while the surfaces at 450 and 600 mm from the center settled around 0.8 mm.

5.2.1.5 Test 5: 50-mm-Thick Topsoil over 150-mm Geocell-Reinforced Soil-Aggregate Mixture

The vane shear tests showed a 4.5% CBR subgrade. The DCP tests indicated the base course CBR at 5% and the subgrade CBR at 7%. The LWD tests indicated the base elastic modulus was 15.7 MPa.

Figure 5.20 presents the permanent and elastic rebound deformations of the loading plate. Figure 5.21 presents the interface pressures at different pressure cell locations. The surface deformations at distances of 300, 450, and 600 mm from the center are presented in Figure 5.22.

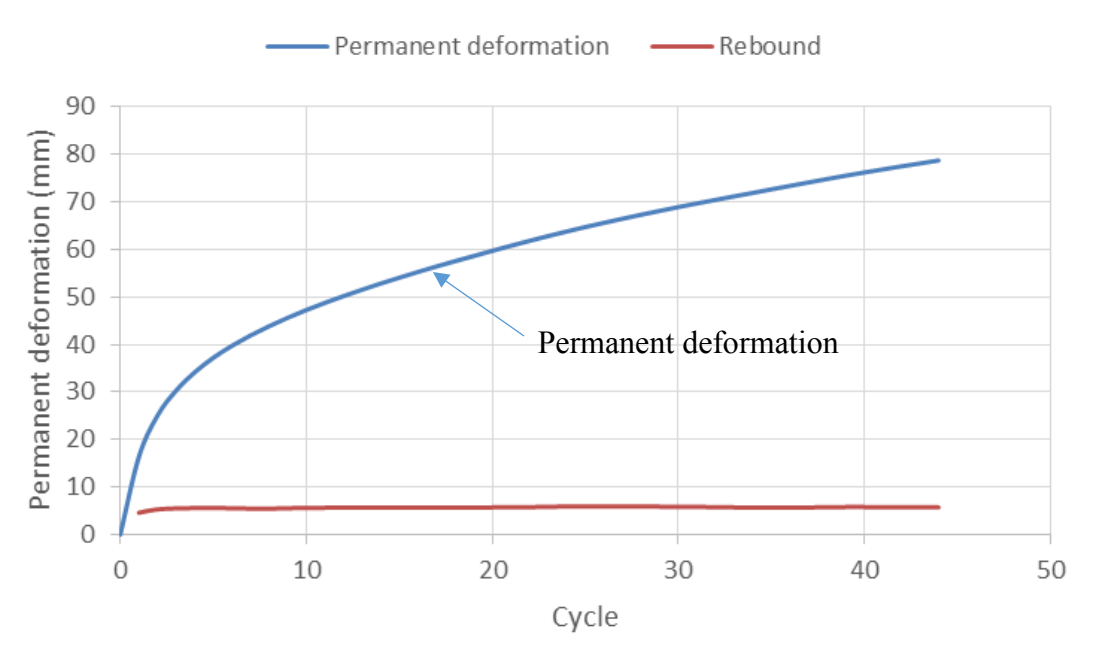

Figure 5.20: Permanent and Elastic Rebound Deformations of the Loading Plate in Test 5

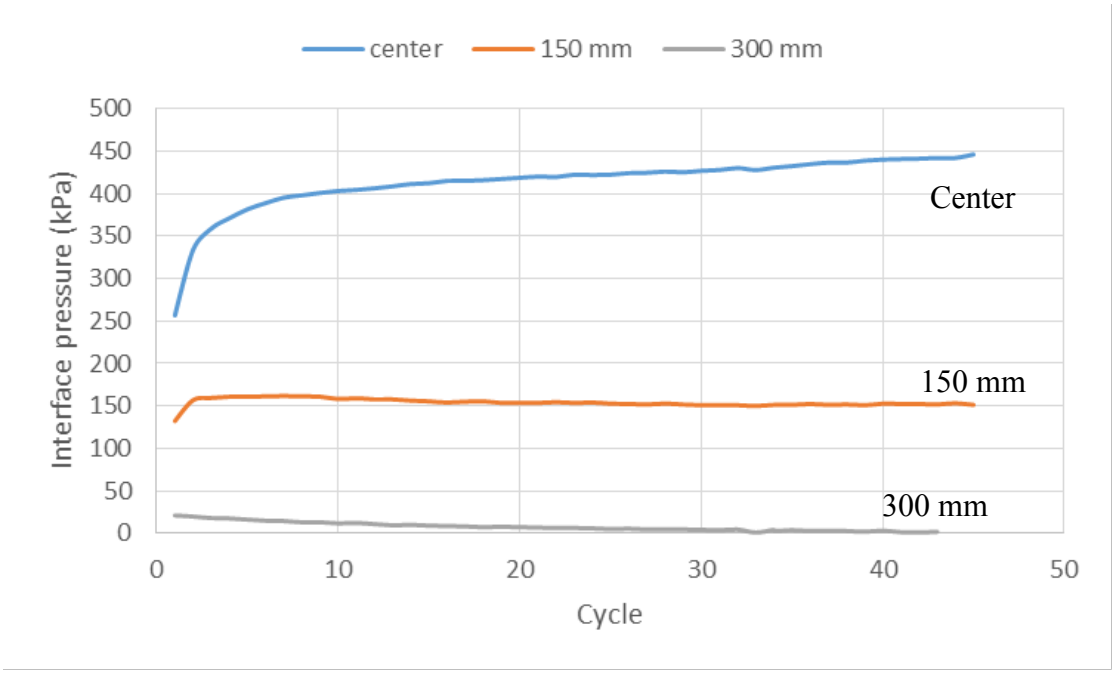

Figure 5.21: Interface Pressures at Various Locations in Test 5

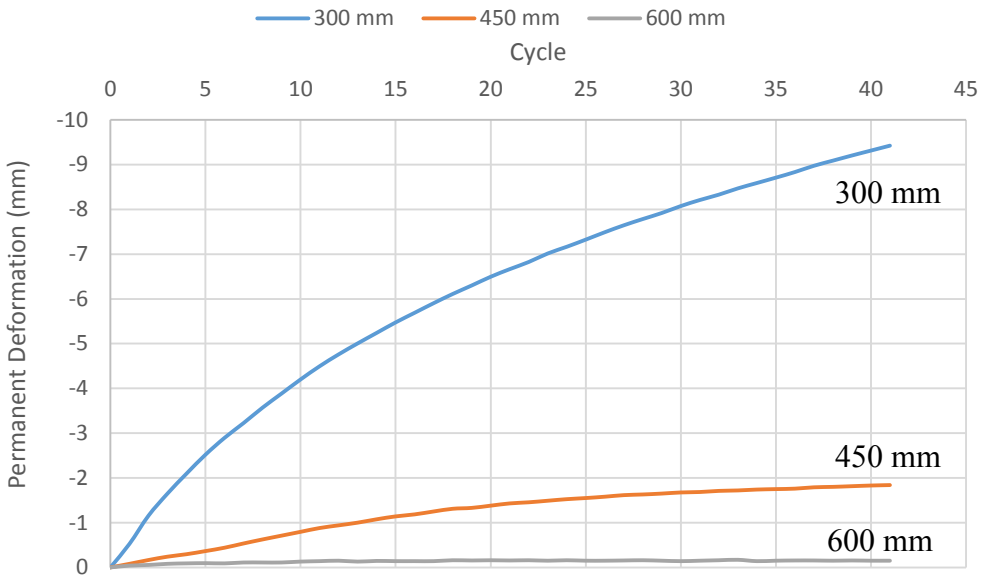

Figure 5.22: Surface Permanent Deformations at Distances from the Center in Test 5

Test 5 only lasted 39 cycles before reaching 75-mm permanent deformation. After failure, the test was continued to 44 cycles. The average elastic deformation was 5.7 mm. Both the earth pressure cells at the center and 150 mm from the center showed an increase in the pressure within the first 4 cycles. The center interface pressure continued increasing to 450 kPa while the interface pressure at 150 mm from the center slightly decreased after the first 4 cycles and maintained at 150 kPa. The interface pressure at 300 mm from the center decreased from 21 kPa initially to 1 kPa at the 40th cycle. The surface of the test section showed relatively large heave at the distances of 300 and 450 mm from the center, while the surface at a distance of 600 mm from the center remained unchanged. At the distance of 300 mm from the center, the surface heaved up approximately 9 mm, while at 450 mm from the center, the surface heaved approximately 2 mm at the end of the test. These heaves indicated the failure of the soil cover.

5.2.1.6 Test 6: 200-mm-Thick Geocell-Reinforced Topsoil

The vane shear tests showed a 4.5% CBR subgrade. The DCP tests indicated the base course CBR at 2.3% and the subgrade CBR at 4.4%. LWD tests indicated the base elastic modulus was 10.9 MPa.

Figure 5.23 presents the permanent and elastic rebound deformations of the loading plate with the number of cycles. Figure 5.24 presents the interface pressures at different pressure cell locations. The surface deformations at the distances of 300, 450, and 600 mm are presented in Figure 5.25.

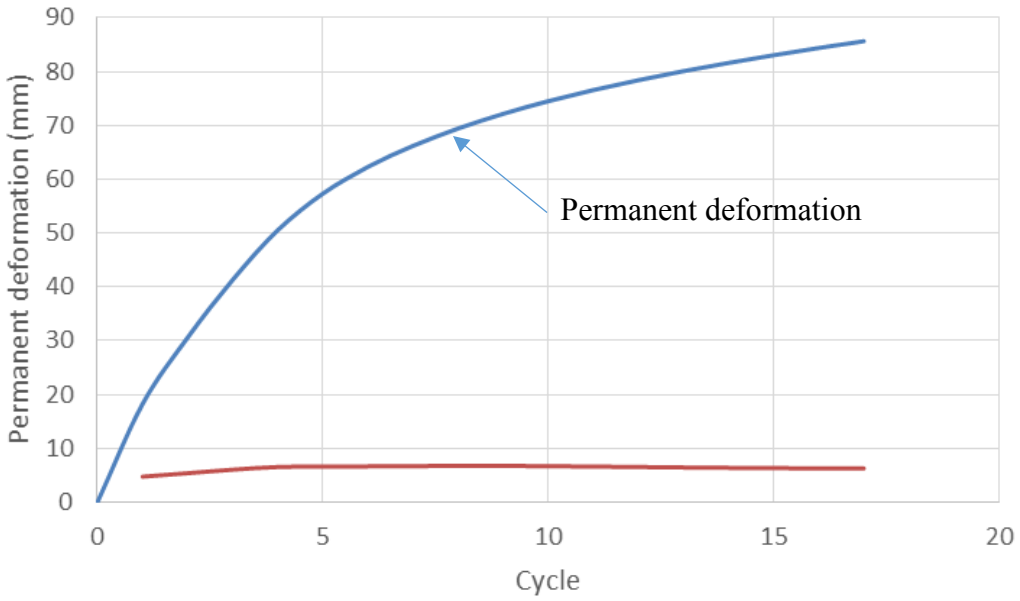

Figure 5.23: Permanent and Elastic Rebound Deformations of the Loading Plate in Test 6

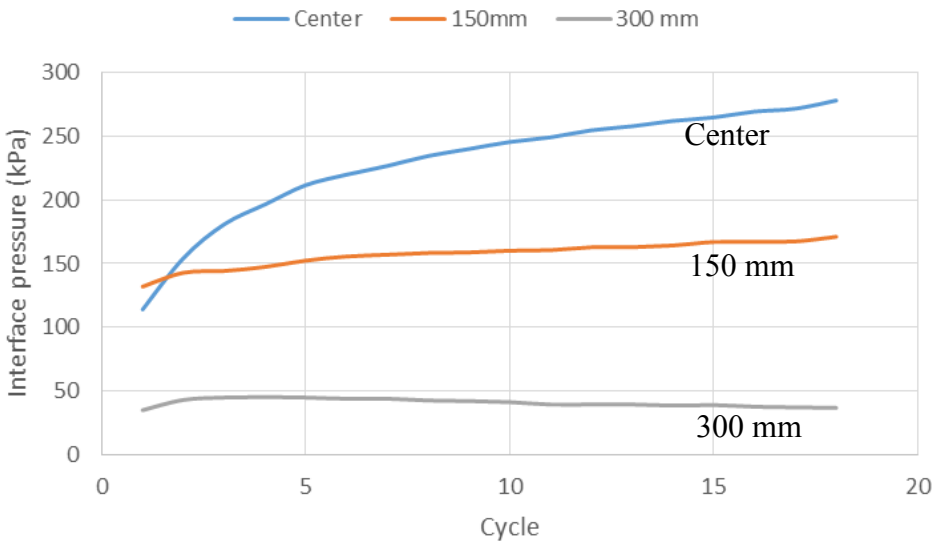

Figure 5.24: Interface Pressures at Various Locations in Test 6

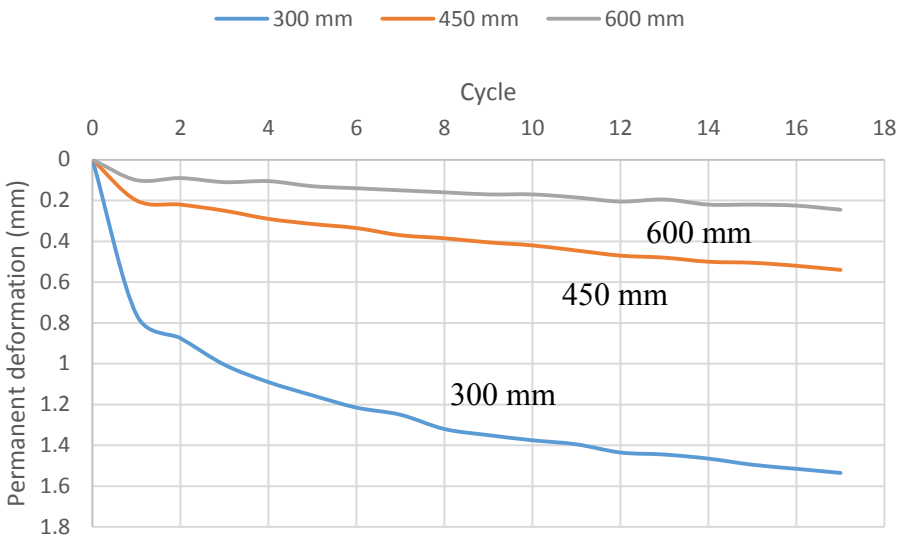

Figure 5.25: Surface Permanent Deformations at Distances from the Center in Test 6

In Test 6, the test section reached the 75 mm failure criterion at the 11th cycle. The test was then terminated at the 18th cycle. The average elastic deformation was 6.3 mm. The interface pressures at both the center and the distance of 150 mm from the center increased with the number of cycles. The interface pressure at the center increased from 114 kPa to 278 kPa at the 18th cycle and showed no sign of stabilization. The interface pressure at the distance of 150 mm from the center increased more gradually as compared with that at the center, for example, 132 kPa at the 1st cycle and 171 kPa at the 18th cycle. The interface pressure at the distance of 300 mm increased from 35 kPa to 45 kPa in the first 5 cycles and then decreased to 37 kPa at the end of the test. The surface deformations indicated the surface of the test section settled slightly at the end of the test.

5.2.1.7 Discussions

The permanent deformation and elastic deformation under the loading plate as well as the subgrade and base course strengths from each test are listed in Table 5.2. In this table, the DCP test data are used to calculate the subgrade and base CBR values.

The only two test sections in Tests 5 and 6 failed due to the excessive deformation, both of which contained a topsoil cover layer. The topsoil was compacted at the moisture content of

21% to produce the maximum dry density. As compared with the aggregate cover and the soil-aggregate mixture cover, the topsoil cover was much softer and weaker, thus yielding lower elastic moduli and higher elastic deformations.

Both Test Sections 2 and 3 consisted of a 200-mm-thick mixture base course. However, at 20,000 cycles, the reinforced section (i.e., Test 3) outperformed the unreinforced section (i.e., Test 2) by a large margin. The plate permanent deformation of the reinforced section at 20,000 cycles was less than half of that of the unreinforced section, despite the subgrade in the unreinforced section being stronger. In addition, the elastic modulus of Test Section 3 was 17.5% higher than that of Test Section 2, which might result from the combined effect of the different compaction method and the geocell reinforcement.

Test Sections 3 and 4 performed similarly. Both sections had the LWD elastic modulus of 34 MPa and the elastic deformation of 3.4 mm. Test Section 3 had a slightly less permanent deformation at 20,000 cycles than Test Section 4. The 50-mm AB-3 aggregate cover layer showed no more improvement than the 50-mm soil-aggregate mixture cover layer. Both Test Sections 3 and 4 performed slightly better than Test Section 1 despite Test Section 1 consisting of the base course with a higher CBR value.

All test sections except Test Section 5 had less than 2.5 mm surface settlement throughout the test based on the displacement measurements. In Test 5, the surface heaved at all three measured locations because of the failure of the topsoil cover.

Table 5.2: Summary of Deformation Under Loading Plate for Geocell Study

Section No.	*Subgrade CBR*	*Base CBR*	*Base elastic modulus*	*Plate permanent deformation at 20,000 cycles*	*Average plate elastic deformation*
	%	**%**	**MPa**	**mm**	**mm**
1	6.1	11	-	39	2.9
2	7.5	4.9	29.1	65	2.9
3	6.1	8	34.2	32	3.4
4	6	8.2	34.3	37	3.4
5	7	5	15.7	[?]	5.7
6	4.4	2.3	10.9	[?]	6.3

[?] Test terminated prior to 20,000 cycles due to the excessive deformation

Note: CBR data obtained by DCP tests

Figure 5.26 presents the comparison of the interface pressures at the 15th cycle. Section 3 and Section 4 showed significantly lower center interface pressure, which indicated the geocell-reinforced base effectively reduced the pressure on subgrade directly blow the loading plate. Section 5 showed the greatest center pressure partially due to the base consisting of a low strength cover layer and a strong reinforced layer. The weak cover layer reduced the effective thickness of the base and failed before the reinforced base was mobilized.

Figure 5.27 presents the comparison of interface pressures at the 20,000th cycle for all six test sections. The interface pressure at the distance of 300 mm in Test Section 2 and the interface pressure at the center in Test Section 3 were estimated based on the applied load and the pressures measured by functional pressure cells. The interface pressures at the center at the 20,000th cycle were higher than those at the 15th cycle. The interface pressures at the center in Test Sections 3 and 4 were lower than those in Test Sections 1 and 2.

The bearing capacity of the subgrade in unreinforced, geotextile or geocell-reinforced, and geogrid-reinforced sections can be evaluated by Equation 5.3 (Giroud & Han, 2004a; Pokharel et al., 2010):

$$q = N_c c_u \qquad \textbf{Equation 5.3}$$

Where:

q = bearing capacity, kPa;

N_c = bearing capacity factor, 3.14 for an unreinforced section, 5.14 for a woven geotextile or geoccell section, and 5.71 for a geogrid section; and

c_u = undrained shear strength, kPa.

The undrained shear strength, c_u, of each test section was approximately deduced from the CBR value of the subgrade soil using Equation 5.4 (Pokharel, 2010):

$$c_u = 20CBR \qquad \textbf{Equation 5.4}$$

Based on the calculation, the vertical stress at the center was lower than the bearing capacity of subgrade in all sections at both the 15th cycle and the 20,000th cycle. Thus, the excess

deformations in Sections 5 and 6 were most likely caused by the failure of base due to the use of the topsoil cover.

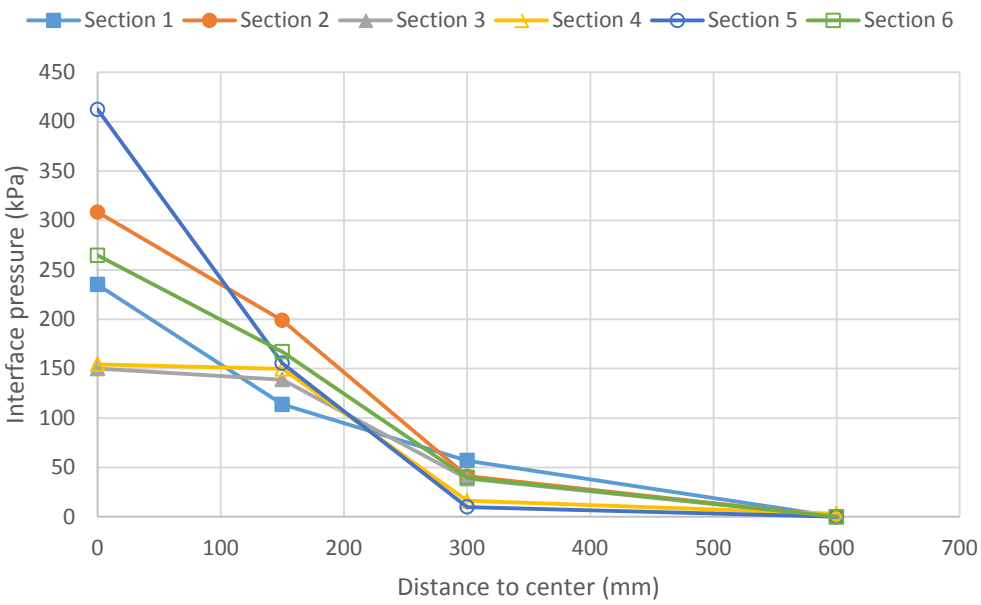

Figure 5.26: Interface Pressure Distributions for All Test Sections at the 15th Cycle

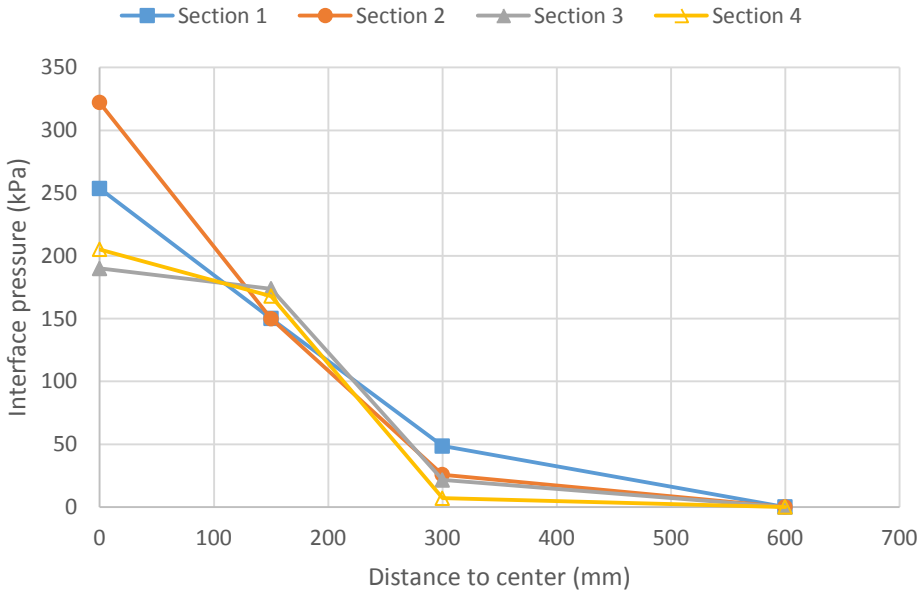

Figure 5.27: Interface Pressure Distributions for Test Sections 1 to 4 at the 20,000th Cycle

5.2.2 Geogrid-Reinforced Bases

Eight test sections under cyclic plate loading tests were evaluated in this study. Four test sections consisted of approximately 5% CBR subgrade while the other four consisted of approximately 3% CBR subgrade. As the geocell tests suggested, the sections with a topsoil cover layer reached the 75-mm permanent deformation failure criteria much sooner than other sections, thus for the geogrid test sections, a topsoil cover layer was not constructed. Table 5.3 presents a summary of soil conditions and base combinations of geogrid test sections. In addition to the same equipment used in the geocell test, telltales were installed on the top of subgrade to monitor the subgrade deformation. A telltale was made of a steel rod inside a copper tube. One end of the steel rod was welded to a steel washer, which was placed on the subgrade. The steel rod could move freely inside the copper tube. The displacements of steel rods, which were also measured by LVDTs at 10 Hz frequency, represent the displacements of the subgrade.

Table 5.3: Summary of Soil Conditions and Base Combinations for Geogrid Test Sections

Test No.	Stabilized condition	CBR by DCP (%)		
		Subgrade	Base course	
			AB-3	AB-3-soil mixture
7	Unreinforced	3.3	14.3	
8	Geogrid-reinforced	3.5	13.7	
9	Unreinforced	3.1		10.5
10	Geogrid-reinforced	3.4		9.8
11	Unreinforced	4.8	14.6	
12	Geogrid-reinforced	5.2	15.5	
13	Unreinforced	4.6		9.5
14	Geogrid-reinforced	4.9		10.2

5.2.2.1 Test 7: Unreinforced Test Section with AB-3 Base and 3% CBR Subgrade

In Test 7, the test section reached the 75-mm failure criterion at approximately the 180th cycle as shown in Figure 5.28. The center permanent deformation increased rapidly within the first 25 cycles and then increased at a slower rate without any sign of stabilization. The surface deformation at the distance of 0.5 m from the center showed no significant change. The interface pressures at the center increased with the number of cycles as shown in Figure 5.29. The interface pressure at the center increased from 208 to 260 kPa at the 180th cycle. The interface pressure at the distance of 0.18 m from the center increased slightly from 170 to 187 kPa within the first 25 cycles then started to decrease, and at the 180th cycle, the interface pressure was 172 kPa, approximately the same as the initial pressure. The interface pressure at the distance of 0.3 and 0.45 m decreased with the increasing number of loading cycles and eventually reached zero.

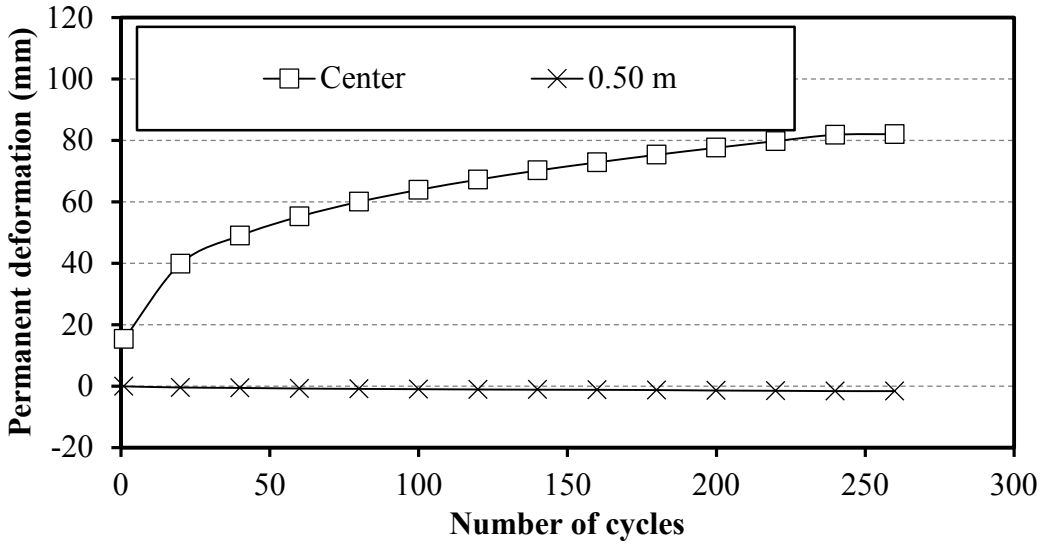

Figure 5.28: Permanent Deformations vs. Number of Loading Cycles for the Unreinforced Test Section with AB-3 Base and 3% CBR Subgrade

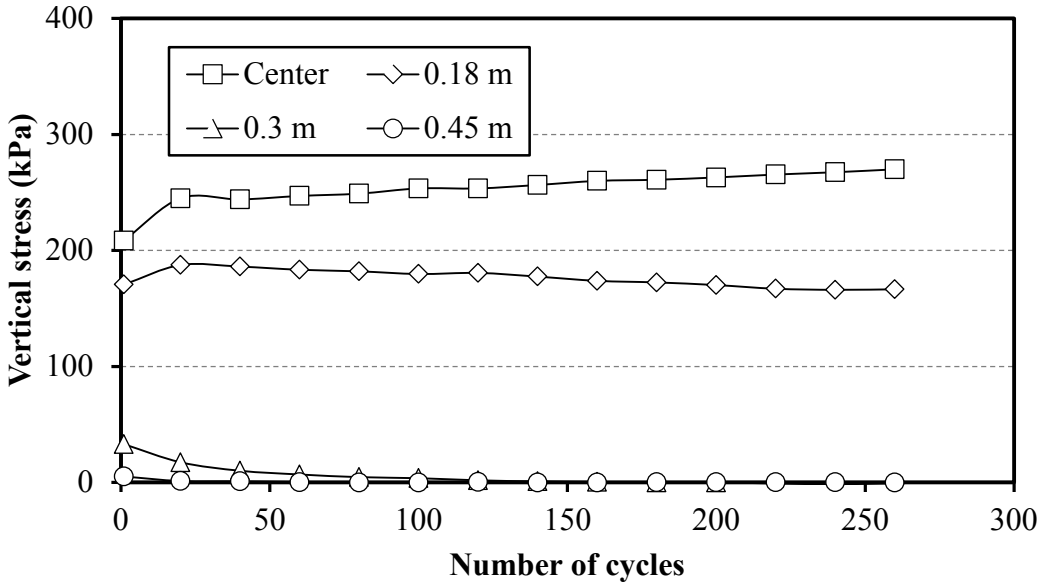

Figure 5.29: Vertical Stresses at the Interface vs. Number of Loading Cycles for the Unreinforced Test Section with AB-3 Base and 3% CBR Subgrade

5.2.2.2 Test 8: Geogrid-Reinforced Test Section with AB-3 Base and 3% CBR Subgrade

In Test 8, the test section reached the 75-mm failure criterion at approximately the 790th cycle as shown in Figure 5.30. The center permanent deformation increased rapidly within the first 40 cycles and then increased at a slower rate without any sign of stabilization. The deformation at the distance of 0.5 m from the center showed no significant change. The interface pressure at the center increased with the number of cycles as shown in Figure 5.31. The interface pressure at the center increased from 215 to 285 kPa from the beginning to the 580th cycle. The interface pressure at the distance of 0.18 m from the center increased rapidly from 98 to 257 kPa within the first 40 cycles, surpassing the interface pressure at the center. Then the interface pressure at 0.18 m from the center increased in a much slower rate and peaked at the 160th cycle and maintained a steady pressure in later loading cycles. The interface pressure at the distance of 0.3 and 0.45 m decreased with the increasing number of loading cycles and eventually stabilized at 10 and 0 kPa, respectively.

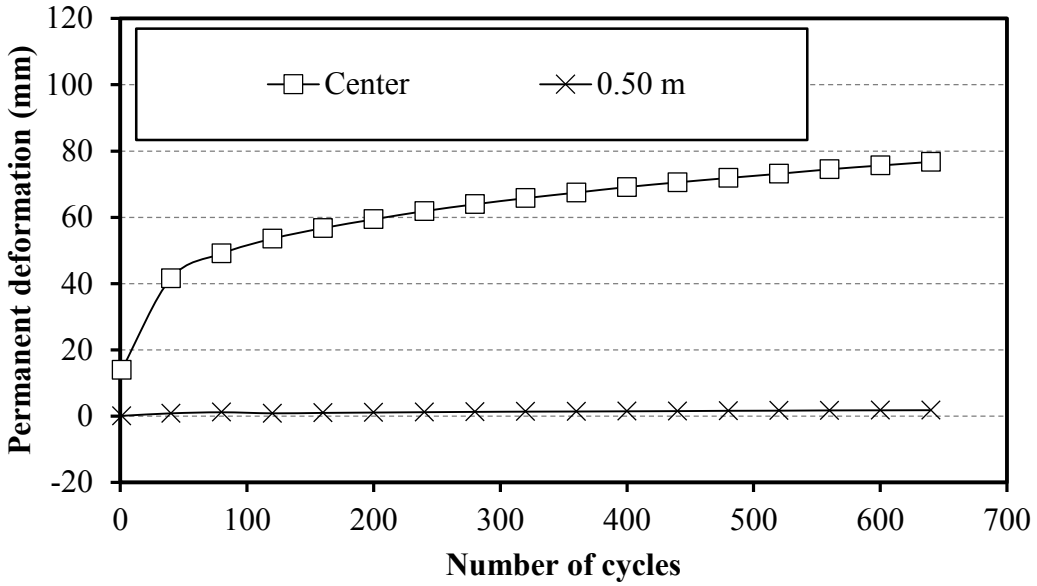

Figure 5.30: Permanent Deformations vs. Number of Loading Cycles for the Geogrid-Reinforced Test Section with AB-3 Base and 3%-CBR Subgrade

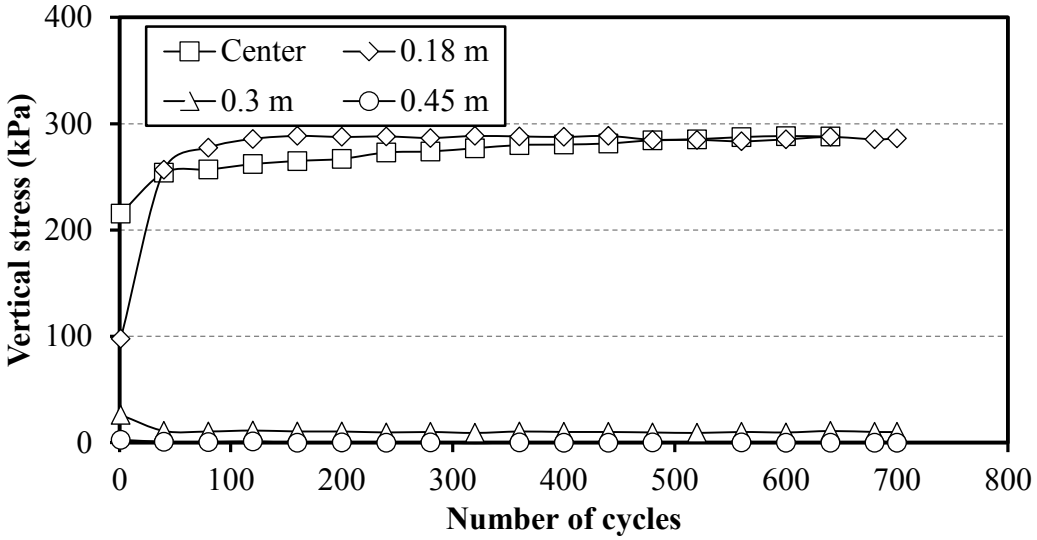

Figure 5.31: Vertical Stresses at the Interface vs. Number of Loading Cycles for the Geogrid Stabilized Test Section with AB-3 Base and 3% CBR Subgrade

5.2.2.3 Test 9: Unreinforced Test Section with AB-3 Base and 5% CBR Subgrade

In Test 9, the test section did not reach the 75-mm failure criterion and was terminated at 2,000 cycles as shown in Figure 5.32. At the 2,000th cycle, the permanent deformation at the center was 69 mm. The center permanent deformation increased rapidly to 38 mm within the first 100 cycles and then increased at a slower rate until the 2,000th cycle. The deformations at the distances of 0.18, 0.3, and 0.45 m from the center were small. The interface pressures at the center increased with the number of cycles as shown in Figure 5.33. The interface pressure at the center increased from 244 to 297 kPa within the first 1,000 cycles, then maintained at approximate 300 kPa in the later loading cycles. The interface pressure at the distance of 0.18 m was maintained at approximate 255 kPa throughout the test. The interface pressure at the distances of 0.3 and 0.45 m was less than 10 kPa throughout the test.

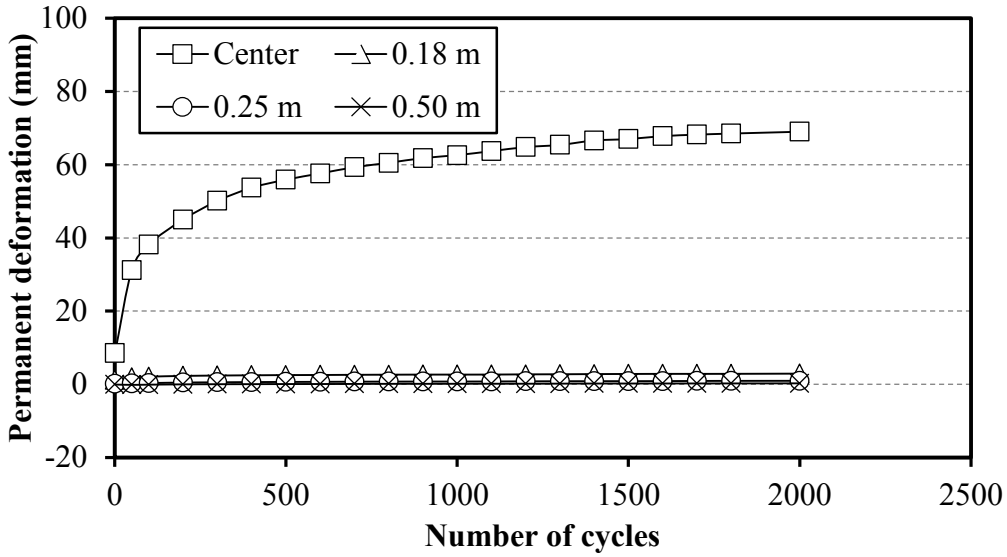

Figure 5.32: Permanent Deformations vs. Number of Loading Cycles for the Unreinforced Test Section with AB-3 Base and 5% CBR Subgrade

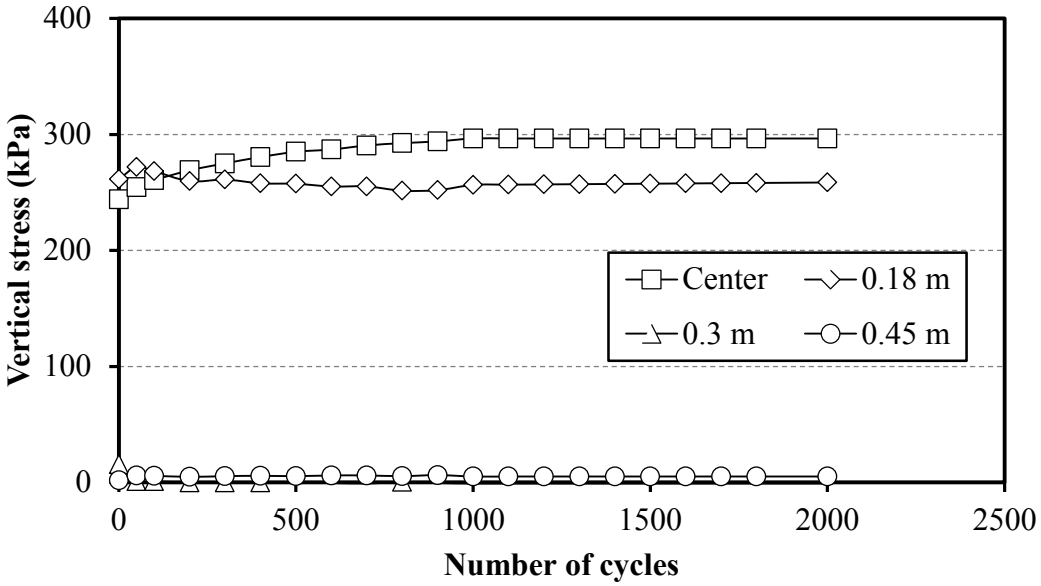

Figure 5.33: Vertical Stresses at the Interface vs. Number of Loading Cycles for the Unreinforced Test Section with AB-3 Base and 5% CBR Subgrade

5.2.2.4 Test 10: Geogrid-Reinforced Test Section with AB-3 Base and 5% CBR Subgrade

In Test 10, the test section did not reach the 75-mm failure criterion and was terminated at 3,000 cycles as shown in Figure 5.34. At the 3,000th cycle, the permanent deformation at the center was 61 mm. Then the center permanent deformation increased with the progress of the test at a slower rate and showed the sign of stabilization at the end of the test. The deformations at the distances of 0.18, 0.3, and 0.45 m from the center indicated slight heave; however, their magnitudes were insignificant. Figure 5.35 shows that the interface pressures at the center were maintained at approximate 267 kPa through the test. The interface pressure at the distance of 0.18 m from the center increased from 186 to 307 kPa from the beginning of the test to the 700th cycle then decreased to 248 kPa by the end of the test. The interface pressure at the distances of 0.3 and 0.45 m from the center decreased with the progress of the test. The interface pressure at the distance of 0.3 m from the center decreased from 35 kPa at the beginning of the test to 3 kPa at the end. The interface pressure at the distance of 0.45 m from the center was small.

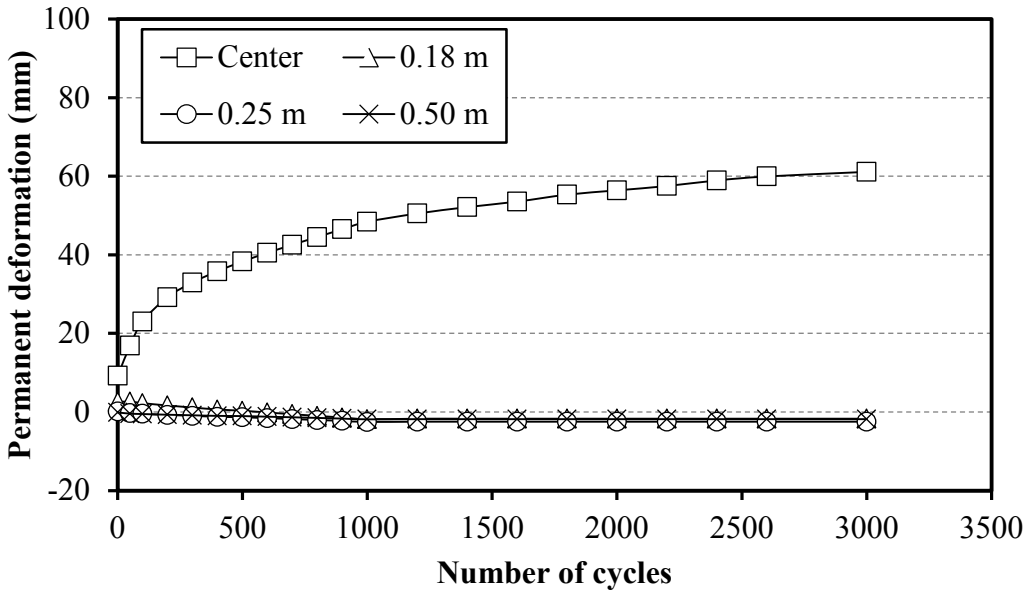

Figure 5.34: Permanent Deformations vs. Number of Loading Cycles for the Geogrid-Reinforced Test Section with AB-3 Base and 5% CBR Subgrade

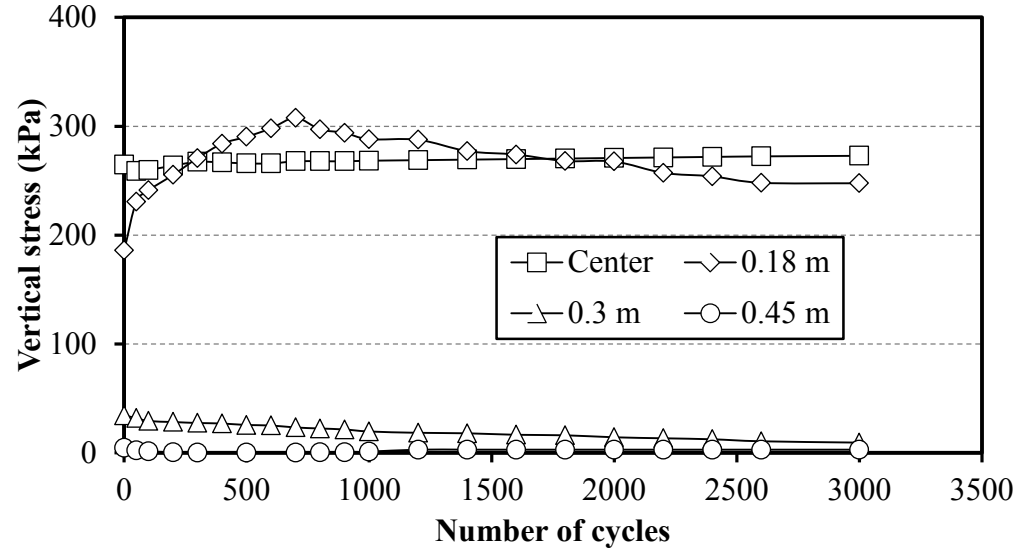

Figure 5.35: Vertical Stresses at the Interface vs. Number of Loading Cycles for the Geogrid-Reinforced Test Section with AB-3 Base and 5% CBR Subgrade

5.2.2.5 Test 11: Unreinforced Test Section with the Mixture Base and 3% CBR Subgrade

In Test 11, the test section reached the 75-mm failure criterion at the 105th cycles as shown in Figure 5.36. The deformations at distances of 0.18, 0.3, and 0.45 m from the center showed no significant change. The interface pressures at the center increased with the number of cycles as shown in Figure 5.37. The interface pressure at the center increased from 281 kPa at the start of the test to 329 kPa at the end. The interface pressure at the distance of 0.18 m from the center increased from 150 to 167 kPa within the first 20 cycles, then decreased to 157 kPa. The interface pressure at the distance of 0.3 m decreased from 22 to 0 kPa within the first 80 cycles. The interface pressure at 0.45 m from the center was small.

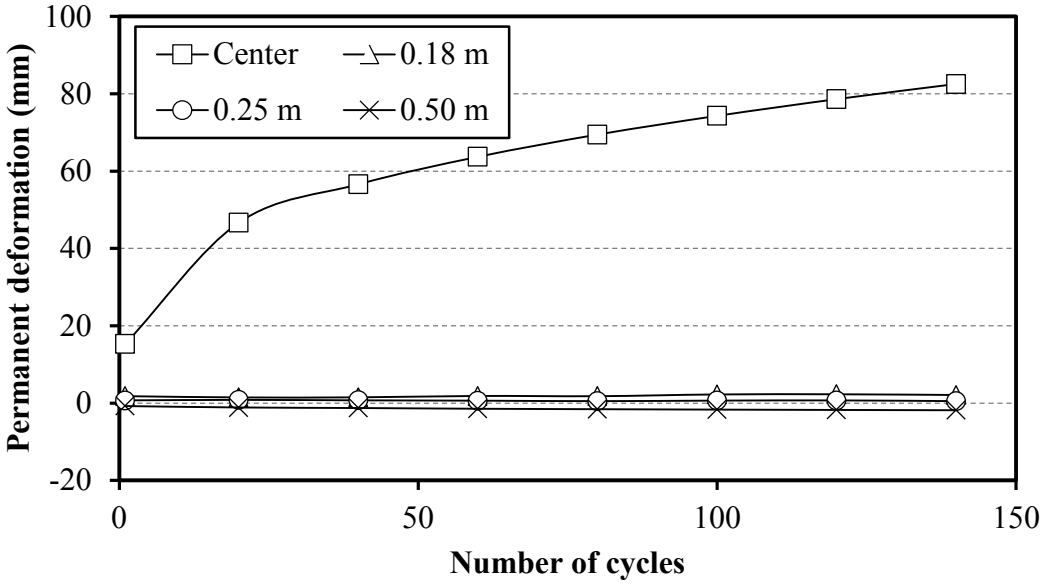

Figure 5.36: Permanent Deformations vs. Number of Loading Cycles for the Unreinforced Test Section with Mixture Base and 3% CBR Subgrade

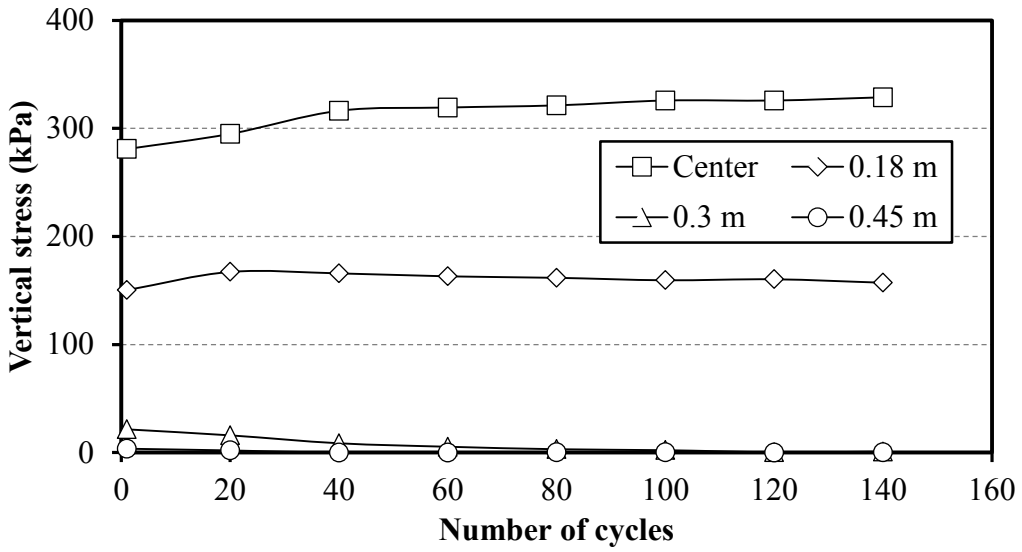

Figure 5.37: Vertical Stresses at the Interface vs. Number of Loading Cycles for the Unreinforced Test Section with Mixture Base and 3% CBR Subgrade

5.2.2.6 Test 12: Geogrid-Reinforced Section with the Mixture Base and 3% CBR Subgrade

In Test 12, the test was terminated at the 390th cycle due to mechanical issue of the equipment as shown in Figure 5.38; the permanent deformation at the center was 74 mm at the 390th cycle. Deformations at distances of 0.18, 0.3, and 0.45 m from the center showed no significant change. The interface pressure at the center increased from 267 to 303 kPa within the first 20 cycles, then decreased slightly to 293 kPa by the end of the test as shown in Figure 5.39. The interface pressure at the distance of 0.18 m from the center showed a similar trend as the interface pressure at the center, i.e., increased rapidly from 144 to 197 kPa within the first 20 cycles then was maintained at approximate 206 kPa in the later loading cycles. The interface pressure at the distance of 0.3 m from the center decreased slightly from 22 to 17 kPa within the first 20 cycles, then was maintained at approximate 17 kPa in the rest of the test. The interface pressure at 0.45 m from the center was small.

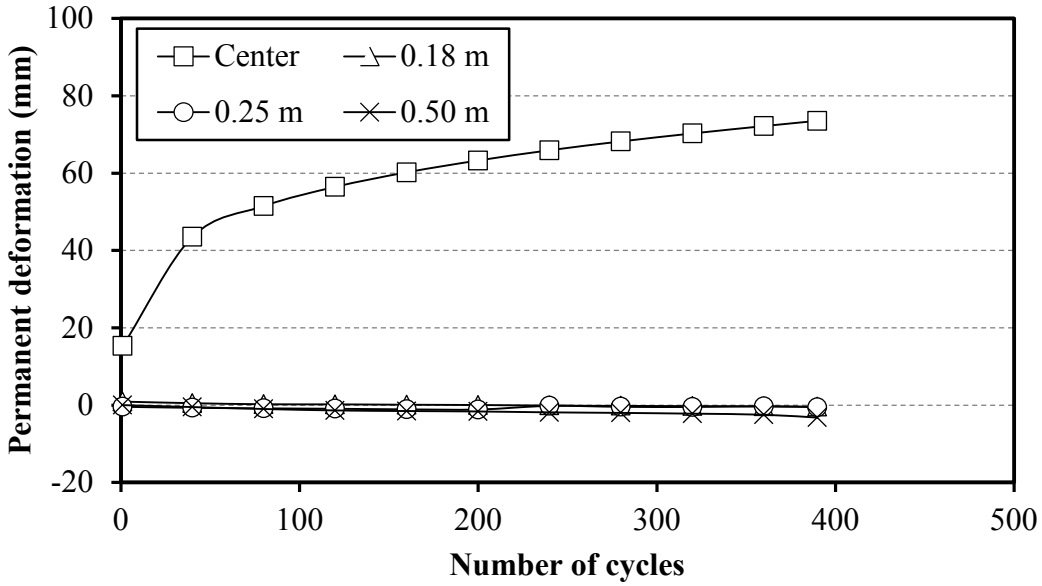

Figure 5.38: Permanent Deformations vs. Number of Loading Cycles for the Geogrid-Reinforced Test Section with Mixture Base and 3% CBR Subgrade

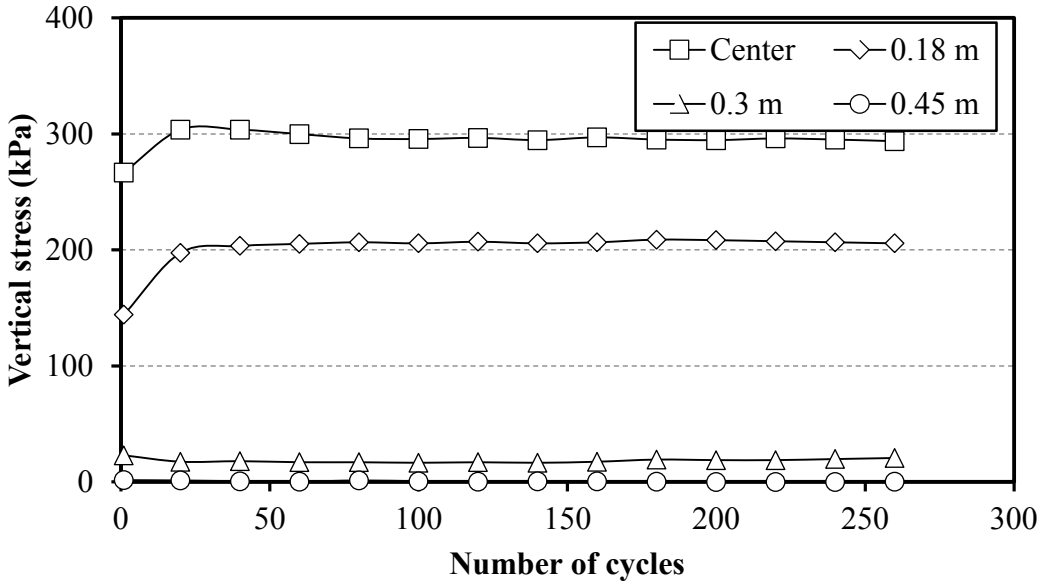

Figure 5.39: Vertical Stresses at the Interface vs. Number of Loading Cycles for the Geogrid-Reinforced Test Section with the Mixture Base and 3% CBR Subgrade

5.2.2.7 Test 13: Unreinforced Section with the Mixture Base and 5% CBR Subgrade

In Test 13, the test section did not reach the 75-mm failure criterion and was terminated at 2,000 cycles as shown in Figure 5.40. At the 2,000th cycle, the permanent deformation at the center was 71 mm. The center permanent deformation increased with the progress of the test and showed the sign of stabilization. Deformations at distances of 0.18, 0.3, and 0.45 m from the center were small. The interface pressures at the center and 0.18 m from the center as presented in Figure 5.41 were similar and both increased with the progress of the test. The interface pressure at the center increased from 236 to 290 kPa in the first 800 cycles, and then increased slightly to 304 kPa by the end of the test. The interface pressure at the distance of 0.18 m from the center increased from 242 to 282 kPa as the test progressed. The interface pressure at the distance of 0.3 m decreased from 22 kPa at the beginning of the test to 0 kPa at the end. The interface pressure at the distance of 0.45 m from the center was small.

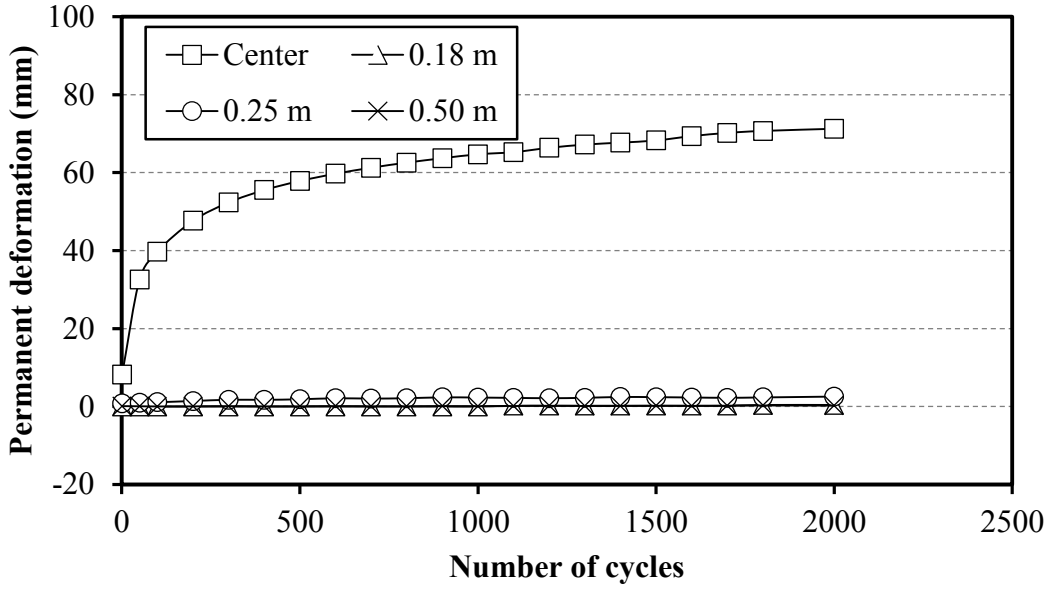

Figure 5.40: Permanent Deformations vs. Number of Loading Cycles for the Unreinforced Test Section with the Mixture Base and 5% CBR Subgrade

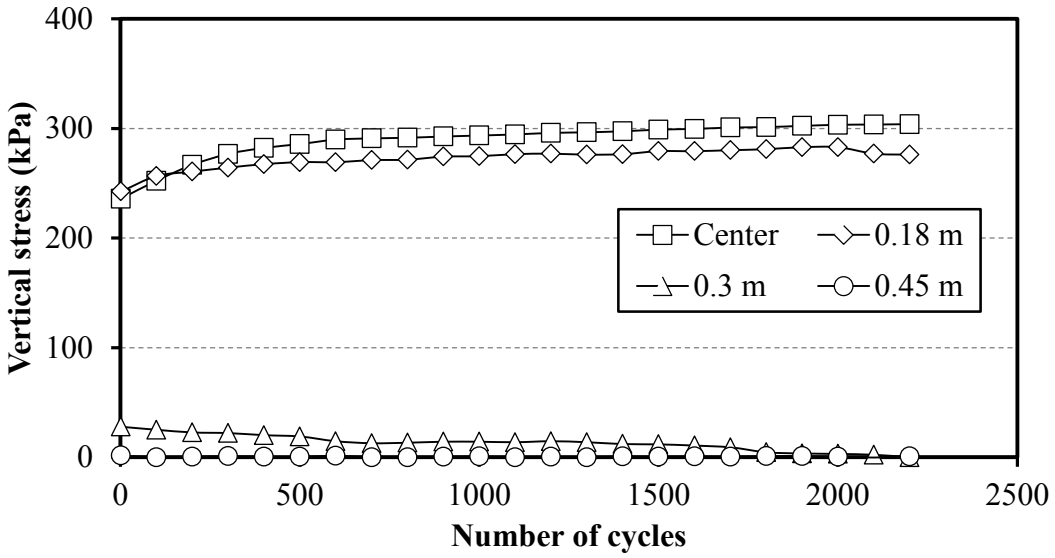

Figure 5.41: Vertical Stresses at the Interface vs. Number of Loading Cycles for the Unreinforced Test Section with Mixture Base and 5%-CBR Subgrade

5.2.2.8 Test 14: Geogrid-Reinforced Section with the Mixture Base and 5% CBR Subgrade

In Test 14, the test section did not reach the 75-mm failure criterion and was terminated at the 3,000th cycle as shown in Figure 5.42. At the 3,000th cycle, the permanent deformation at the center was 66 mm. The center permanent deformation increased with the progress of the test and showed the sign of stabilization. Deformation at distances of 0.18, 0.3, and 0.45 m from the center indicated slight heave, however, their magnitudes were insignificant. The interface pressure at the center increased slightly from 246 kPa at the beginning to 279 kPa at 1,200 cycles as shown in Figure 5.43, then was maintained at approximate 280 kPa for the rest of the test. The interface pressure at the distances of 0.3 m from the center increased with the number of loading cycles from 201 kPa at the beginning to 288 kPa at the end. The interface pressure at the distance of 0.3 m decreased from 35 kPa at the beginning of the test to 12 kPa at the end. The interface pressure at the distance of 0.45 m from the center was small.

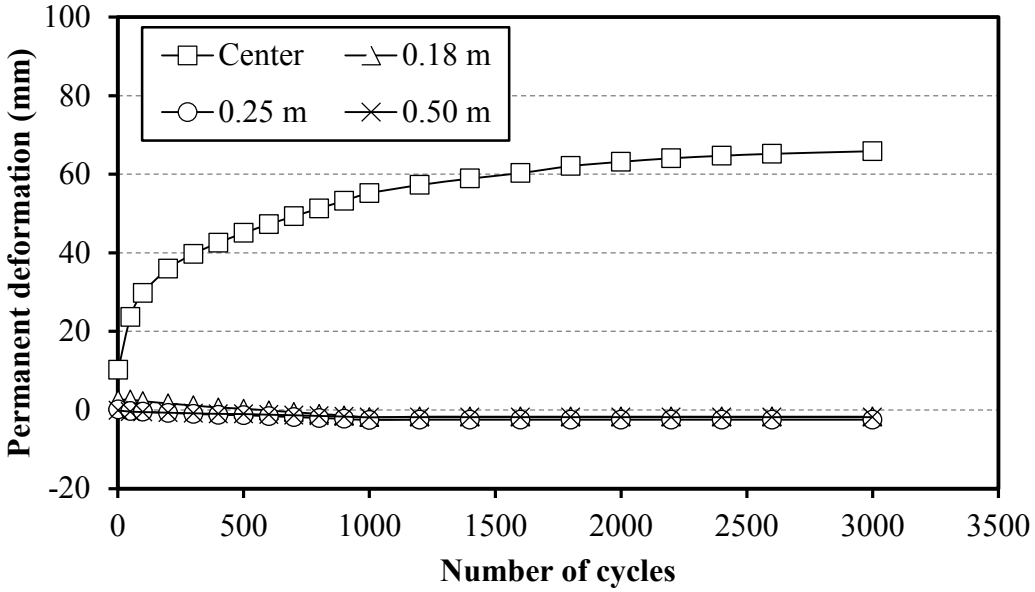

Figure 5.42: Permanent Deformations vs. Number of Loading Cycles for the Geogrid-Reinforced Test Section with the Mixture Base and 5% CBR Subgrade

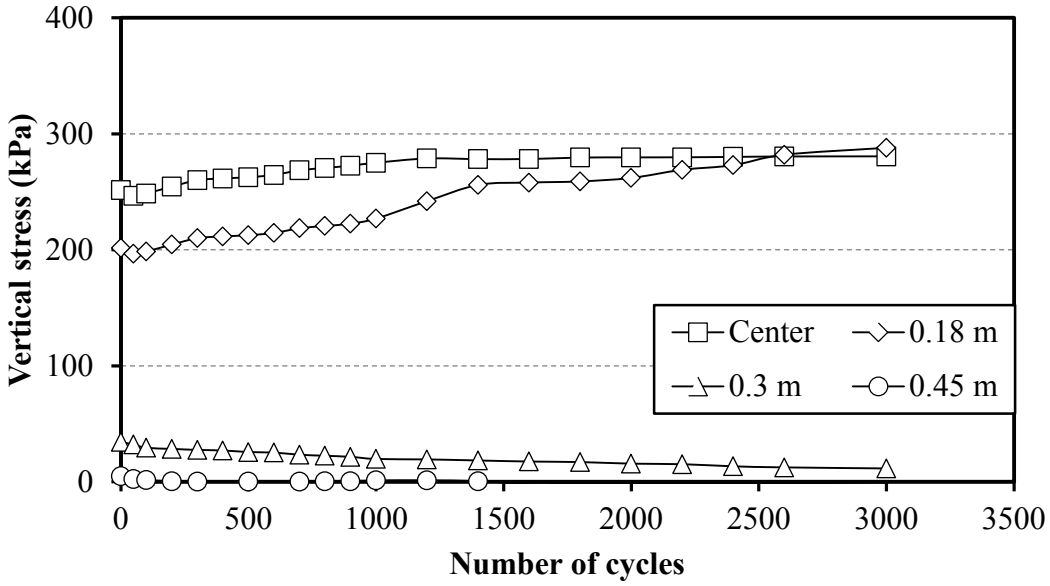

Figure 5.43: Vertical Stresses at the Interface vs. Number of Loading Cycles for the Geogrid-Reinforced Test Section with the Mixture Base and 5% CBR Subgrade

5.2.2.9 Discussion

Figures 5.44 and 5.45 show the surface permanent deformations of all the test sections. The increase rate of the permanent deformation at the initial stage was high and decreased with the increase of the loading cycles. Figure 5.44 shows that the permanent deformations were significantly reduced by the inclusion of the geogrid. The test sections with the soil-AB-3 aggregate mixture base course were weaker than those with the AB-3 aggregate base course in terms of the number of cycles to reach the same permanent deformation. For the test sections with the subgrade CBR at 5%, as shown in Figure 5.45, the number of cycles increased significantly to reach the same permanent deformations as compared with the test sections with the subgrade CBR at 3%. In addition, the geogrid-reinforced test sections had lower permanent deformations. The surface permanent deformations of the test sections with the AB-3-soil mixture bases were slightly higher those of the test sections with the AB-3 bases. However, their differences were not as significant as those of the test sections with the subgrade CBR at 3%, as shown in Figure 5.44. This result indicates that, for a test section with stronger subgrade, the quality of the base course was not as significant as that for a test section with weak subgrade. The main reason is that the test sections with stronger subgrade could avoid a bearing failure so that the accumulation of the permanent deformation became stable, while that of the test sections with weaker subgrade was unstable.

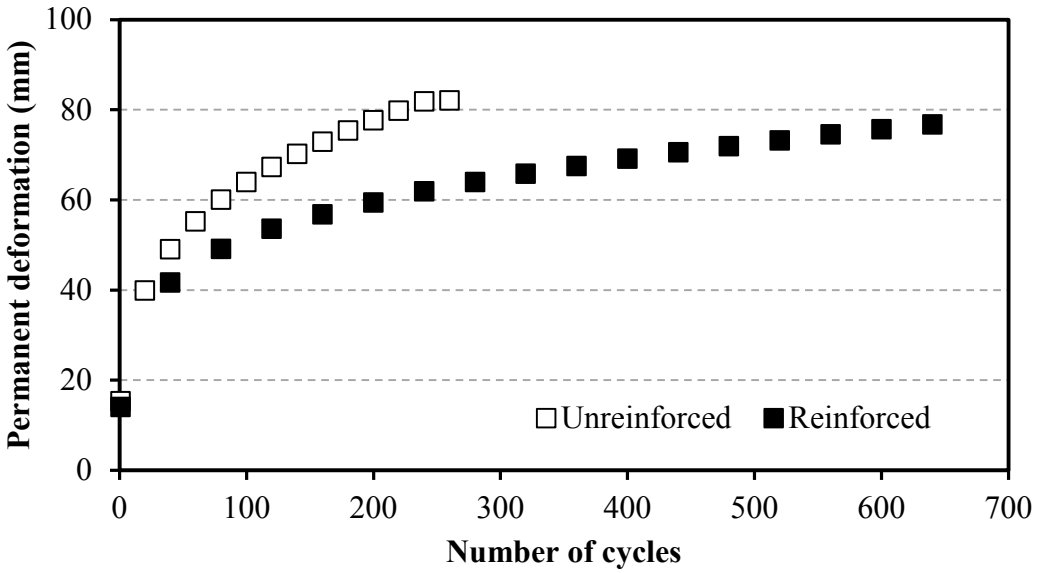

(a) AB-3 base

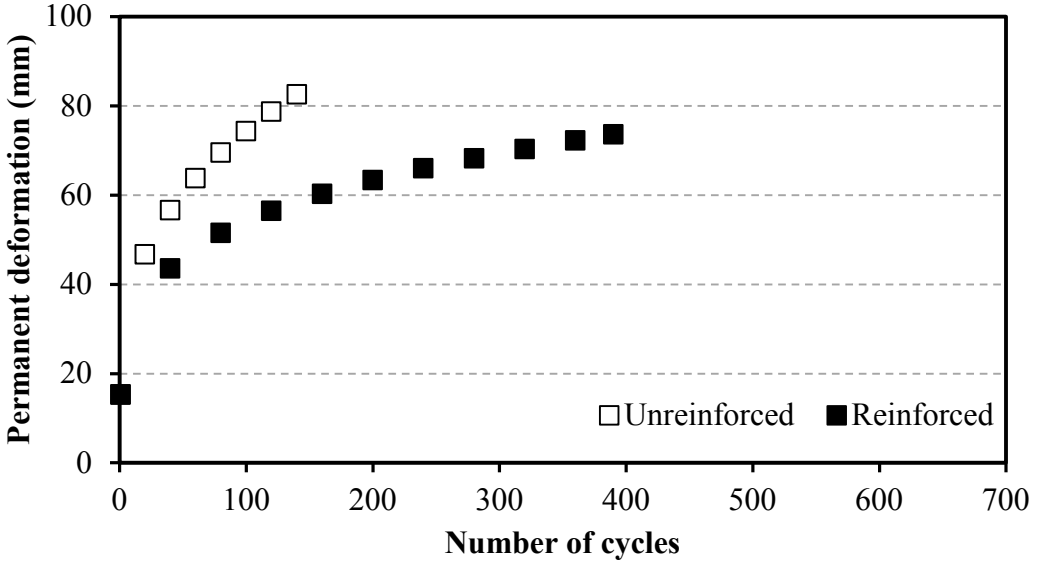

(b) Soil-AB-3 mixture base

Figure 5.44: Permanent Deformations vs. Number of Cycles for the Test Section with Subgrade CBR of 3%

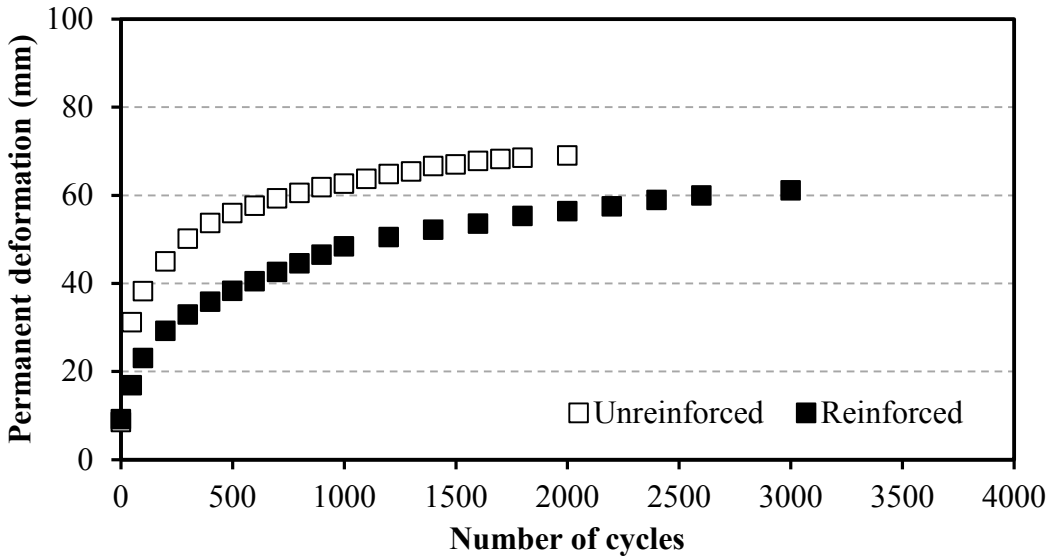

(a) AB-3 base

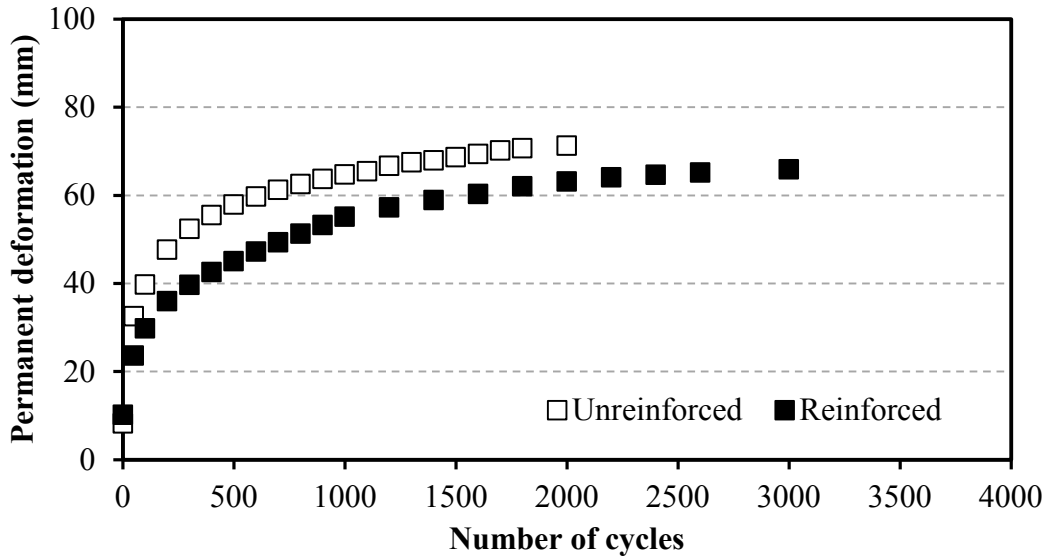

(b) Soil-AB-3 mixture base

Figure 5.45: Permanent Deformations vs. Number of Cycles for the Test Section with Subgrade CBR of 5%

Over 3% or 5% CBR subgrade, the geogrid-reinforced mixture performed better than the unreinforced AB-3 aggregate. The geogrid-reinforced mixture over a 3% CBR subgrade reached 75 mm at approximate 400 cycles while the unreinforced AB-3 base over the same subgrade failed at approximately 200 cycles. The geogrid-reinforced mixture over a 5% CBR subgrade sustained over 1,500 cycles before reaching the 75-mm failure criteria while the unreinforced AB-3 base failed at approximately 500 cycles.

Figures 5.46 and 5.47 show the vertical stresses at the interface in all the test sections. Overall, the vertical stresses decreased with the inclusion of geogrid reinforcement. The initial stresses in the unreinforced and reinforced sections were approximately the same because the geogrid was not mobilized at the same deformation. With the increase of the load cycles, the vertical stresses increased gradually. This result indicates the deterioration of the base course as suggested by Giroud and Han (2004a). The use of the geogrid slowed down the rate of base deterioration.

As compared with those of the test sections with AB-3 bases, the vertical stresses of the test sections with soil-AB-3 mixture bases were higher because the modulus of the soil-AB-3 mixture base was lower than that of the AB-3 base. According to the layered elastic theory, the decrease of the modulus ratio of the base course to subgrade results in an increase of the vertical stress at the interface. Similarly, the increase of the subgrade modulus causes the decrease of the modulus ratio as well. Therefore, the vertical stresses of the test sections with the subgrade CBR at 5% were higher than those of the test sections with the subgrade CBR at 3%.

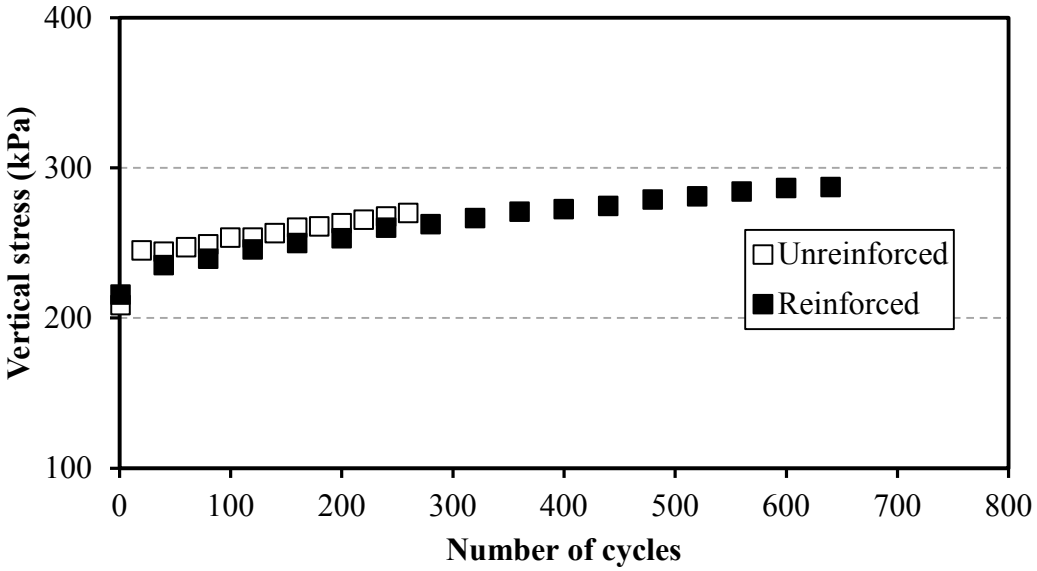

(a) AB-3 base

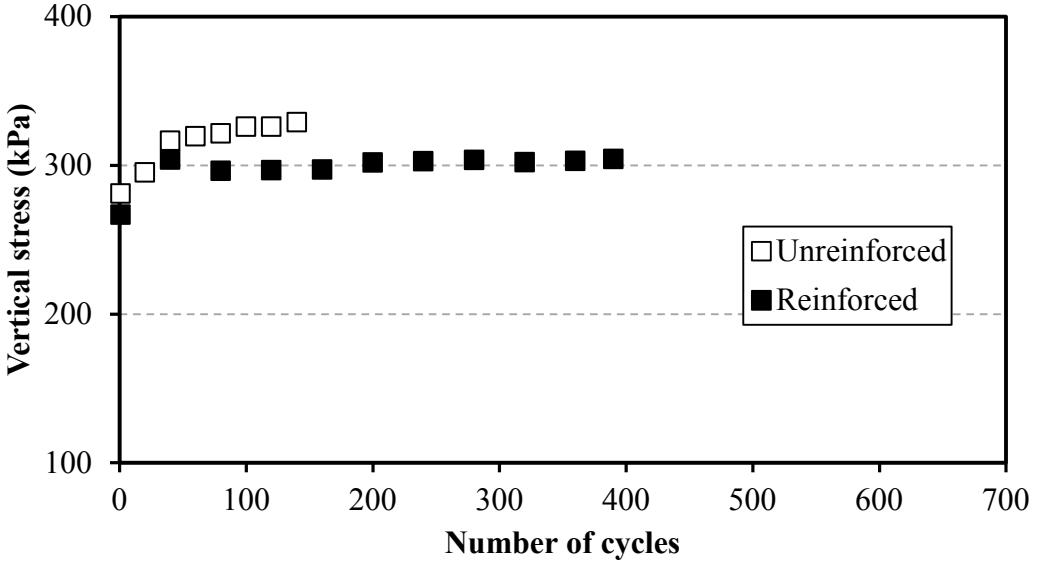

(b) Soil-AB-3 mixture base

Figure 5.46: Vertical Stress at the Interface vs. Number of Cycles for the Test Section with Subgrade CBR of 3%

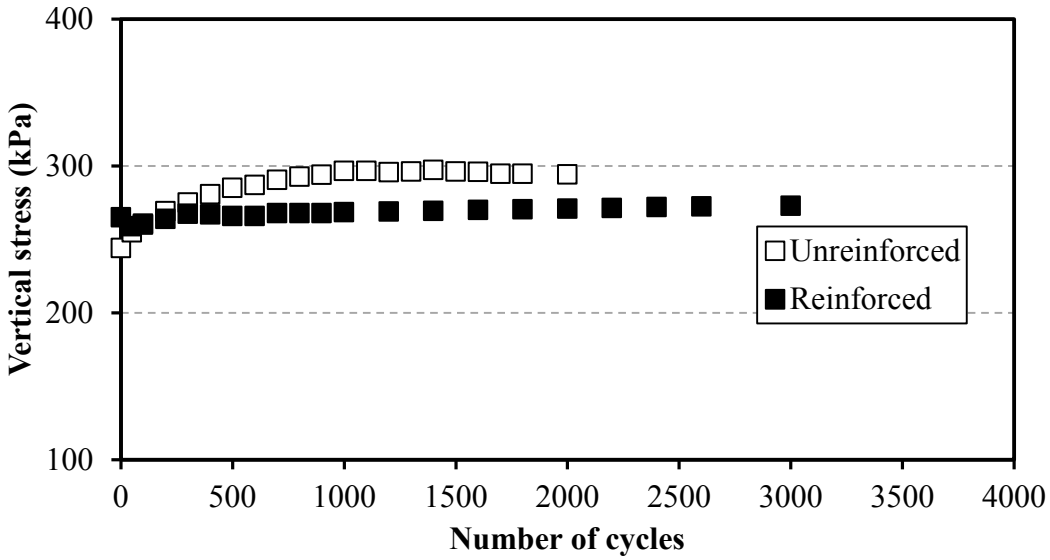

(a) AB-3 base

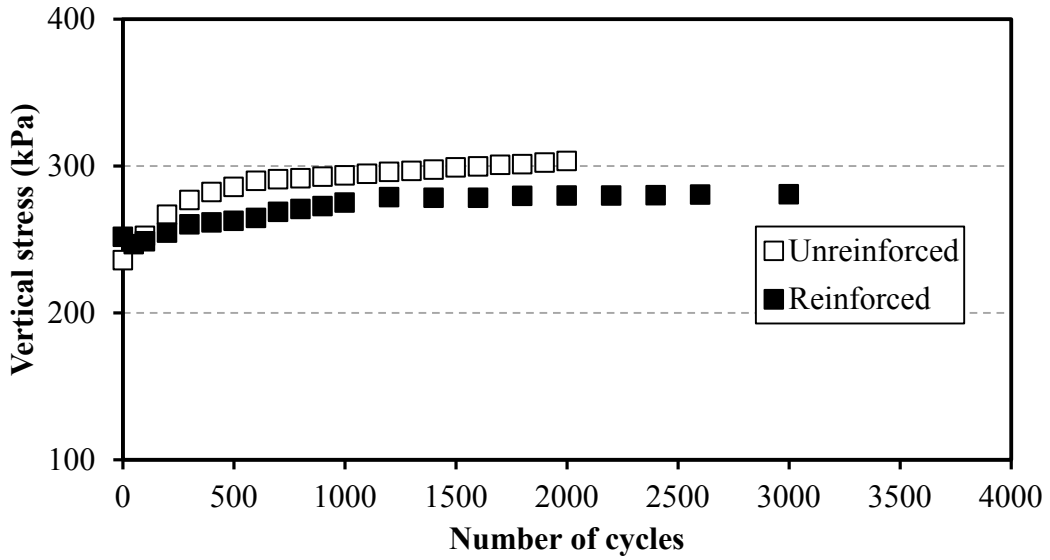

(b) Soil-AB-3 mixture base

Figure 5.47: Vertical Stress at the Interface vs. Number of Cycles for the Test Section with Subgrade CBR of 5%

5.2.3 Traffic Beneficial Ratio

To evaluate the benefits provided by geosynthetic reinforcement, a traffic beneficial ratio (TBR) is often used in practice and defined here as the ratio of the number of cycles for the test section with geosynthetic reinforcement to that without reinforcement at a specific permanent deformation over the same subgrade condition as follows:

$$\mathbf{TBR} = \frac{N_{reinforced}}{N_{unreinforced}}$$

The calculated traffic beneficial ratios at various permanent deformations from this study are provided in Table 5.4. This table indicates the effectiveness of geosynthetics increased with the increase of permanent deformation or loading cycles. At 50-mm permanent deformation, the geogrid-reinforced base supported at least twice the number of load cycles than the unreinforced base. For the geocell reinforcement, because the geocell-reinforced mixture section did not reach 50-mm permanent deformation, the TBR was calculated at 25-mm permanent deformation. The geocell-reinforced mixture base underwent over 50 times more loading cycles than the unreinforced mixture base at 25-mm permanent deformation.

Table 5.4: Traffic Beneficial Ratios at Different Permanent Deformations Provided by Geosynthetics

Section			Traffic Beneficial Ratio at Permanent Deformation (mm)		
Subgrade CBR	**Base course**	**Reinforcement**	**25**	**50**	**70**
3%	AB-3	Geogrid	1.9	2.0	2.6
5%	AB-3	Geogrid	3.6	3.9	
3%	Mixture	Geogrid	2.1	2.7	3.8
5%	Mixture	Geogrid	1.8	4.8	
5%	Mixture	Geocell	51.4		

The TBR concept can also be applied to compare the number of load cycles of geosynthetic-reinforced mixture base with that of the conventional unreinforced aggregate base (AB-3 aggregate in this study). This TBR is termed as an equivalent TBR. Table 5.5 presents the equivalent TBRs for the geosynthetic-reinforced mixture sections to the conventional unreinforced aggregate section at a specific permanent displacement. In Table 5.5, the geogrid-reinforced mixture sections of 150-mm thick were compared to the AB-3 aggregate base of 150-mm thick over the similar CBR subgrade while the geocell-reinforced mixture sections of 200-mm thick were compared to the AB-3 aggregate base of 200-mm thick over the similar CBR subgrade. Test Sections 5 and 6 were left out of the comparison, for the reason as previously discussed, i.e., the topsoil cover developed excessive permanent deformations and was considered unsuitable for the application of unpaved shoulders or roads discussed in this report. Table 5.5 shows that the geosynthetic-reinforced mixture bases had a larger number of load cycles than the conventional aggregate base. Therefore, the geosynthetic-reinforced mixture can be used to replace aggregate in the application of unpaved shoulders or roads.

Table 5.5: Equivalent TBRs of Geosynthetic-Reinforced Mixture Bases over the Conventional Aggregate Base

Section			Equivalent TBR at Permanent Deformation (mm)		
Subgrade CBR	**Base course**	**Reinforcement**	**25**	**50**	**70**
3%	Mixture	Geogrid	3.8	1.7	4.5
5%	Mixture	Geogrid	1.7	2.5	
5%	Mixture	Geocell	2.1		
5%	AB-3+Mixture	Geocell	1.4		

5.3 Cost Analysis

Design of unpaved roads, such as shoofly detours, requires a tolerable number of load cycles and does not require vegetation; therefore, aggregate bases are preferred because they are more effective to support loads. Since aggregate bases do not require mixing with topsoil or onsite soil, they may be more cost-effective as well. As discussed earlier, geosynthetic reinforcement (geogrid or geocell) can increase the tolerable number of load cycles at the same base thickness at least twice if the tolerable permanent deformation is 50 mm or larger. In other words, to achieve the same performance (i.e., same tolerable permanent deformation), a thinner geosynthetic-reinforced base course is needed than an unreinforced base course. Since both geosynthetics and aggregate have costs, a cost analysis should be performed to evaluate whether the saving of the aggregate base is sufficient to offset the cost of geosynthetic. Since geogrid costs less than geocell, geogrid is often more cost-effective when aggregate base is used.

Design of unpaved shoulders depends on whether vegetation is needed. If no vegetation is needed, aggregate base is also preferred. However, if vegetation is needed, soil-aggregate mixture base is preferred. Based on this study, a mixture of 50% soil and 50% aggregate by weight is recommended because it can ensure good vegetation growth and have a reasonable structural capacity for load cycles. However, the soil-aggregate mixture has a limited structural capacity. Geosynthetic, geocell or geogrid, can be used to increase the mixture's structural capacity to meet the demand of high load cycles. Geocell is more effective in enhancing the performance of the soil-aggregate mixture base than geogrid because geocell can provide better lateral confinement. The use of geosynthetic can also reduce the required base thickness of soil-aggregate mixture to achieve the same performance.

Chapter 6: Conclusions and Recommendations

In this study, a one-year-long vegetation test and 14 large-scale cyclic plate loading tests were conducted on different base courses consisting of AB-3 aggregate, soil-aggregate mixture, and topsoil with and without geocell or geogrid reinforcement to investigate their effects on vegetation and structural capacities. Based on the test results, the following conclusions were drawn:

1. Throughout the one-year test period, no definite evidence of geocell or geogrid reinforcement limiting the vegetation growth in unpaved shoulders was found.
2. The type of soil cover had a significant effect on the vegetation growth at the initial establishment stage. The soil cover containing a high percentage of aggregate retarded the establishment of vegetation while the soil cover containing a high percentage of fines promoted the establishment of vegetation.
3. The 50/50 soil-aggregate mixture showed no significant difference from the native topsoil on the ability to sustain the already established vegetation. The AB-3 aggregate and 65/35 soil-aggregate mixture did limit the biomass production of vegetation, thus, it was not recommended for the application of vegetated shoulders.
4. Both geocell and geogrid reinforcement effectively reduced permanent deformations under cyclic loading.
5. The effectiveness of geocell reinforcement depended on the composition of the base course. The geocell-reinforced soil-aggregate mixture base with a mixture cover or an aggregate cover performed slightly better than the unreinforced aggregate base of the same thickness over 5% CBR subgrade.

6. The high-plasticity topsoil cover failed rapidly under cyclic loading; therefore, it should not be used if unpaved shoulders are expected to carry traffic.
7. The geogrid-reinforced soil aggregate mixture base performed significantly better than the unreinforced aggregate base of the same thickness over 3% and 5% CBR subgrade.

Based on the analysis and discussion of the test data, the following recommendations can be made:

1. The soil mixture consisting of 50% AB-3 aggregate and 50% topsoil showed similar ability on sustaining vegetation as the topsoil. With the inclusion of geocell or geogrid reinforcement, the 50/50 soil-aggregate mixture also had enhanced structural capacities, which were higher than AB-3 aggregate at the same thickness. Therefore, the 50/50 soil-aggregate mixture is recommended as the base material for vegetated unpaved shoulders. To improve the structural capacity of the soil-aggregate mixture, geocell is recommended.
2. The topsoil cover promoted the vegetation establishment. However, during cyclic loading tests, it was found that the topsoil cover was the main contributor for the excessive permanent deformations. Therefore, the topsoil cover is not recommended for the application of vegetated unpaved shoulders if subjected to traffic loading.
3. For unpaved roads, such as shoofly detours, aggregate bases are recommended. To improve the performance of aggregate bases on weak subgrade or moderate subgrade, geogrid is recommended.

The influence of moisture content on the strength of the 50/50 soil-aggregate mixture was not investigated in this study. Further studies are needed to verify the performance of the mixtures at various moisture contents.

References

Abu-Farsakh, M.Y., Nazzal, M.D., & Mohammad, L.N. (2007). Effect of reinforcement on resilient and permanent deformations of base course material. *Transportation Research Record, 2004*, 120-131.

Al-Qadi, I.L., Brandon, T.L., Valentine, R.J., Lacina, B.A., & Smith, T.E. (1994). Laboratory evaluation of geosynthetic-reinforced pavement sections. *Transportation Research Record, 1439*, 25-31.

ASTM D1557-12e1. (2012). *Standard test methods for laboratory compaction characteristics of soil using modified effort (56,000 ft-lbf/ft3 (2,700 kN-m/m3))*. West Conshohocken, PA: ASTM International. doi: 10.1520/D1557-12E01, www.astm.org

ASTM D2974-14. (2014). *Standard test methods for moisture, ash, and organic matter of peat and other organic soils*. West Conshohocken, PA: ASTM International. doi: 10.1520/D2974-14, www.astm.org

ASTM D6951 / D6951M-09. (2015) *Standard test method for use of the dynamic cone penetrometer in shallow pavement applications*. West Conshohocken, PA: ASTM International. doi: 10.1520/D6951_D6951M-09R15, www.astm.org

ASTM E1756-08. (2008). *Standard test method for determination of total solids in biomass.* West Conshohocken, PA: ASTM International. doi: 10.1520/E1756-08, www.astm.org

Bathurst, R.J., & Karpurapu, R. (1993). Large-scale triaxial compression testing of geocell-reinforced granular soils. *Geotechnical Testing Journal, 16*(3), 296-303.

Chen, Q., Abu-Farsakh, M., & Tao, M. (2009). Laboratory evaluation of geogrid base reinforcement and corresponding instrumentation program. *Geotechnical Testing Journal, 32*(6), 516-525.

Chow, J.C., Watson, J.G., Lowenthal, D.H., Solomon, P.A., Magliano, K.L., Ziman, S.D., & Willard Richards, L. (1992). PM10 source apportionment in California's San Joaquin Valley. *Atmospheric Environment. Part A. General Topics, 26*(18), 3335-3354.

Dunnett, N.P., Willis, A.J., Hunt, R., & Grime, J.P. (1998). A 38-year study of relations between weather and vegetation dynamics in road verges near Bibury, Gloucestershire. *Journal of Ecology, 86*(4), 610-623.

Gantenbein, B. (2006, April 6). Unique application: Greendale resurfacing job includes green shoulder. *Western Builder*, pp. 8-9.

Gibson, D.J., & Newman, J.A. (2001). Festuca arundinacea Schreber (F. elatior L. ssp. arundinacea (Schreber) Hackel). *Journal of Ecology, 98*(2), 304-324.

Giroud, J.P., & Han, J. (2004a). Design method for geogrid-reinforced unpaved roads. I. Development of design method. *Journal of Geotechnical and Geoenvironmental Engineering, 130*(8), 775-786.

Giroud, J.P., & Han, J. (2004b). Design method for geogrid-reinforced unpaved roads. II. Calibration and applications. *Journal of Geotechnical and Geoenvironmental Engineering, 130*(8), 787-797.

Giroud, J.P., & Noiray, L. (1981). Geotextile-reinforced unpaved road design. *Journal of the Geotechnical Engineering Division, 107*(9), 1233-1254.

Google Maps. (2015). [University of Kansas West Campus, Lawrence, KS] [Satellite imagery]. Retrieved October 2013, from https://www.google.com/maps/@38.9514565,-95.2731543,191m/data=!3m1!1e3

Haas, R., Walls, J., & Carroll, R. (1988). Geogrid reinforcement of granular bases in flexible pavements. *Transportation Research Record, 1188*, 19-27.

Han, J., Yang, X., Leshchinsky, D., & Parsons, R.L. (2008). Behavior of geocell-reinforced sand under a vertical load. *Transportation Research Record, 2045*, 95-101.

Henson, J.F. (2001). *Plant guide: Tall fescue*. Baton Rouge, LA: USDA NRCS National Plant Data Center.

Indraratna, B., Hussaini, S.K.K., & Vinod, J.S. (2013). The lateral displacement response of geogrid-reinforced ballast under cyclic loading. *Geotextiles and Geomembranes, 39*, 20-29.

Kansas Department of Transportation (KDOT). (2013). *Seed/native wildflower mixes*. Topeka, KS: Author.

Kansas Department of Transportation (KDOT). (2014). *Road design manual, volume I (part A & B), November 2011 edition, revised May 2014*. Topeka, KS: Author.

Leenders, J.K., van Boxel, J.H., & Sterk, G. (2007). The effect of single vegetation elements on wind speed and sediment transport in the Sahelian zone of Burkina Faso. *Earth Surface Processes and Landforms, 32*(10), 1454-1474.

Leng, J., & Gabr, M.A. (2002). Characteristics of geogrid-reinforced aggregate under cyclic load. *Transportation Research Record, 1786*, 29-35.

Madhavi Latha, G., Rajagopal, K., & Krishnaswamy, N. (2006). Experimental and theoretical investigations on geocell-supported embankments. *International Journal of Geomechanics, 6*(1), 30-35.

Mekkawy, M.M., White, D.J., Jahren, C.T., & Suleiman, M.T. (2010). Performance problems and stabilization techniques for granular shoulders. *Journal of Performance of Constructed Facilities, 24*(2), 159-169.

Mitchell, J.K., Kao, T., & Kavazanjian, E., Jr. (1979). *Analysis of grid cell reinforced pavement bases*. Fort Belvoir, VA: Defense Technical Information Center.

Moosmüller, H., Gillies, J.A., Rogers, C.F., DuBois, D.W., Chow, J.C., Watson, J.G., & Langston, R. (1998). Particulate emission rates for unpaved shoulders along a paved road. *Journal of the Air & Waste Management Association, 48*(5), 398-407.

Munson, S.M., Belnap, J., Okin, G.S., & Schlesinger, W.H. (2011). Responses of wind erosion to climate-induced vegetation changes on the Colorado Plateau. *Proceedings of the National Academy of Sciences of the United States of America, 108*(10), 3854-3859.

Perkins, S.W. (1999). *Geosynthetic reinforcement of flexible pavements: Laboratory based pavement test sections* (Report No. FHWA/MT-99-001/8138). Helena, MT: Montana Department of Transportation.

Perkins, S.W., & Ismeik, M. (1997). A synthesis and evaluation of geosynthetic-reinforced base layers in flexible pavements: Part I. *Geosynthetics International, 4*(6), 549-604.

Pokharel, S.K. (2010). *Experimental study on geocell-reinforced bases under static and dynamic loading* (Doctoral dissertation). University of Kansas, Lawrence, KS.

Pokharel, S.K., Han, J., Leshchinsky, D., Parsons, R.L., & Halahmi, I. (2010). Investigation of factors influencing behavior of single geocell-reinforced bases under static loading. *Geotextiles and Geomembranes, 28*(6), 570-578.

Pokharel, S.K., Han, J., Manandhar, C., Yang, X., Leshchinsky, D., Halahmi, I., & Parsons, R.L. (2011). Accelerated pavement testing of geocell-reinforced unpaved roads over weak subgrade. *Transportation Research Record, 2204*, 67-75.

Presto Geosystems. (2009a). Geoterra® Structural Mat System: Specification summary. Retrieved from http://www.prestogeo.com/downloads/5d2eF5tVoSthZ7S2FTHJYktElB46cxYUp3ZuxIGbz01vRs2k1A/GEOTERRA%20Specification%20Summary.pdf

Presto Geosystems. (2009b). Geoterra® Structural Mat System: Specification & installation guideline. Retrieved from http://www.prestogeo.com/downloads/BqEa3J4VQhW59e3bvwoA5sECWXdrensKrJC2DYHkuCjthbLTOz/GEOTERRA%20Specification%20and%20Installation%20Guideline-eng.pdf

Presto Geosystems. (2011). Genuine Geoweb® GW30V - 150 mm (6 in) depth: Performance & material specification summary. Retrieved from http://www.prestogeo.com/downloads/YNjJj6EykMeI87iE9Sx4FxrNzFrvYrwx6W7fRBT3NxBLukPt3D/Geoweb%20GW30v6_summary.pdf

Qian, Y., Han, J., Pokharel, S.K., & Parsons, R.L. (2011). Stress analysis on triangular-aperture geogrid-reinforced bases over weak subgrade under cyclic loading: An experimental study. *Transportation Research Record, 2204*, 83-91.

Raeside, M.C., Friend, M.A., Behrendt, R., Lawson, A.R., & Clark, S.G. (2012). A review of summer-active tall fescue use and management in Australia's high-rainfall zone. *New Zealand Journal of Agricultural Research, 55*(4), 393-411.

Rahman, M.A., Arulrajah, A., Piratheepan, J., Bo, M.W., & Imteaz, M.A. (2014). Resilient modulus and permanent deformation responses of geogrid-reinforced construction and demolition materials. *Journal of Materials in Civil Engineering, 26*(3), 512-519.

Rea, C., & Mitchell, J.K. (1978). Sand reinforcement using paper grid cells. In *Symposium on Earth Reinforcement* (pp. 644-663). New York, NY: American Society of Civil Engineers.

Sharma, R., Chen, Q., Abu-Farsakh, M., & Yoon, S. (2009). Analytical modeling of geogrid reinforced soil foundation. *Geotextiles and Geomembranes, 27*(1), 63-72.

Thakur, J.K., Han, J., & Parsons, R.L. (2013). Creep behavior of geocell-reinforced recycled asphalt pavement bases. *Journal of Materials in Civil Engineering, 25*(10), 1533-1542.

Thakur, J.K., Han, J., Pokharel, S.K., & Parsons, R.L. (2012). Performance of geocell-reinforced recycled asphalt pavement (RAP) bases over weak subgrade under cyclic plate loading. *Geotextiles and Geomembranes, 35*, 14-24.

Tingle, J., & Jersey, S. (2005). Cyclic plate load testing of geosynthetic-reinforced unbound aggregate roads. *Transportation Research Record, 1936*, 60-69.

Tingle, J., & Jersey, S. (2009). Full-scale evaluation of geosynthetic-reinforced aggregate roads. *Transportation Research Record, 2116*, 96-107.

Udo, K., & Takewaka, S. (2007). Experimental study of blown sand in a vegetated area. *Journal of Coastal Research, 23*(5), 1175-1182.

United States Department of Agriculture (USDA) Natural Resources Conservation Service Plant Materials Program. (2002a). Plant fact sheet: Perennial ryegrass. Retrieved from: http://plants.usda.gov/factsheet/pdf/fs_lope.pdf

United States Department of Agriculture (USDA) Natural Resources Conservation Service Plant Materials Program. (2002b). Plant fact sheet: Tall fescue. Retrieved from http://plants.usda.gov/factsheet/pdf/fs_loar10.pdf

Van de Ven, T.A.M., Fryrear, D.W., & Spaan, W.P. (1989). Vegetation characteristics and soil loss by wind. *Journal of Soil and Water Conservation, 44*(4), 347-349.

Yang, X., & Han, J. (2013). Analytical model for resilient modulus and permanent deformation of geosynthetic-reinforced unbound granular material. *Journal of Geotechnical and Geoenvironmental Engineering, 139*(9), 1443-1453.

Yang, X., Han, J., Pokharel, S.K., Manandhar, C., Parsons, R.L., Leshchinsky, D., & Halahmi, I. (2012). Accelerated pavement testing of unpaved roads with geocell-reinforced sand bases. *Geotextiles and Geomembranes*, 32, 95-103.

K-TRAN

KANSAS TRANSPORTATION RESEARCH AND NEW-DEVELOPMENT PROGRAM

AD ASTRA PER ASPERA

Kansas

Department of Transportation